NOTE TO USERS

This reproduction is the best copy available.

UNIVERSITY OF CINCINNATI

August 11, 19 76

I hereby recommend that the thesis prepared under my supervision by FRANK A. ASCOLI

entitled Dose Parameters for Pediatric Nuclear Medicine Procedures

be accepted as fulfilling this part of the requirements for the degree of Masters in Radiological Science

Approved by:

James G Kereiakes

J. R. Thomas

Edward R Ekern

Form 668—Grad. School

DOSE PARAMETERS FOR PEDIATRIC NUCLEAR MEDICINE PROCEDURES

A Thesis submitted to the

Division of Graduate Studies
of the University of Cincinnati

in partial fulfillment of the
requirements for the degree of

MASTER OF SCIENCE

in the Department of Radiological Sciences
of the College of Medicine

1976

by

Frank A. Ascoli
B.S., Northeastern University, 1972

Abstract

This thesis presents detailed calculations of the dosage to the metaphyses of the distal femur and proximal tibia and fibula of two children, ages 4 and 13. Parameters studied for each child include: mass and dimensions of the growth plate area; effective half-life and cumulated activity for ^{99m}Tc-EHDP; and mean dose per unit cumulated activity for the disc geometry of the metaphyses. Consideration is given to the use of the gamma camera for conjugate view counting. The effects of source to collimator distance, source length, and absorber thickness on the absolute count rate are evaluated. In addition, S factors for the various radionuclides have been calculated for spheres and ellipsoids of masses down to one gram.

Acknowledgment

I wish to thank Dr. James Kereiakes for his guidance throughout this project and his welcomed advice during the past year; Dr. Stephen Thomas for the many hours spent initiating the protocol studies; Dr. Michael Gelfand for the all important clinician's point of view; my wife, Paulette, for graciously typing the manuscript and for her endless understanding, encouragement, and belief in us; and finally Amy, who, knowingly or not, has been a constant source of inspiration.

Table of Contents

List of Figures

List of Tables

Introduction

The question of dosage from radionuclides used in diagnostic procedures on infants and children continues to remain of paramount interest amoung researchers concerned with minimizing the child's exposure from such procedures. Although dosimetric information in available for adults, only occasional reference is found to doses received by children. Kereiakes et al. have warned of the inaccuracies which may be introduced as a result of extrapolating pediatric dose from adult dose tables (21). Consideration in using adult dose to estimate pediatric dose must be given to the biological differences attributed to age. It has been shown, for example, that thyroid uptake is elevated from about 30 percent in adults to 80 percent in newborn euthyroid infants (38) and that the localization of bone-seeking agents may vary with age in animals (39).

A specific case in pediatric nuclear medicine where neither adult nor animal data exists is the localization of bone seeking agents in the epiphyses of children. Total bone activity and radiation dosages have been estimated for adults (34), (35), (40) and presumably apply for children as well; however, as the scintigram in figure 3b shows, the active growth plates in children have a significantly higher uptake than compact bone. An attempt will be made in this study of

two children receiving ^{99m}Tc-EHDP (ethane-1-hydroxyl-1, 1-diphosphonate) bone scanning agent to quantitate the activity in the growth plates and calculate self dosage.

As shown in figure 3b, the growth plates of the knee may be approximated by disc geometry. For this reason, the knees were chosen for study, since other epiphyses in children present rather complex geometries (41).

Growth plate dosages were calculated in this study according to the schema of Loevinger and Berman (7). Basically, the method calls for measurements on the biological action of the isotope and the derivation of physical constants appropriate to the radionuclide and geometry under study. In practice, the biological and physical factors may be difficult to obtain. Since geometrical factors are implicit in internal dosimetry calculations, Monte Carlo type computations are usually performed. Unfortunately, Monte Carlo data is not available for disc geometry and therefore analytical calculations must be used.

Biological data, i.e. the cumulated activity, may be obtained by the method of Thomas et al. (29) directly from equipment found in most nuclear medicine labs. The Ohio Nuclear and DataSystem 150 Computer at the Children's Hospital in Cincinnati were used for this

study. The very fact that biological data can be obtained in a clinical lab will hopefully mean that more measurements will be done than in the past, and more data on children collected.

Subramanian and McAfee have presented data for technetium labeled sodium tripolyphosphate localization in the fractured tibia's of rabbits (35). Their results show significantly increased uptake in the callus, and form the only basis of comparison of growth plate uptake in children. Similiar fracture data has not been found for the EHDP compounds. Obviously, more studies are needed before any definitive statements can be made about the distribution of ^{99m}Tc-EHDP in the growth plates of children.

Biological and Effective Half-Life.

When a radionuclide is administered internally to a patient, a complicated pattern of uptake and elimination takes place. Assuming that the uptake is rapid relative to the elimination for most clinically used isotopes and most tissues, the radiation dose to tissue is usually delivered during the elimination phase. Elimination is characterized both by biological removal and physical decay of the radionuclide. The physical decay of the isotope is easily quantitated by a knowledge of its decay constant, λ_p. A mathematical model for the biological removal, however, would involve a complicated function of the actual "turnover" rates of the various tissues involved, since activity is both entering and leaving the tissue at all times (1). As a first approximation, it will be assumed that the elimination phase is exponential, i.e., the fraction of the isotope eliminated biologically per unit time can be characterized as λ_b.

Physical decay and biological removal are independent and simultaneous. Letting λ_{eff} be the fraction which disappears per unit time by both processes, it follows that

$$\lambda_{eff} = \lambda_p + \lambda_b \qquad [1]$$

or

$$T_{1/2(eff)} = \frac{T_{1/2(p)} T_{1/2(b)}}{T_{1/2(p)} + T_{1/2(b)}} \qquad [2]$$

The average concentration of radioactivity in tissue, therefore, decreases exponentially according to

$$C(t) = C_o e^{-\frac{0.693 t}{T_{1/2(eff)}}} \qquad [3]$$

where C_o is the average concentration at time t=0.

The effective half-life is an essential parameter in any calculations involving dose to a tissue. But, as mentioned briefly above, its true value is rarely predicted with accuracy. The biological half-life may depend on the amount of inactive carrier received by the patient before, during, or after the injection of radionuclide. It may also, for large doses, depend on the amount of radioactivity injected, since the tissue itself may be altered by large doses of radioactivity. Also, biological half-life may be related in a complex way to the metabolism of other tissues in the body, which in turn are unpredictable functions of the physical state of the patient (1).

The effective half-life will be assumed exponential for the purposes of this study. As will be shown in the experimental phase, the exponential model is a good approximation.

The MIRD Equations

A. Introduction

The dose delivered by internally administered radioisotopes depends upon such factors as: energy of the radiation, type of radioactive decay, geometry of the region in which the radioisotope is distributed, physical position of a point of interest within the tissue, concentration of the isotope within the region, biological elimination from the region, surrounding media, and the mass and density of the tissue.

Geometric and energy considerations were accounted for in earlier works by use of a "geometrical" factor, g_p (1), (6):

$$g_p = \int_V \frac{e^{-\mu_{eff} r}}{r^2} dV \qquad [4]$$

The MIRD equations replace the geometrical factor with a more exact expression, ϕ, the absorbed dose fraction, to be described later in this study. Nevertheless, g_p is a valid approximation useful in internal dosimetry and forms the basis of the absorbed fraction data for the epiphyseal plate geometry presented in this work.

Tables of g_p and $\overline{g}$ (useful when average dose to a specific volume from a uniformly distributed radioisotope is desired) are available (1), (6). These are approximations since they depend on an effective

attenuation coefficient for primary radiation. This coefficient has been approximated at .03 for radium energies (3), but in fact may vary considerably for energies less than .2 MeV and greater than 2 MeV.

In equation 4, μ_{eff} is the effective absorption coefficient per centimeter of tissue. Its value depends on the fraction of scattered radiation that is absorbed within the tissue and is therefore a function of energy, density, and geometry. In their original work, Loevinger et al. reasoned that μ_{eff} would have a value somewhere between zero and the true absorption coefficient μ_a depending upon the source to point distance (1). For distances up to one mean-free path of primary radiation, $\mu_{eff} \sim 0$, and from one to three mean-free paths, $\mu_{eff} \sim \mu_a$. The value for μ_a is given as 0.03 cm^{-1} and is approximately constant in the range 0.2 to 2.0 MeV (1). Although a good approximation, other authors recommend not using an attenuation coefficient but rather an energy absorption coefficient (4), (5). The attenuation coefficient is determined by the number of interactions that occur between incident photons and matter per unit length of material. The energy absorption coefficient, however, refers to the amount of energy dissipated by the secondary electrons set in motion as a result of these interactions. Since energy dissipated can be equated to energy absorbed, μ_{en} is more

appropriate for dosimetry.

For this study, μ_{en} will be obtained from tables in Johns(2) and in practice applied to each of the gamma type decay energies of the particular radioisotope.

B. General Dose Equation

The simpliest case for the calculation of dose to a region is a situation involving an equilibrium distribution (7), i.e. where the energy absorbed per gram is in equilibrium with the energy emitted per gram. The equilibrium absorbed dose is then

$$D_{eq} = 2.13\left(\sum_i n_i \overline{E_i}\right)\int_0^\infty C(t)\,dt \quad \text{rad} \qquad [5]$$

The integral of C(t)dt over all time is defined as the cumulative concentration, $\tilde{C}$, and has units of μCi-hr/g. $\overline{E_i}\ n_i$ has units of MeV per disintegration and accounts for the fractional amount of a specific decay energy per disintegration. The constant 2.13 is obtained from

$$1.602 \times 10^{-6}\left(\frac{\text{erg}}{\text{MeV}}\right) \times 10^{-2}\left(\frac{\text{rad}}{\text{erg/g}}\right) \times 3.70 \times 10^{4}\left(\frac{\text{dis/sec}}{\mu\text{Ci}}\right) \times 3.60 \times 10^{3}\left(\frac{\text{sec}}{\text{hr}}\right)$$

and has units of $\frac{\text{g-rad-dis}}{\mu\text{Ci-hr-MeV}}$. Equation 5 may be rewritten as

$$D_{eq} = \tilde{C}\sum_i \Delta_i \quad \text{rad} \qquad [6]$$

Where

$$\Delta_i = 2.13\, n_i \overline{E}_i \quad \frac{\text{g-rad}}{\mu\text{Ci-hr}} \qquad [7]$$

Equation 6 is valid for uniformly-distributed radionuclides in a finite homogeneous material, provided boundary effects are negligible. Boundary effects do become significant when the isotope is a gamma emitter. To account for geometrical considerations, Loevinger and Berman have included an absorbed fraction term in their method of dosimetry. It is briefly defined here for the i th type of radiation as the energy absorbed in target volume v from source region r divided by the energy emitted by source region r. Symbolically represented as ϕ_i, the absorbed fraction is analogous to the geometrical factor $\overline{g}$, except that energy dependence is implicit, and newer methods of computation exist.

The energy emitted by source region r is given by

$$U_r = \tilde{A}_r \Delta_i \quad \text{g-rad} \qquad [8]$$

where

$$\tilde{A} = \int_{t_1}^{t_2} A(t)\, dt \quad \mu\text{Ci-hr} \qquad [9]$$

is the cumulative activity, and Δ_i is the equilibrium dose constant in $\frac{\text{g-rad}}{\mu\text{Ci-hr}}$. The energy absorbed in target volume v is given by

$$U_{(v \leftarrow r)} = m_v \overline{D}_i(v \leftarrow r) \quad \text{g-rad} \qquad [10]$$

Therefore,

$$\phi_i(v \leftarrow r) = \frac{m_v \bar{D}_i(v \leftarrow r)}{\tilde{A}_r \Delta_i} \qquad [11]$$

The specific absorbed fraction is given by

$$\bar{\Phi}_i(v \leftarrow r) = \frac{\phi_i(v \leftarrow r)}{m_v} \quad g^{-1} \qquad [12]$$

Using these relationships, a general dose equation can be written as

$$\bar{D}(r_1 \leftarrow r_2) = \tilde{A}_2 \sum_i \Delta_i \bar{\Phi}_i(r_1 \leftarrow r_2) \text{ rad} \qquad [13]$$

This is the dose to a region r_1 from a region r_2 and is the basic MIRD dose equation: It has no limitations on size or composition of source and target regions. Equation 13 allows dosage to be calculated directly in rads, and as previously mentioned, $\bar{\Phi}_i$ provides more accuracy over $\bar{g}$.

The remainder of this study will be concerned with the special but common case where source organ and target organ are identical. Equation 13 then becomes

$$\bar{D}(v \leftrightarrow v) = \tilde{A}_v \sum_i \Delta_i \bar{\Phi}_i(v \leftrightarrow v) \quad \text{rad} \qquad [14]$$

Values for the equilibrium dose constant, Δ_i, are obtain from Dillman (9) and are listed in Appendix A along with the decay schemes of most clinically used radioisotopes.

Appendix B lists values of ϕ_i computed by

Brownell et al. (10), and Ellett and Humes (11). These values were calculated by utilizing the Monte Carlo technique of photon diffusion. More will be said shortly about other methods of calculating specific absorbed fraction. The values of ϕ_i are given for several specific organ configurations which are usually encountered clinically.

C. The Specific Absorbed Fraction, Φ_i

The calculation of absorbed fractions for finite media is greatly facilitated by the use of Monte Carlo techniques. In the work done by Brownell et al. (10) and Ellett et al. (12), (13), the path of a single gamma ray is traced through an absorbing medium with probability functions used to determine the individual events.

In the Monte Carlo program, the initial direction of a photon is determined through a random number generator. This effectively simulates an isotropic source. The distance traversed by the photon is determined by sampling the exponential probability distribution, as a function of photon energy. Since the program includes photoelectric, Compton and total cross sections, a probability of interaction can also be sampled. Photoelectric interaction terminates the photon transport, while Compton interaction would be governed by a Klein-Nishina scattering distribution. Histories of the pho-

tons are thus recorded, and absorbed fractions calculated.

Prior to successful machine photon diffusion techniques, absorbed fractions for a uniform isotropic model could still be calculated directly from the point function (7). Considering an infinite uniform absorber, the distribution of absorbed energy about an isotropic point source is a function of distance from the source and can be expressed as a fraction of emitted energy absorbed per gram. This is called the point isotropic specific absorbed fraction, $\Phi_{ph}(x)$.

$$\Phi_{ph}(x) = \frac{\mu_{en} e^{-\mu x}}{\rho 4\pi x^2} \cdot B_{en}(\mu x) \quad g^{-1} \qquad [15]$$

The quantity $\frac{\mu_{en} e^{-\mu x}}{\rho 4\pi x^2}$ accounts for energy absorbed from the primary photons: $\frac{e^{-\mu x}}{4\pi x^2}$ is the point kernel, and $\frac{\mu_{en}}{\rho}$ is the mass energy absorption coefficient. The factor $B_{en}(\mu x)$ is the point isotropic energy-absorption buildup factor and accounts for the effect of the scattered photons.

Assuming that

$$B_{en}(\mu x) e^{-\mu x} = e^{-\mu_{eff} x} = e^{-\mu_{en} x} \qquad [16]$$

equation 15 becomes

$$\Phi_{ph}(x) = \frac{\mu_{en}}{\rho 4\pi x^2} e^{-\mu_{en} x} \quad g^{-1} \qquad [17]$$

The absorbed fraction ϕ can be obtained from geometrical factors g_p and $\bar{g}$ by extention of the above point

function.

$$\Phi_{ph}(x) m_v = \frac{\mu_{en}}{4\pi} \int_V \frac{e^{-\mu_{en} x}}{x^2} dV \qquad [18]$$

$$\Phi_{ph}(x) m_v = \frac{\mu_{en}}{4\pi} g_p$$

since

$$g_p = \int_V \frac{e^{-\mu_{en} r}}{r^2} dV \qquad [4]$$

The absorbed fraction then becomes

$$\phi_{ph}(v \leftarrow r) = \frac{\mu_{en}}{4\pi} g(r \leftarrow v) \qquad [19]$$

For the purposes of this study, where target and source are identical and the activity is uniformly distributed throughout the tissue,

$$\phi = \frac{\mu_{en}}{4\pi} \bar{g} \qquad [20]$$

where $\bar{g}$ is given in cm, and ϕ, as expected, becomes unitless.

Monte Carlo type calculations are preferred over an analytical approach, and extensive tables of specific absorbed factions and absorbed fractions computed by Monte Carlo methods exist (12), (13), (10), (11). Several important tables are listed in Appendix B. The geometry of the growth plate in children, however, does not appear to have been considered in the Monte Carlo approach to absorbed fraction. Calculations for "disc" geometry must

therefore be done using analytical data from Focht (6) Loevinger (1), and Widman (4).

Widman et al. (4) have provided a table of absorbed fractions for cylinders containing a uniformly distributed source which may be extrapolated to solve the problem of disc geometry. Table 1 and figure 1 give the absorbed fractions as a function of cylinder height (H) and radius (R) and also mean free path (μR). As pointed out, ϕ includes energy dependence; therefore, the use of table 1 is to be preferred over the geometrical factor calculations of Focht (6) and Loevinger (1).

Figure 2 shows the model used by Widman to analytically solve for absorbed fractions. A cylinder of radius R and height H contains a uniformly distributed gamma-ray source of intensity τ energy emitted per unit volume.

U = energy absorbed

ϕ = ratio of absorbed energy to emitted energy

μ = linear absorption coefficient

dU = energy absorbed in volume dV from energy emitted by source dV'

$$= \frac{\mu\tau}{4\pi} \frac{e^{-\mu r}}{r^2} dV\, dV' \qquad [21]$$

then

$$U = \frac{\mu\tau}{4\pi} \int dV \int \frac{e^{-\mu r}}{r^2} dV' \qquad [22]$$

TABLE I: ABSORPTION FRACTION (Cylinders)

μR \ H/R	0.2	0.3	0.5	0.7	1.0	1.5	2	3	5	7	10	15	20	100	∞
7.0	.652	.730	.804	.840	.866	.887	.897								
5.0	.568	.651	.739	.783	.818	.846	.860	.872							.901
4.0	.511	.595	.689	.738	.779	.810	.827	.843	.854						.877
3.0	.438	.520	.616	.671	.718	.757	.777	.797	.813						.837
2.0	.342	.415	.508	.564	.617	.663	.688	.712	.733	.743	.747				.764
1.5	.281	.346	.431	.485	.537	.585	.613	.641	.665	.674	.680				.698
1.0	.208	.259	.330	.377	.425	.471	.500	.530	.554	.565	.575	.580	.582		.593
0.7	.156	.196	.253	.293	.333	.375	.401	.430	.455	.467	.474	.482	.486		.494
0.5	.117	.148	.193	.225	.258	.294	.317	.342	.366	.376	.385	.392	.396		.404
0.4	.096	.122	.160	.187	.216	.247	.267	.290	.313	.323	.331	.336	.340		.348
0.3	.074	.094	.124	.146	.169	.194	.211	.231	.250	.260	.267	.273	.275		.284
0.2	.051	.065	.086	.101	.118	.137	.149	.164	.180	.186	.193	.198	.201	.207	.207
0.15	.038	.049	.066	.077	.090	.105	.115	.127	.140	.146	.150	.155	.158	.162	.163
0.10	.026	.033	.045	.053	.062	.072	.079	.088	.096	.101	.105	.108	.110	.115	.115
0.07	.018	.024	.032	.037	.044	.051	.056	.063	.069	.073	.076	.078	.079	.082	.083
0.05	.013	.017	.023	.027	.032	.037	.041	.045	.050	.053	.055	.057	.058	.061	.061
0.04	.011	.014	.018	.022	.025	.030	.033	.037	.041	.043	.044	.046	.047	.050	.050
0.03	.008	.010	.014	.016	.019	.022	.025	.028	.031	.032	.034	.035	.036	.038	.038
0.02	.005	.007	.009	.011	.013	.015	.017	.019	.021	.022	.023	.023	.024	.026	.026

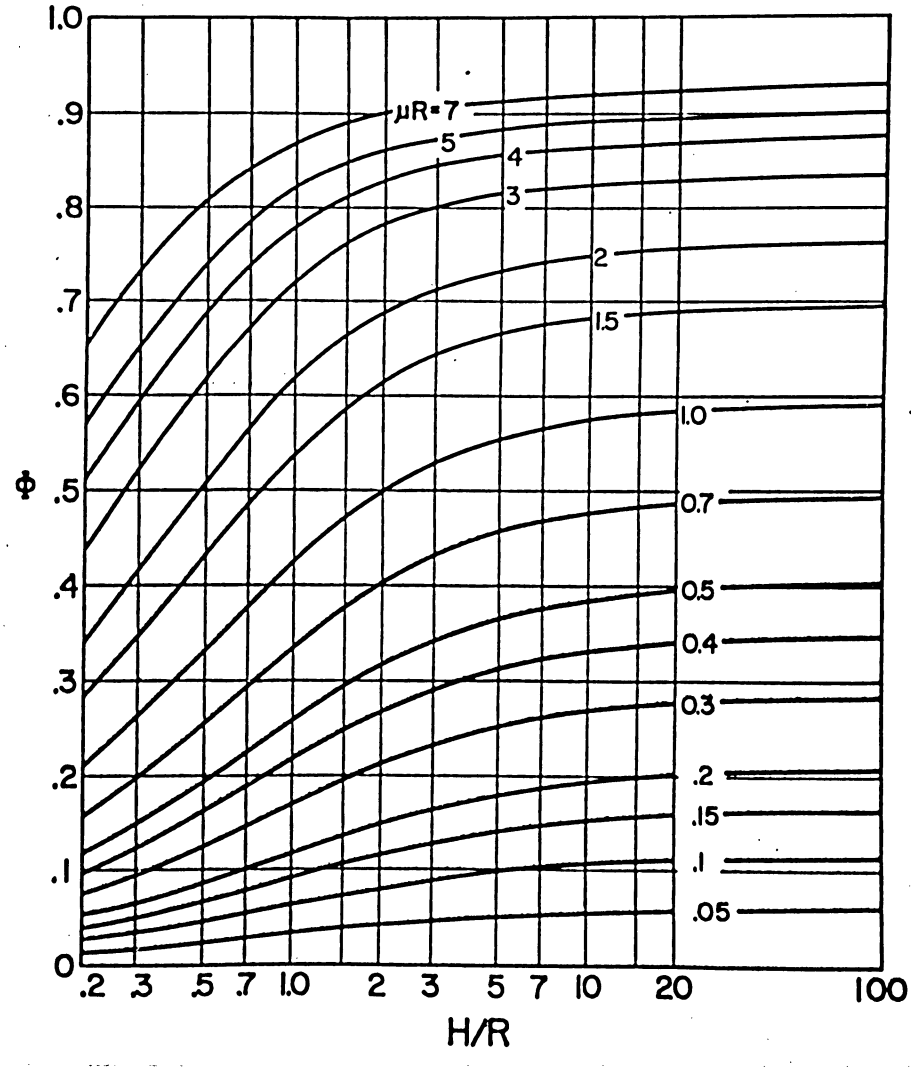

FIGURE 1: Absorbed fractions for various cylinders and mean free paths (4)

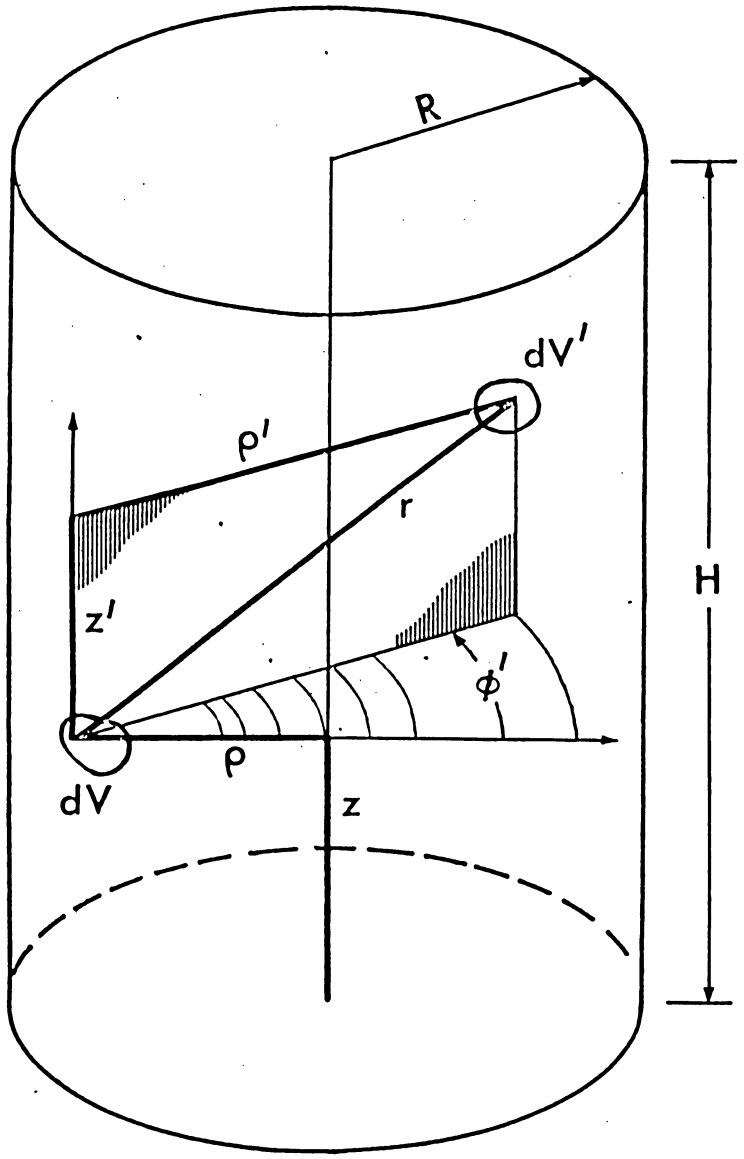

FIGURE 2: Cylinder containing a uniformly distributed gamma emitter (4)

and

$$\phi = \frac{\mu}{4\pi^2 R^2 H} \int dV \int \frac{e^{-\mu r}}{r^2} dV' \qquad [23]$$

since the total emitted energy is given by $\pi R^2 H \tau$.

As was also previously noted, the linear absorption coefficient μ should be replaced by the absorber density ρ times the mass energy attenuation coefficient μ_{en}/ρ.

Table 2 gives the $\bar{g}$ values determined by Focht et al. (6) based upon a linear absorption coefficient of .028. Table 3 gives the results of absorbed fraction calculations based upon Widman's approach compared to the $\bar{g}$ factor approach. For purposes of this comparison, a cylinder height of 1 cm is assumed, and the radius is varied between 1 and 5 cm. The linear absorption coefficient is assumed to be .028. Equation 20 is used to compute absorbed fractions from geometrical factors.

As seen from table 3, agreement rapidly diminishes for low values of $\bar{g}$, but is generally quite good for higher $\bar{g}$ values. This trend was also reported by Widman et al (4) and is unexplainable.

The specific case to be considered in this study is epiphyseal growth plate in children: the distal head of the femur, and proximal head of the tibia and fibula. The geometry is basically that of a disc. Absorbed fractions will be calculated by extrapolation of table 1

TABLE 2

AVERAGE GEOMETRICAL FACTOR, $\bar{g}$, FOR CYLINDERS CONTAINING A UNIFORMLY DISTRIBUTED γ-RAY EMITTER

(μ = 0.028)

Length of Cylinder (cm)	Radius of Cylinder (cm)										
	1	2	3	5	7	10	15	20	25	30	35
1	3.8	7.5	10.2	13.0	13.5	13.8	15.1	16.0	17.5	18.0	19.0
2	6.5	11.7	15.7	21.6	23.2	25.2	28.1	30.5	32.8	35.4	37.3
3	8.4	14.7	19.8	27.7	31.0	34.5	39.2	42.9	46.5	49.5	52.5
5	10.6	18.8	25.6	36.0	42.4	48.5	56.1	62.6	68.2	73.0	77.2
7	11.6	21.4	29.3	41.4	50.0	59.0	68.7	77.8	84.7	90.2	93.8
10	12.7	23.6	33.0	47.1	57.8	70.2	83.2	94.0	103	109	113
15	13.7	25.6	36.4	53.2	66.1	81.4	99.7	113	123	130	135
20	14.2	26.7	38.0	56.3	72.2	89.6	111	127	139	147	152
30	14.5	27.6	39.7	59.9	76.8	98.8	124	144	159	172	179
40	14.8	28.2	40.7	62.4	80.0	103	133	156	175	187	197
50	14.8	28.4	41.3	64.1	82.2	106	139	165	185	199	208
60	14.8	28.7	41.7	65.5	84.0	109	143	171	193	206	216
70	14.8	28.8	41.9	65.6	85.3	111	146	174	196	212	222
80	14.8	28.8	42.1	65.8	86.0	112	148	176	198	214	226
90	14.8	28.9	42.3	66.0	86.5	113	149	177	199	216	228
100	14.8	29.2	42.5	66.2	86.8	114	150	179	201	218	230

Table 3

ϕ from Widman Versus Calculated ϕ by $\bar{g}$ Approach (μ= .028, H = 1 cm)

Radius (cm)	μR	H/R	$\bar{g}$	ϕ Widman	ϕ Geom	Difference
1	.028	1.0	3.8	.018	.008	+ 125%
2	.056	.50	7.5	.026	.017	+ 53%
3	.084	.33	10.2	.030	.023	+ 30%
4	.112	.25	11.6	.033	.026	+ 27%
5	.140	.20	13.0	.036	.029	+ 24%
30	.84	.33*	109	.237	.243	- 2%

* H = 10cm

and will be limited to technetium-99m decay energies.

Figure 3a shows the various aspects of epiphyseal bone, in particular the distal femur. Figure 3b is a scintigram of the anterior left knee of a child, approximately 24 hours post injection, and readily shows the increased uptake of the growth plates. Johnson has described this area as one of the most rapidly growing growth plates in the body (14). For a two year old child, he has reported a growth plate thickness of 2 mm. Trueta has recorded thicknesses between 2.5 mm and 3.5 mm in a ten year old child (15). For the absorbed fraction determinations which follow, a growth plate thickness of 3.0 mm will be assumed. Disc radii from 1 to 5 cm will be included in this study, although Johnson (14) has pointed out that the distal growth plate does show accelerated growth on the medial side, and in fact the medial-lateral growth rate per year may be twice that of the anterior-posterior growth rate.

The calculation of absorbed fraction for disc geometry with a uniform distribution of ^{99m}Tc requires a knowledge of the mean free path for each of the decay energies of electromagnetic radiation from technetium. Appendix A shows the decay of ^{99m}Tc; the penetrating energies of concern are:

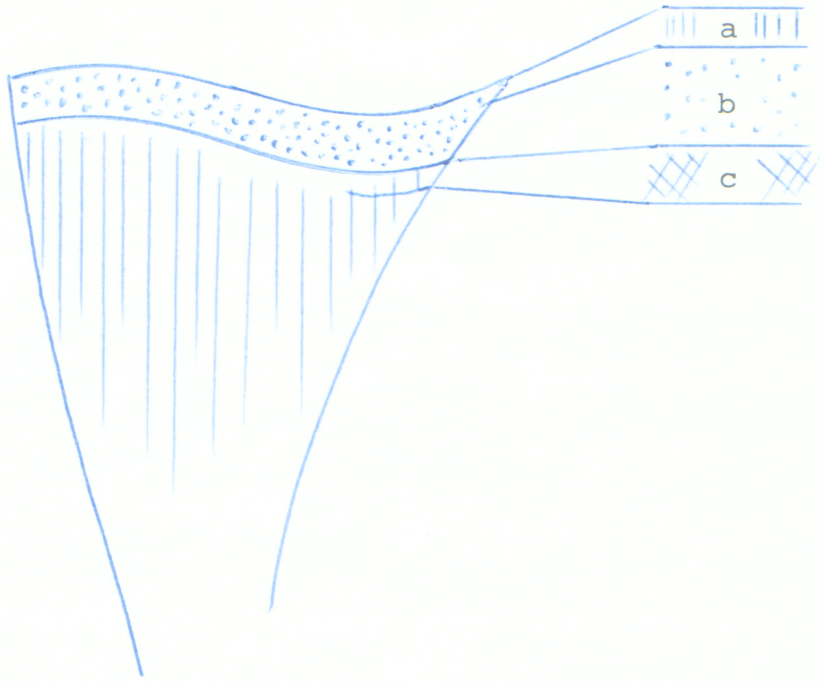

Zones:

a. Hyaline (resting cartilage)

b. Translucent (active cellular cartilage)

c. Bright pink (capillary brush border)

FIGURE 3a: Growth plate complex of the distal femur (14)

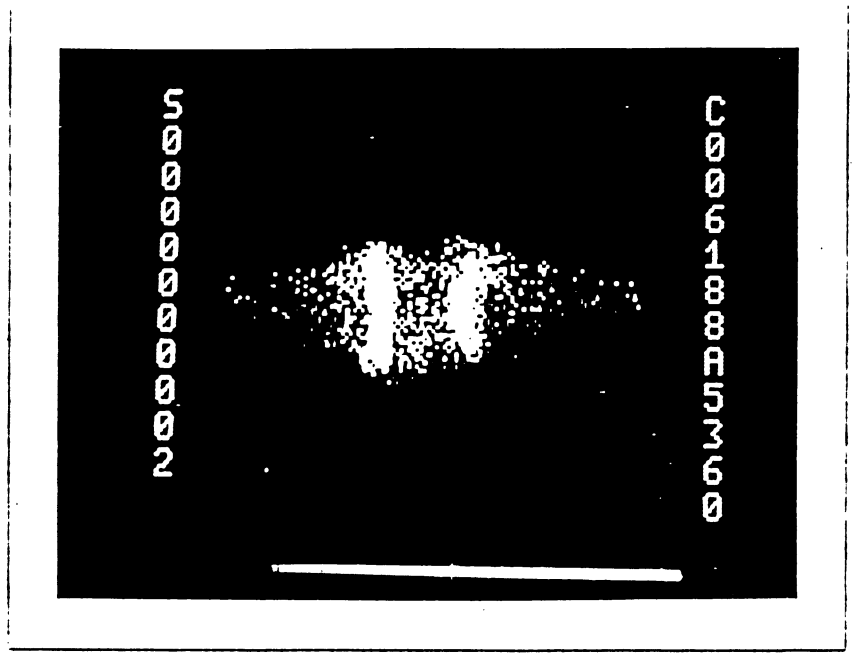

FIGURE 3b: Scintigram of anterior left knee, approximately 24 hours post injection

.1405 MeV
.1426 MeV
.0183 MeV
.0182 MeV
.0206 MeV

The energy absorption coefficient, μ_{en}, for each of these energies can be obtained from Johns (2). Calculations can be greatly simplified by assuming a growth plate density comparable to muscle or water. Evans has reported on the dry specimen density of human cancellous bone (16). Densities vary over a wide range, depending upon age and sex. An average density appears to be 0.7 g/cc. Since the epiphyses have only a thin outer layer of dense compact bone (hyaline cartilage) and are otherwise constructed of porous, marrow filled cancellous bone (17), a density of 1.0 seems to be a good approximation.

Figure 4 is a graph of the energy absorption coefficient (cm^{-1}) versus photon energy (MeV) for an absorber having a density of 1.0. Values of μ_{en} corresponding to the decay energies of ^{99m}Tc can be found in table 4.

Figures 5 and 6 present an extrapolation of Widman's absorbed fractions to include flat discs. These curves should be verified by Monte Carlo techniques. Table 5 gives ϕ_i for each decay energy of interest as a function of mean free path and radius for a standard disc height of 3 mm. For conversion electrons, Auger electrons, K fluorescent radiation from material with a Z less than

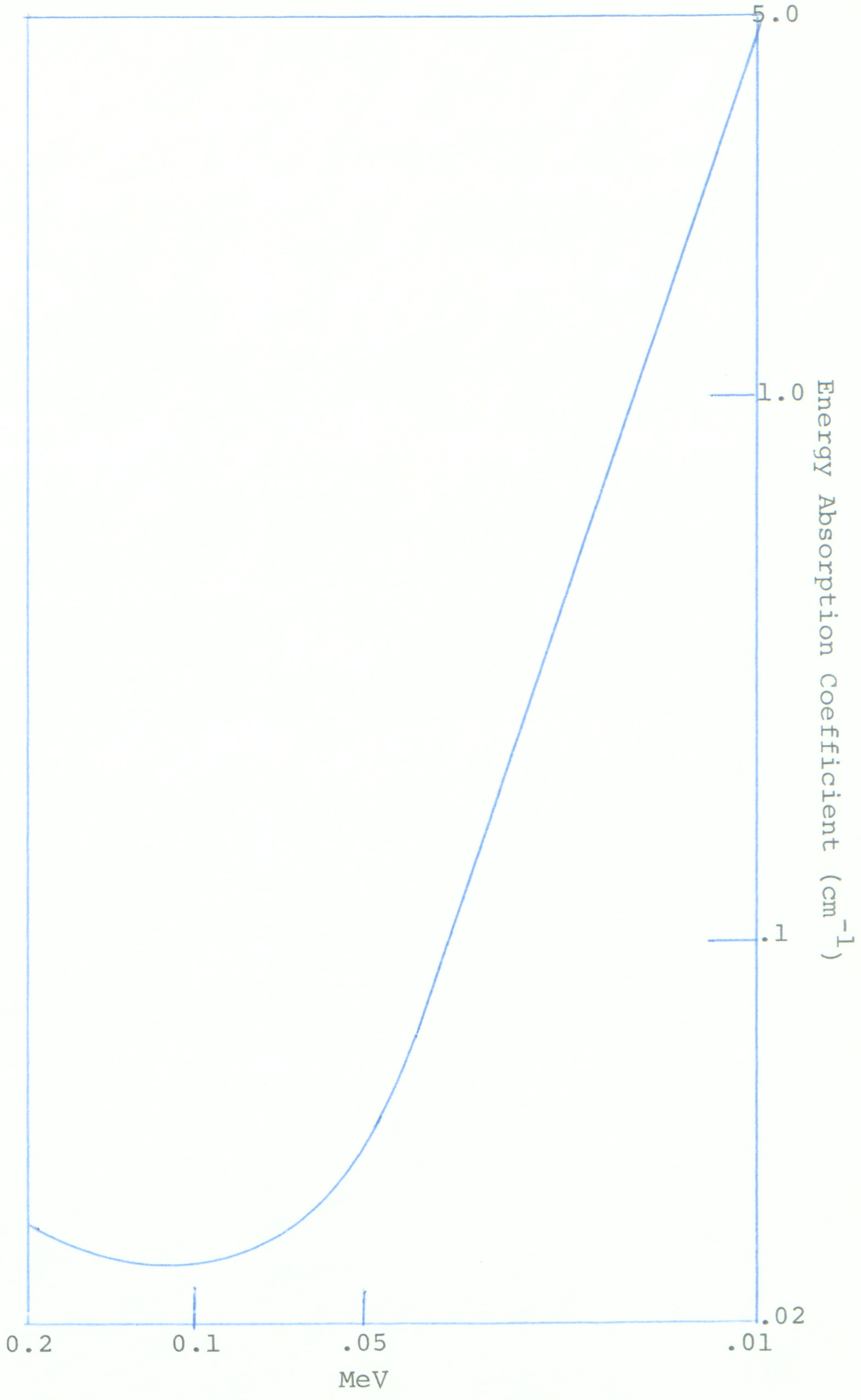

FIGURE 4: Energy absorption coefficient versus photon energy for a unit density absorber. (2)

Table 4

μ_{en} for Tc-99m decay energies of interest.

Energy (MeV)	μ_{en} (cm^{-1})
.1405	.027
.1426	.027
.0183	.72
.0182	.72
.0206	.50

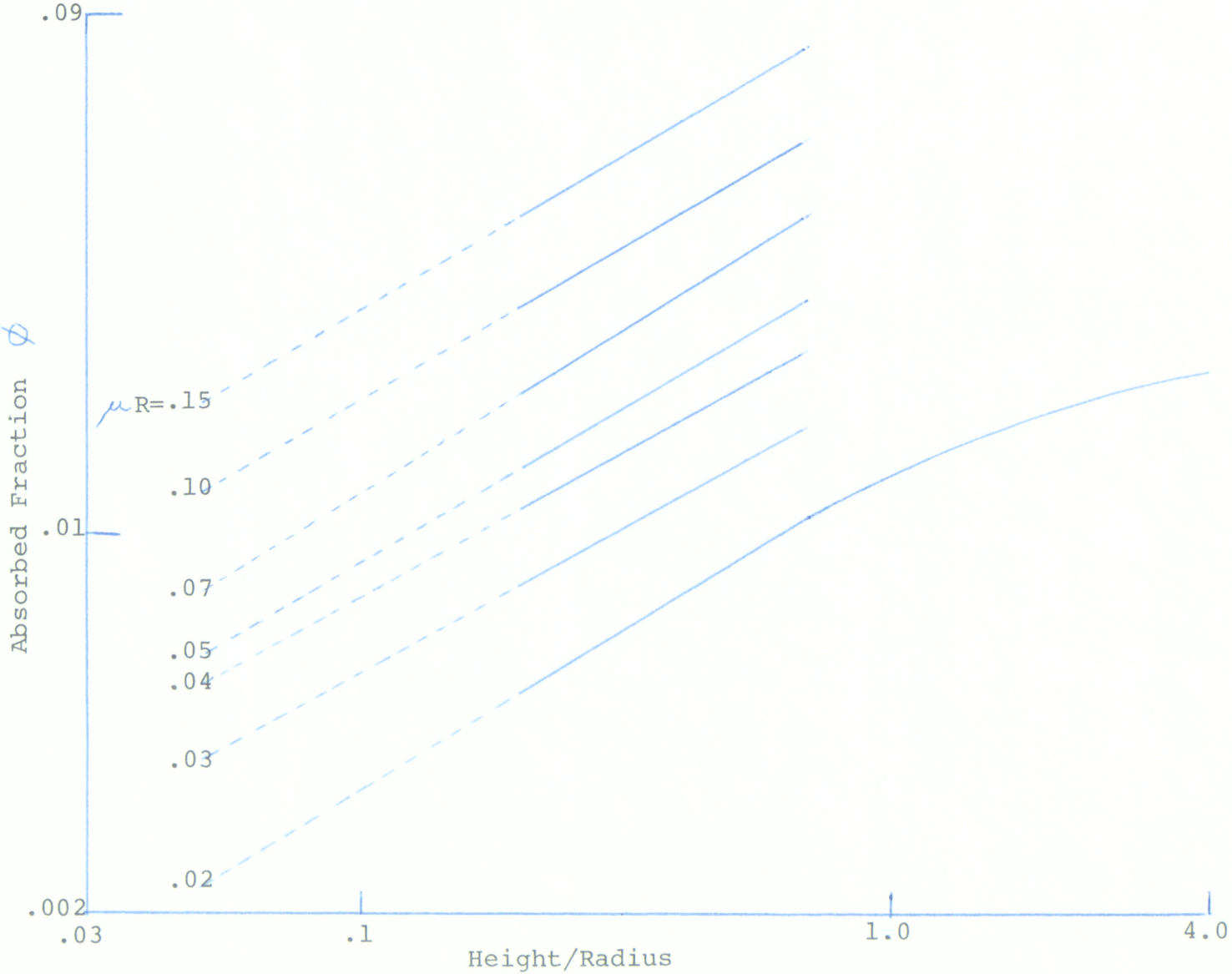

FIGURE 5: Absorbed fractions for cylinders (4)

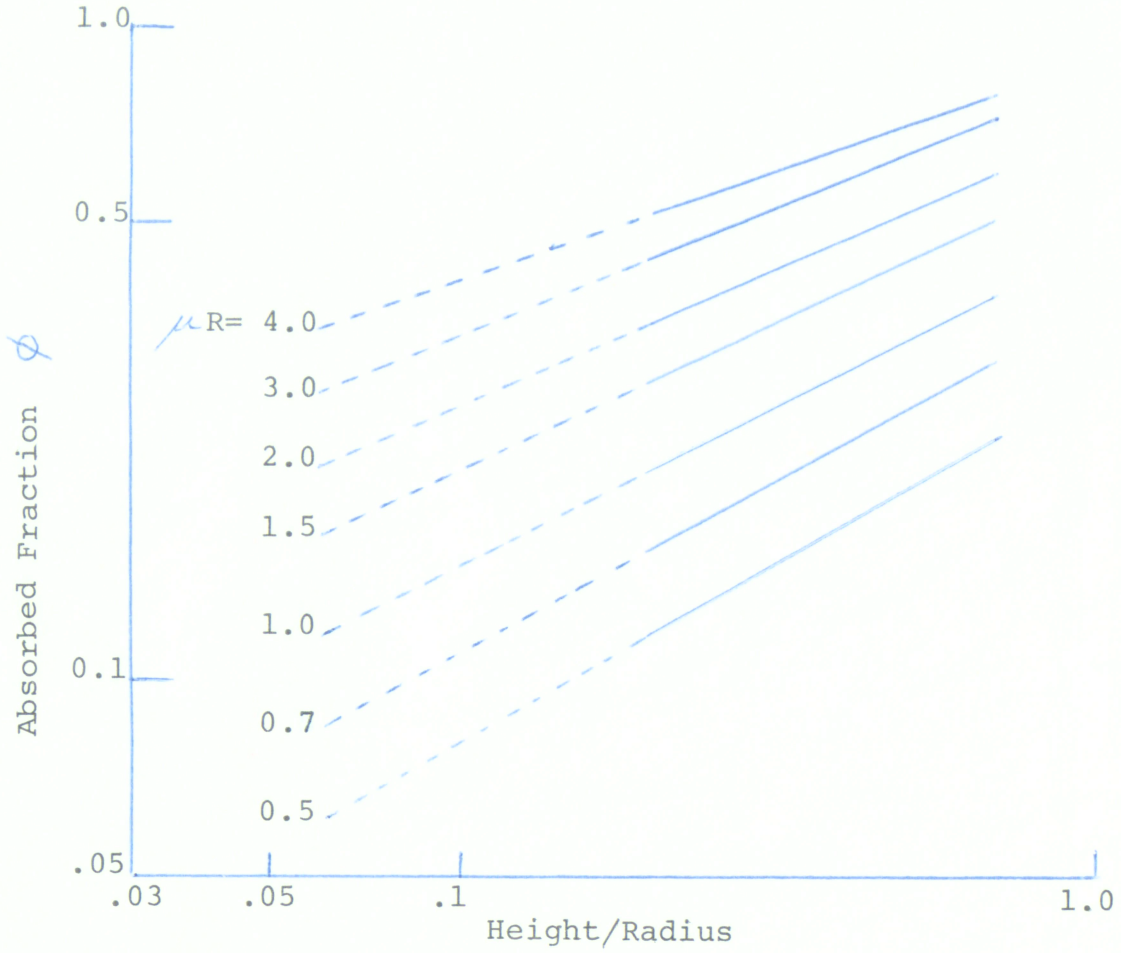

FIGURE 6: Absorbed fractions for cylinders (4)

Table 5

ϕ_i as f (R, μen) H = 3 mm

^{99m}Tc decay energy	Radius (cm)	H/R	μR	ϕ_i
.1405	1	.3	.027	.009
	2	.15	.054	.012
	3	.10	.081	.014
	4	.075	.108	.016
	5	.06	.135	.017
.1426	1	.3	.027	.009
	2	.15	.054	.012
	3	.10	.081	.014
	4	.075	.108	.016
	5	.06	.135	.017
.0183	1	.3	.72	.205
	2	.15	1.44	.235
	3	.10	2.16	.270
	4	.075	2.88	.290
	5	.06	3.6	.310
.0182	1	.3	.72	.205
	2	.15	1.44	.235
	3	.10	2.16	.270
	4	.075	2.88	.290
	5	.06	3.6	.310
.0206	1	.3	.50	.148
	2	.15	1.0	.180
	3	.10	1.5	.210
	4	.075	2.0	.230
	5	.06	2.5	.240

35, and all electromagnetic radiations below 11 keV, the absorbed fraction equals 1.0 (2), (18). Finally, table 6 summarizes the absorbed fractions for each radius to be used in a later calculation.

The density of the epiphyseal plates has been approximated as 1.0; cases do exist however, where the density of the tissue of interest cannot be assumed to be that of muscle or water. In these cases, Brownell et al. have formulated a scaling rule (10): the value of absorbed fraction corresponding to a mass m in a unit density medium will correspond to a mass m/ρ^2 in a medium of density ρ. Likewise, a conversion exists for materials of differing electron density: if a new material has n electrons/g, and the reference has n_o (3.308×10^{23} electrons/g), a table entry refering to mass m of the reference will refer to mass $\left(\frac{n_o}{n}\right)^3 (m)$ of the new material. The above rules apply to the tables in Appendix B.

The geometry of the epiphyseal plates must be considered a worse possible case to obtain absorbed fraction data on. The majority of dosimetry in nuclear medicine is performed upon well defined organs. The tables in Appendix B lend themselves well to the situation of target organ-source organ identical. For improved accuracy, self dose plus dosage received from other tissues in the body need to be considered. To perform these sophisticated calculations, Snyder et al. developed

Table 6

Summary of ϕ_i

Decay energy	Radius (cm) 1	2	3	4	5
.1405 MeV	.009	.012	.014	.016	.017
.1426	.009	.012	.014	.016	.017
.0183	.205	.235	.270	.290	.310
.0182	.205	.235	.270	.290	.310
.0206	.148	.180	.210	.230	.240

a reference man computer code, and ran Monte Carlo type computations to obtain data essential to the solution of target organ-source organ different (19), (20). The question of dosimetry in pediatric nuclear medicine, however, remained unanswered by the reference man concept.

Kereiakes et al. warned of the inaccuracies of extrapolating pediatric data from adult data (21) and urged the establishment of a series of standard children. Fisher and Snyder reported on the design of six phantoms corresponding to ages 0 (newborn), 1-, 5-, 10-, 15-, and 20 years (22). These phantoms were obtained by isotropically "shrinking" the head, trunk and legs of the Reference Man by a factor thought to be representative of the particular age group under study. Although a good approximation, these phantoms did not consider changes in organ shape with age. Hwang et al. noted that the physiological geometry of a child is diferent than that of an adult (22), and proceeded to develop phantoms for children one and five years of age from current biological data. Jones et al. have similarly developed a fifteen year old standard phantom (24). The phantoms developed by Jones and Hwang are adaptable to Monte Carlo calculations and data useful for calculating dosage is presented in their reports.

To simplify the presentation of data collected from such phantom work, the concept of absorbed dose per unit

cumulated activity has been developed and has been given the name "S factor". This factor will be described in the next section, and a calculation will be done on the unusual disc geometry presented in this study.

The "S" Factor

Snyder et al. have advocated the use of an "S factor" to facilitate dose calculations (20), (25). S has the units of rads per microcurie-hour, and is defined as

$$S(r_k \leftarrow r_h) = \sum_i \Delta_i \Phi_i (r_k \leftarrow r_h)$$

$$= \frac{\sum_i \Delta_i \Phi_i (r_k \leftarrow r_h)}{m_k} \quad \frac{\text{rad}}{\mu\text{Ci-hr}} \qquad [24]$$

where r_k and r_h refer to target organ and source organ, respectively. The general dose equation formulated by the MIRD Committee

$$\bar{D}(r_1 \leftarrow r_2) = \tilde{A} \sum_i \Delta_i \bar{\Phi}_i (r_1 \leftarrow r_2) \quad \text{rad} \qquad [13]$$

can then be re-written as

$$\bar{D}(r_k \leftarrow r_h) = \tilde{A}_h S(r_k \leftarrow r_h) \quad \text{rad} \qquad [25]$$

If there are a number of source organs to be considered, the total average dose to target organ r_k is given by

$$\bar{D}(r_k) = \sum \bar{D}(r_k \leftarrow r_h)$$

$$= \sum_h \tilde{A}_h S(r_k \leftarrow r_h) \quad \text{rad} \qquad [26]$$

Most of the biological data necessary for estimating dose is included in the cumulated activity $\tilde{A}_h$. S consists of quantities which are unique for a specific radionuclide and a specific target-source combination: it can therefore be determined without prior knowledge of radionuclide distribution.

In the calculation of S it is again assumed that the isotope is uniformly distributed in the source organ. The equilibrium dose constants are obtained from Appendix A, and the absorbed fractions from Appendix B. While S has been calculated for the revised MIRD adult phantom (25) and for several standard children based on ^{99m}Tc decay energies, the S factors presented in this study can be used in pediatric dosimetry for target organ-source organ identical and for the following radionuclides: ^{99m}Tc, ^{125}I, ^{131}I, ^{123}I, ^{127}Xe, ^{133}Xe, ^{169}Yt, ^{201}Tl, ^{11}C, ^{75}Se, ^{57}Co, ^{59}Fe, ^{67}Ga, ^{45}Ca, ^{51}Cr, ^{43}K, ^{111}In, ^{129}Cs, and ^{113m}In.

The determination of the S factors was simplified by writing a Fortran IV computer program, a listing of which appears in Appendix C. The program is general, only the data cards containing the equilibrium dose constants and the decay energies of the particular radionuclide need to be changed for each run. The six specific organ shapes included in the program are given below. All organ shapes, unless otherwise specified, are assumed

to be imbedded in a scattering medium. The values of S are given in Appendix D, and also appear in reference (36).

Mass	Shape
1-100 grams	Small unit density spheres (axes ratios 1:1:1)
	Small unit density ellipsoids (axes ratios 1:2:4)
	Small unit density ellipsoids (axes ratios 1:3:8)
300-6000 grams	Small unit density spheres and thick ellipsoids (axes ratios 1:1:1 and 1:0.667:1.333)
	Unit density flat ellipsoids (axes ratios 1:0.5:2.0)
2000-140,000 grams	Unit density ellipsoids (axes ratios 1:1.8:9.27)

Before performing S factor calculations on the epiphyseal plates of interest, it is necessary to consider the mass of each disc. Masses may be calculated from a knowledge of the volume and density of each plate. Volume is given by $\pi R^2 H cm^3$ where H is constant at .3 cm. Since the density is close to 1.0 for these growth plates, mass can be calculated and appears below.

Raduis (cm)	Volume cm^3	Mass g
1	0.94	0.94
2	3.77	3.77
3	8.48	8.48
4	15.08	15.08
5	23.56	23.56

Data from Appendix A, table 6, and the mass values above are used in the S calculation which appears in Appendix E. Results appropriate for use with ^{99m}Tc appear in table 7. Values listed in table 7 follow the general trend of values obtained from Monte Carlo data for absorbed fraction, i.e. decreasing for an increase in mass. Comparing table 7 with S factors listed for ellipsoids, axes ratio 1:3:8 (Appendix D), gives the following:

Mass (g)	S Disc	S Ellipsoid
.94	.042	.042
3.77	.011	.01164
8.48	.005	.00512
15.08	.003	.00329
23.56	.002	.00206

The S factors for the ellipsoid are calculated from Monte Carlo data. S factors for the discs appear to be good estimates.

In the general dose equation for internally administered radionuclides, $\tilde{A}$, the cumulated activity, accounts for the biological actions of the administered drug, as opposed to the S factor, which can be determined without any knowledge of the biological system under study. Cumulated activity is a function of uptake and elimination, and may very well be the most difficult term of the dose equation to obtain. The next section will describe some methods of estimating $\tilde{A}$.

Table 7

S Factors for Discs, ^{99m}Tc Energies

Radius (cm)	S (rad/μCi-hr)
1	.042
2	.011
3	.005
4	.003
5	.002

$\tilde{A}$-Cumulated Activity

The cumulated activity, $\tilde{A}$, is related to the activity A by

$$\tilde{A} = \int_{t_1}^{t_2} A(t)\,dt \qquad \mu\text{Ci-hr} \qquad [9]$$

The activity A(t) in an organ or tissue depends upon such factors as: the amount of administered activity, the site and rate of intake, rate of biological uptake and removal and the physical decay of the radionuclide. MIRD Pamphlet 1 (7) introduced the concept of a distribution factor q(t) which in this paper will be defined as the fractional amount of the administered radionuclide in a region at any time t. Therefore,

$$A(t) = A(0)\,e^{-\lambda t}\,q(t) \qquad \mu\text{Ci} \qquad [27]$$

where

A(o) = the initial activity of the radionuclide (μCi)

λ = the physical decay constant

In actuality, the biological decay may not follow an exponential, and q(t) may have to be expressed as the sum of a number of exponential components (7)

$$q(t) = \sum_j q_j\,e^{-\lambda_j t} \qquad [28]$$

where the λ_j's are the biological decay constants. Curve fitting programs, or a method of orthogonal polynomials with significance testing for "lack of fit", would have to be employed to determine the values of q_j and λ_j in the power series expansion.

Substituting equation 28 into equation 27 yields

$$A(t) = A(0)e^{-\lambda t}\sum_j q_j e^{-\lambda_j t}$$

$$= A(0)\sum_j q_j e^{-[\lambda+\lambda_j]t} \qquad [29]$$

Equation 9 then becomes

$$\tilde{A} = \int_{t_1}^{t_2} A(0)\sum_j q_j e^{-[\lambda+\lambda_j]t}\, dt$$

$$= A(0)\sum_j q_j \int_{t_1}^{t_2} e^{-[\lambda+\lambda_j]t}\, dt$$

$$= A(0)\sum_j \frac{q_j}{\lambda+\lambda_j}\left(1-e^{-[\lambda+\lambda_j]t}\right)\Bigg|_{t_1}^{t_2} \qquad [30]$$

Taking $t_1 = 0$, and $t_2 = \infty$

$$\tilde{A}_\infty = A(0)\sum_j \frac{q_j}{\lambda+\lambda_j} \ \mu\text{Ci-hr} \qquad [31]$$

Adapting the notation of Kereiakes et al. (26), and substituting an effective half-life for $\lambda+\lambda_j$, equation 31 can be re-written as

$$\tilde{A}_\infty = 1.44\, T_{1/2(\text{eff})}\sum_j A_j(0) \ \mu\text{Ci-hr} \qquad [32]$$

where

$A_j(0)$ = the activity (μCi) at t=0 of the j^{th} component with j^{th} biological half-time measured in hours.

When A(t) can be approximated by a straight line on semi-log paper, the cumulated activity in the source organ can be given by

$$\tilde{A}_\infty = 1.44\, T_{1/2(eff)}\, A'(0) \quad \mu\text{Ci-hr} \qquad [33]$$

where

A'(0) = activity (μCi) obtained by extrapolation to t = 0

and $T_{1/2(eff)}$ corresponds to the time at which

$$A(t) = 1/2\ A'(0)$$

Kereiakes et al. (26) also presented a method of computing $\tilde{A}_\infty$ with a high degree of accuracy. A numerical integration can be carried out over A(t); this would make no assumptions about the number of exponential components and their rate constants and would include all cases where uptake time is significant. Using the trapezoidal rule results in

$$\tilde{A}_\infty = \frac{1}{2}\sum_{j=1}^{n=1}(A_j + A_{j+1})(t_{j+1} - t_j) + 1.44\, A_n\, T_p \quad \mu\text{Ci-hr} \qquad [34]$$

where

A_j = activity (μCi) measured at $t=t_j$

A_n = activity (μCi) at the time of the last measurement (t_n)

T_p = physical half-life (hrs) of the radionuclide

Cumulated activity for various radiopharmaceuticals in children were calculated by Kereiakes et al. (27) from in vivo measurements and appear in Appendix F. These values differ from cumulated activities published by Webster et al. (28), which were obtained from estimates of the uptake and effective half-life of radiopharmaceuticals in normal adults and animals. Application of adult data to children should be done with caution until more data from children can be obtained.

Thomas et al. (29) have described a method for determining lesion activity which appears to be adaptable to the problem of obtaining meaningful cumulated activities in children. Their method involves external counting techniques utilizing a "calibrated" gamma camera and an associated computer system. This method will specifically be applied to quantitating the activity in the growth plates of the knee in children.

Combined Transmission-Emission Counting

A. Introduction

The approximate method of extrapolating A'(0) or the more exact method of integrating A(t) both require that the radioactivity within the organ or tissue be quantitated. Such measurements would also be useful in evaluating organ uptake, organ function, and total body retention and turnover of various elements.

Sorenson (30) has reviewed three such methods for quantitatively estimating radioactivity in patients by external gamma-ray counting techniques: a) combined transmission-emission method, b) ratioing of Compton to photopeak counts, and c) the dual-isotope method. The transmission-emission method, also known as conjugate view counting,was adapted by Thomas et al. (29) in their clinical studies and will be applied here to quantitating the activity in the growth plate. This method is particularly useful with gamma type cameras which are interfaced with dedicated mini-computers.

Two general sources of error in all <u>in vivo</u> counting are: a) distance effects, and b) attenuation and scatter effects. The sensitivity of some collimator-detector systems depends strongly on the distance from the source to the detector. A way to minimize this geometric effect (in essence inverse square fall-off) is to use a large array of detectors, or a detector whose surface area is

much larger than the region to be counted. This is an approximation to 2π counting geometry, and should result in fairly constant counts for activity located anywhere within the counting area for a practical range of source to collimator distances, assuming no attenuation. The gamma camera easily supplies this type of geometry. Distance effects will be evaluated in the experimental stage.

Attenuation, however, will vary with differences in source depth and patient thickness. Genna (31) and Ben-Haim and Dudley (32) have shown the geometric mean of conjugate counting measurements to be approximately independent of source depth while dependent upon total patient thickness. Total patient thickness, as will be shown, can be calculated from a knowledge of the linear attenuation coefficient, or simply measured with calipers.

Another factor to be corrected for is the source distribution itself, when not assumed to be a point source. Most internally administered radionuclides will result in volume distributions, and source attenuation and source thickness will have to be considered. A general approach to deriving a correction factor will be presented for the simple yet widely applicable case of a rectangular volume distribution.

B. Conjugate Counting of Point Sources

Figure 7 shows a point source of radioactivity located at a depth d in a patient of thickness T. The collimator of the gamma camera is located beneath the patient, N_{PA} being the number of counts recorded in the PA view, at a distance C from the table. Letting d=0 be a reference point, a relationship must be found between N_{PA} and N_o, the number of counts that would be obtained if the same source were placed in air at d=0.

The relationship between N_{PA} and N_o involves both distance and attenuation. Attenuation is accounted for by

$$N_{PA} = N_a e^{-\mu d} \qquad [35]$$

where

μ = linear attenuation coefficient (cm^{-1})

N_a = number of counts recorded from the same source in air, at a distance d from the reference point.

For a straight bore or stationary, small detector, N_a and N_o are related by the inverse square law. For the gamma camera, however, the solid angle of detection changes little with distance; therefore $N_a/N_o \sim 1$, and

$$N_{PA} = N_o e^{-\mu d} \qquad [36]$$

For the AP counting situation,

$$N_{AP} = N_o e^{-\mu (T-d)} \qquad [37]$$

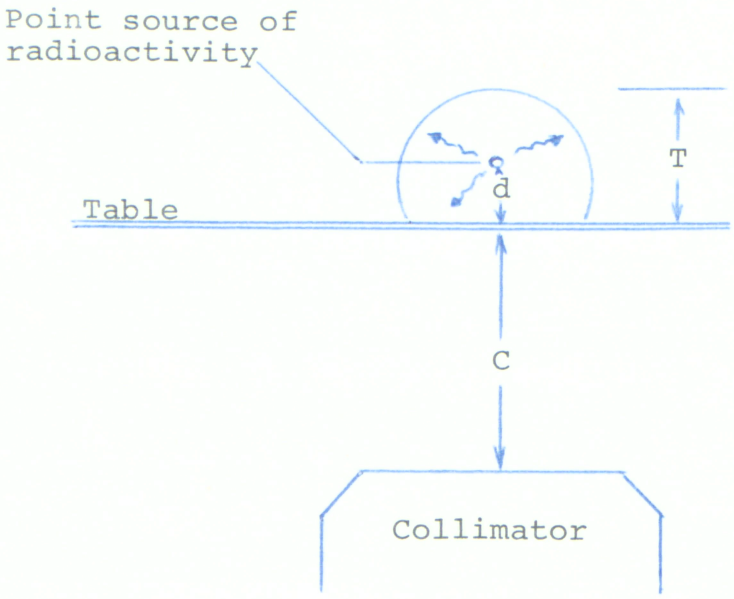

FIGURE 7: Point source of radioactivity in a patient.

Multiplying equation 36 and 37 gives

$$(N_{PA})(N_{AP}) = (N_o)^2 e^{-\mu(T-d+d)}$$

$$\left[(N_{PA})(N_{AP})\right]^{1/2} = N_o e^{-\mu T/2}$$

$$N_o = \left(\frac{N_{PA} N_{AP}}{e^{-\mu T}}\right)^{1/2} \qquad [38]$$

Equation 38 clearly points out the advantage of using a geometric mean: total counts of the source depends upon total thickness and is independent of source position. The overall accuracy of equation 38 depends primarly on the assumptions that a) the source is a point, and b) $N_a = N_o$. For volume sources, equation 38 must be modified.

C. Effects of Source Distribution

Figure 8 shows a uniform volume source imbedded in a scattering medium. The source occupies a fraction, f, of the total patient thickness, T. Let

d = depth of source (cm)

N_o = counts that would be recorded from the same amount of activity concentrated at the reference point (d=o)

x = vertical distance from the table

Then

$\left(\frac{N_o}{fT}\right)$ dx = counts corresponding to a thin layer dx located at the reference point.

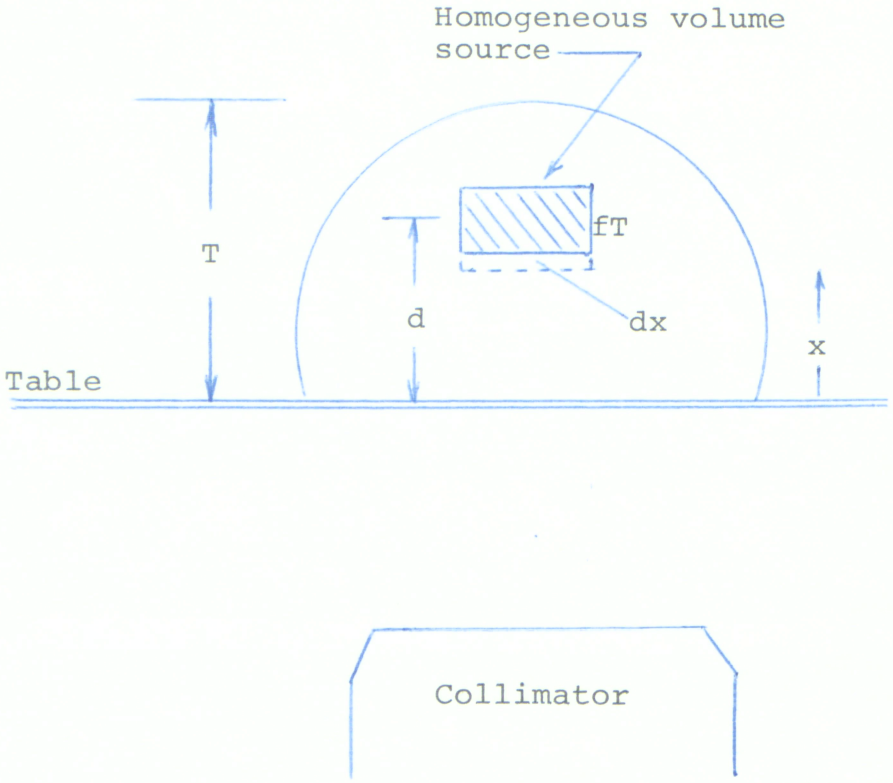

FIGURE 8: Uniform volume source imbedded in a scattering medium.

When dx is places at some depth x,

$$dN_{PA} = \left[\frac{N_o}{fT}\,dx\right] e^{-\mu x} \qquad [39]$$

and the total counts obtained from PA counting would be

$$N_{PA} = \int_{SOURCE} dN_{PA}$$

If the center of the homogeneous source was placed at d,

$$N_{PA} = \int_{d-\frac{fT}{2}}^{d+\frac{fT}{2}} \frac{N_o}{fT} e^{-\mu x}\,dx$$

$$= \frac{N_o}{fT\mu}\left[-e^{-\mu x}\right]_{d-\frac{fT}{2}}^{d+\frac{fT}{2}}$$

$$= \frac{N_o}{fT\mu} e^{-\mu d}\left[e^{fT\mu/2} - e^{-fT\mu/2}\right]$$

$$= \frac{2N_o e^{-\mu d}}{fT\mu} \sinh\frac{fT\mu}{2} \qquad [40]$$

Likewise, for the AP counting,

$$N_{AP} = \frac{2N_o e^{-\mu(T-d)}}{fT\mu} \sinh\frac{fT\mu}{2} \qquad [41]$$

Obtaining the geometric mean of equations 40 and 41 results in

$$(N_{PA})(N_{AP}) = \left(\frac{2N_o}{fT\mu}\right)^2 e^{-\mu T}\left(\sinh\frac{fT\mu}{2}\right)^2$$

or

$$N_o = \left(\frac{N_{PA}N_{AP}}{e^{-\mu T}}\right)^{1/2} \times \frac{fT\mu}{\sinh\frac{fT\mu}{2}} \qquad [42]$$

Letting

$$\frac{\frac{fT\mu}{2}}{\sinh\frac{fT\mu}{2}} \equiv \text{correction factor } f_j$$

and introducing a calibration factor, C (Counts per μCi-min),

$$A_j = \left(\frac{I_{AP}I_{PA}}{e^{-\mu T}}\right)^{1/2} \times \frac{f_j}{C} \qquad [43]$$

where A_j (μCi) is the activity of the source and I_{AP} and I_{PA} are the respective intensities in counts per minute. Equation 43 is a general form of the equation Thomas et al. (29) obtained for quantitating lesion activity, and will suffice for quantitating the activity of the epiphyseal plates.

The term $e^{-\mu T}$ is the transmission through the total thickness and is directly obtained from the patient by taking transmission measurements across the region of

interest: $$e^{-\mu T} = \frac{I}{I_o}$$

where

I = transmitted intensity (cpm)

I_o = standard source intensity (cpm)

then

$$\mu T = \ln \frac{I_o}{I} \qquad [44]$$

Equation 44 may be helpful in evaluating either the linear attenuation coefficient or the thickness of the region of interest, if unknown or not measureable.

The correction factor, f_j, of equation 43 should normally be used; for the specific case of the growth plates, which have a thickness of 3mm and do not appear to lie directly in line with the collimator openenings,

$$f_j = \frac{\frac{1}{2} T\mu/2}{\sinh \frac{1}{2} T\mu/2} \sim 1$$

when μ is approximately that of water or muscle.

D. Summary

The conjugate view counting method described above will yield two important parameters useful in applying the MIRD general dose equation

$$D(r_1 \leftarrow r_2) = \tilde{A}_2 \sum_i \Delta_i \Phi_i(r_1 \leftarrow r_2) \text{ rad} \qquad [13]$$

$$\overline{D}(r_k \leftarrow r_h) = \tilde{A}_h S(r_k \leftarrow r_h) \quad \text{rad} \qquad [25]$$

where

$$\tilde{A} = 1.44\, T_{1/2}(\text{eff})\, A'(0) \quad \mu\text{Ci-hr} \qquad [33]$$

The effective half-life, $T_{1/2\ (\text{eff})}$, and the activity at t=0 (A'(o)) are directly obtainable from conjugate view counting. In practice, the activity at several times e.g. 0, 5, 10, 15 hrs, etc., is quantitated and plotted on semi-log paper. A'(0) can then be extrapolated if the uptake time is assumed negligible compared to the elimination time.

Experimental

A. Introduction

Dosage to the epiphysis of the knee area in two children was determined. The Ohio-Nuclear Gamma Camera and associated DataSystem 150 Computer System at the Children's Hospital of Cincinnati were used for the measurements of cumulated activity. The collimator was a high resolution type, 140 keV peak energy. In both cases, patients received ^{99m}Tc-EHDP bone scanning agent.

Prior consideration was given to: a) the effect of distance (source to collimator) on the total number of counts, b) obtaining a calibration factor, i.e. counts per μCi-min. and c) the transmission factor. In addition, it was determined that in the realm of clinical studies, the counts per channel would not exceed 256, for 16K of memory. These settings allowed for maximum resolution of the epiphyseal plates.

Information on each child, along with source calibration, background and transmission data, was stored on consecutive frames on data tape. Thus, studies could be reviewed at the most convient times. Tape storage is essential to obtain enough data to construct uptake and elimination curves. Data from ^{75}Se L-selenomethionine, for example, would probably need to be collected over 6 months. For the ^{99m}Tc-EHDP studies in this report, data was collected over a 25 hour time span.

B. Source to Collimator Distance Effect

One of the underlying assumptions in the use of equation 43 for quantitating in vivo activity is that the total counts obtained by the imaging system is independent of source to collimator distance over a "practical" range. The range used in this study was 3 cm to 12 cm source to collimator distance. Total counts obtained with varying distance are listed in table 8. Table 9 shows the results of a one way ANOVA on the data of table 8. At $\alpha = .05$, $p > .25$. Equation 43 may therefore be used, with $f_j = 1$, and calibration and transmission factors to be presented in the following sections.

C. Calibration Factor, C

The calibration factor, C $\left(\frac{\text{counts}}{\mu\text{Ci-min}}\right)$ must be determined for each time that the activity, A_j, is to be determined. The standard source, composed of the isotope under study, must a) be of the least thickness as practicable, so that self-absorption is negligible; b) be of sufficient strength to obtain good counting statistics, yet not saturate the data storage capacity of the computer system (256 counts per channel); and c) preferably contain an area approximately equal to the area of tissue or organ to be counted.

Table 8

Standard Counts Versus Source to Collimator Distance, Children's Hospital, Ohio Nuclear Gamma Camera

Distance (cm)						
3	4	5	6	8	10	12
1432	1471	1377	1369	1410	1399	1343
1350	1449	1460	1390	1426	1411	1373
1369	1362	1453				
		1480				
		1440				
		1418				
		1348				

Table 9

Results of One-Way ANOVA on Standard Counts Versus Source to Collimator Distance (Table 8)

Effect	df	SS	MS
Distances	6	11,729	1955
Error	14	24,740	1767
Totals	20	36,469	

$$F_{6,14} = \frac{1955}{1767} = 1.11$$

$$F_{.05,(6,14)} = 2.85$$

Conclusion: distance effect not significant, $P > .25$

One standard can be used throughout the 25 hour time span needed to quantitate ^{99m} Tc-EHDP activity. Calibration factors for each child are given in the data summary tables 10 and 11 based on time post injection. Standard activity can be determined from dose-calibrator measurements, or calculated from the initial activity by use of the decay law, $N=N_o e^{-\lambda t}$.

Background was found to be negligible while obtaining a calibration factor. Standard counts varied from approximately 1300 per 100 channels (1 min) to 7000 per 100 channels (1 min), while background counts for 1 min varied from 1 to 10 per 150 channels interrogated.

D. Transmission Factor, J

The transmission factor is given in equation 43 as $e^{-\mu T}$, where T is the total thickness of the patient across the area of interest, and μ is the effective attenuation coefficient. In practice, J is determined from the ratio of the transmitted counts through the area, divided by the unattenuated counts from the sample.

$$e^{-\mu T} = \frac{I}{I_o} \qquad [44]$$

I_o is simply obtained by counting the standard. I is determined by counting the standard through the area of interest. Since only counts originating from the

standard are to be counted, activity already in the area under study must be subtracted during the measurement of I. Counts taken over the area with no external sources of radiation present are used for this purpose. Tables 10 and 11 show the results of the transmission measurements.

A useful check on the counting method is obtained by a knowledge of total thickness through the area under study. When the thickness T is known, μ can be evaluated from equation 44. The attenuation coefficient should not vary greatly from patient to patient; in this study of the epiphyses of the knee, μ was found to be 0.16 cm^{-1} for both the right and left knees of both children.

E. Conjugate View Counting

Having obtained a calibration factor and a transmission factor, the area of interest must be counted by taking two conjugate views. An AP and a PA were the best methods of counting over the knee areas in this study. Using the "joystick" option on the Data System 150, one may obtain integral counts for any area interrogated. Again, background was found to be negligible.

The growth plate of the knee is qualitatively the most active area of the knee in children who receive ^{99m}Tc-EHDP bone scans. The plate is, however, surrounded by activity in the epiphyses and shafts of the long bones

which may contribute a significant number of counts to the counts obtained over the plate area if the area interrogated is large. An attempt must therefore be made during the counting of the plate to confine the area strictly to that of the highest activity. The results of the AP and PA growth plate counting are given in the patient data summary, tables 10 and 11.

Relative activity within the growth plate has been plotted in figures 9 and 10 for each child. A regression line appears through these points, determined by a Wang exponential least square fit program. The results for the two children under study appear in table 12. Cumulated activity can then be calculated from $T_{1/2\ (eff)}$ and A'(0), and these results appear in tables 13 and 14 for the four growth plates counted. $T_{1/2(eff)}$ can be calculated using equation 4 and the equation of the regression line.

F. Scaling Factor

Since dosage to the growth plates is a function of their physical dimensions, plate diameter must be estimated from available information on the patient. A method for determining plate diameter from the scintigram was evaluated, and a satisfactory "scale factor" was found.

Using a cobalt-57 line source and the high-resolution collimator, varying lengths of line source were imaged on the Ohio-Nuclear Camera and DataSystem 150

Table 10

Patient data for T.S., 4 year old male, 35 lbs. weight.

Received 2.66 mCi ^{99m}Tc-EHDP at time of injection.

A. Calibration Factors

Time post injection (hr)	Standard activity (μCi)	Standard* counts/min	avg. Cal. factor cts/μCi-min
.23	40.5	5982	142
.68	38.5	5269	
4.20	25.0	3456	138
10.43	12.75	1693	
10.77	12.3	1719	140
10.80	12.2	1334	
23.83	32.4**	4558	140

B. Transmission Factors

1. Rt. knee
   Thickness = 6.5 cm
   Source alone = 3692/1 min
   Source through knee = 2870/2 min
   Knee alone = 216/2 min

   μ = 0.16 cm $^{-1}$

2. Lt. knee
   Thickness = 7.0 cm
   Source alone = 3876/1 min
   Source through knee = 2674/2 min
   Knee alone = 226/2 min

   μ = 0.16 cm^{-1}

*based on 100 channels. Counts were also obtained for 150 channels and the average calibration factor adjusted slightly higher as a better estimate of the true source.

**new standard

C. Summary of Conjugate Counts and Activities (T.S.)

$$\left[\frac{I_{AP}I_{PA}}{T}\right]^{1/2} \times \frac{1}{C}$$

Time Post Injection (hrs) (avg)*	Anterior (cts/min)**	Posterior (cts/min)**	Cal. factor (cts/μCi-min)	T=0.36 (μCi)	Relative
1. Rt. Knee - Distal Femur					
.37	2166	2018	142	24.5	0.99
4.47	2281	1855	138	24.8	1.00
10.6	1097	850	140	11.5	0.46
25.16	175	160	140	2.0	0.08
2. Rt. Knee - Proximal Tibia & Fibula					
.37	1525	1392	142	17.1	1.29
4.47	1195	1025	138	13.4	1.00
10.6	577	455	140	6.1	0.45
25.16	102	99	140	1.2	0.09

C. (T.S.)

Time Post Injection (hrs) (avg)*	Anterior (cts/min)**	Posterior (cts/min)**	Cal. factor (cts/μCi-min)	$\left[\frac{I_{AP}I_{PA}}{T}\right]^{1/2} \times \frac{1}{C}$ T=0.32 (μCi)	Relative
3. Lt. Knee - Distal Femur					
.41	2300	2500	142	29.9	1.08
4.46	2350	2000	138	27.8	1.00
10.6	1150	1050	140	13.9	0.50
25.3	190	185	140	2.4	0.09
4. Lt. Knee - Proximal Tibia & Fibula					
.42	1650	1560	142	20.0	1.20
4.46	1400	1200	138	16.6	1.00
10.6	650	500	140	7.2	0.43
25.3	130	95	140	1.4	0.08

* Average, based on anterior and posterior times

** Adjusted, may be slightly higher than "hottest" area depending upon counts obtained from area slightly larger than "hottest"

Table 11

Patient data for J.S., 13 year old male, 80 lbs. Received 10.96 mCi ^{99m}Tc-EHDP at time of injection.

A. Calibration Factors

Time Post injection (hrs)	Standard activity (μCi)	Standard counts/min	avg. Cal. Factor cts/μCi-min
.43	38.5	6368	
.35	34.9	6157	170 ± 6
3.05	26.0	4658	179
8.27	14.0	2346	
8.30	13.9	2276	166 ± 2
22.82	44.7	3880/.5	
22.83		3681/.5	170 ± 5

B. Transmission Factors

1. Rt. Knee
   Thickness = 9.25 cm
   Source alone = 4335/.5 min
   Source through knee = 2328/1 min
   Knee alone = 853/2 min

   $\mu = 0.16\ cm^{-1}$

2. Lt. Knee
   Thickness = 9.5 cm
   Source alone = 3687/.5 min
   Source through knee = 2122/1 min
   Knee alone = 905/2 min

   $\mu = 0.16\ cm^{-1}$

C. Summary of Conjugate Counts and Activities (J.S.)

$$\left[\frac{I_{AP}I_{PA}}{T}\right]^{1/2} \times \frac{1}{C}$$

Time Post Injection (hrs) (avg)*	Anterior (cts/min)**	Posterior (cts/min)**	Cal. factor (cts/μCi-min)	T=0.22 (μCi)	Relative
1. Rt. Knee - Distal Femur					
0.25 ± .05	4900	2800	170 ± 6	46.5	0.56
3.3	8000	6000	179	82.5	1.00
8.5	4100	3250	166 ± 2	46.9	0.57
23.1	575	500	170 ± 5	6.7	0.08
2. Rt. Knee - Proximal Tibia & Fibula					
0.25 ± .05	3350	2350	170 ± 6	35.2	0.63
3.3	5500	4000	179	55.9	1.00
8.5	2850	1700	166 ± 2	28.3	0.51
23.1	450	350	170 ± 2	5.0	0.09

*

** See notes, table 10

C. (J.S.)

$$\left[\frac{I_{AP} I_{PA}}{T}\right]^{1/2} \times \frac{1}{C}$$

$T = 0.23$

Time Post Injection (hrs) (avg)*	Anterior (cts/min)**	Posterior (cts/min)**	Cal. factor (cts/μCi-min)	(μCi)	Relative
3. Lt. Knee - Distal Fermur					
0.12 ± .04	2600	2600	170 ± 6	31.9	0.38
3.22	8000	6500	179	84.0	1.00
8.5	4350	3250	166 ± 2	47.2	0.56
23.05 ± .15	575	525	170 ± 5	6.7	0.08
4. Lt. Knee - Proximal Tibia & Fibula					
0.12 ± .04	1700	1950	170 ± 6	22.3	0.43
3.22	5750	3450	179	51.9	1.00
8.5	3000	2000	166 ± 2	30.8	0.59
23.05 ± .15	450	275	170 ± 5	4.3	0.08

*
**} See notes, table 10

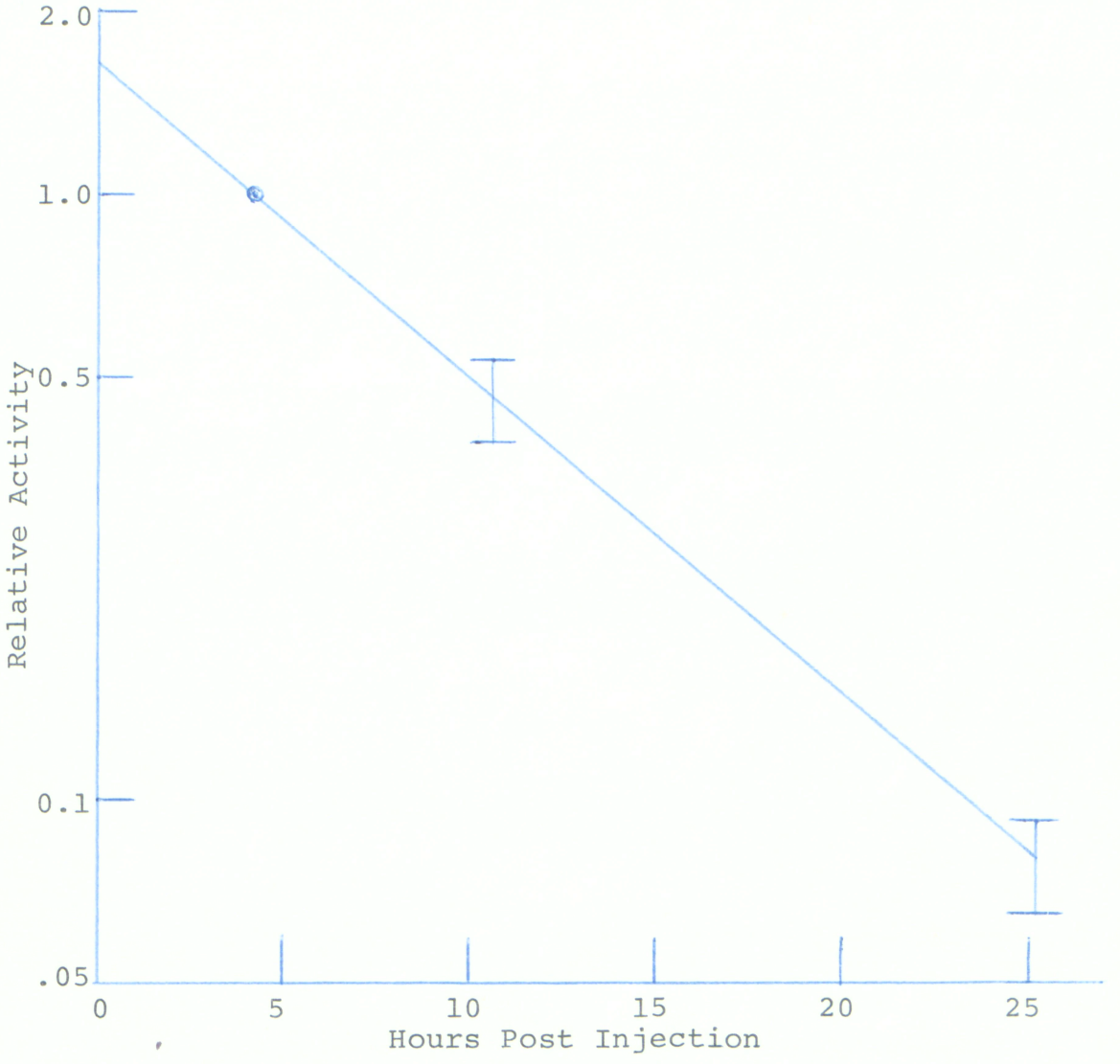

FIGURE 9: Relative activity for the growth plates of the knee, patient T.S. Activities of the right and left distal femurs and proximal tibias and fibulas have been normalized to 1.0 at 4.47 hours. Error bars denote 3 standard deviations.

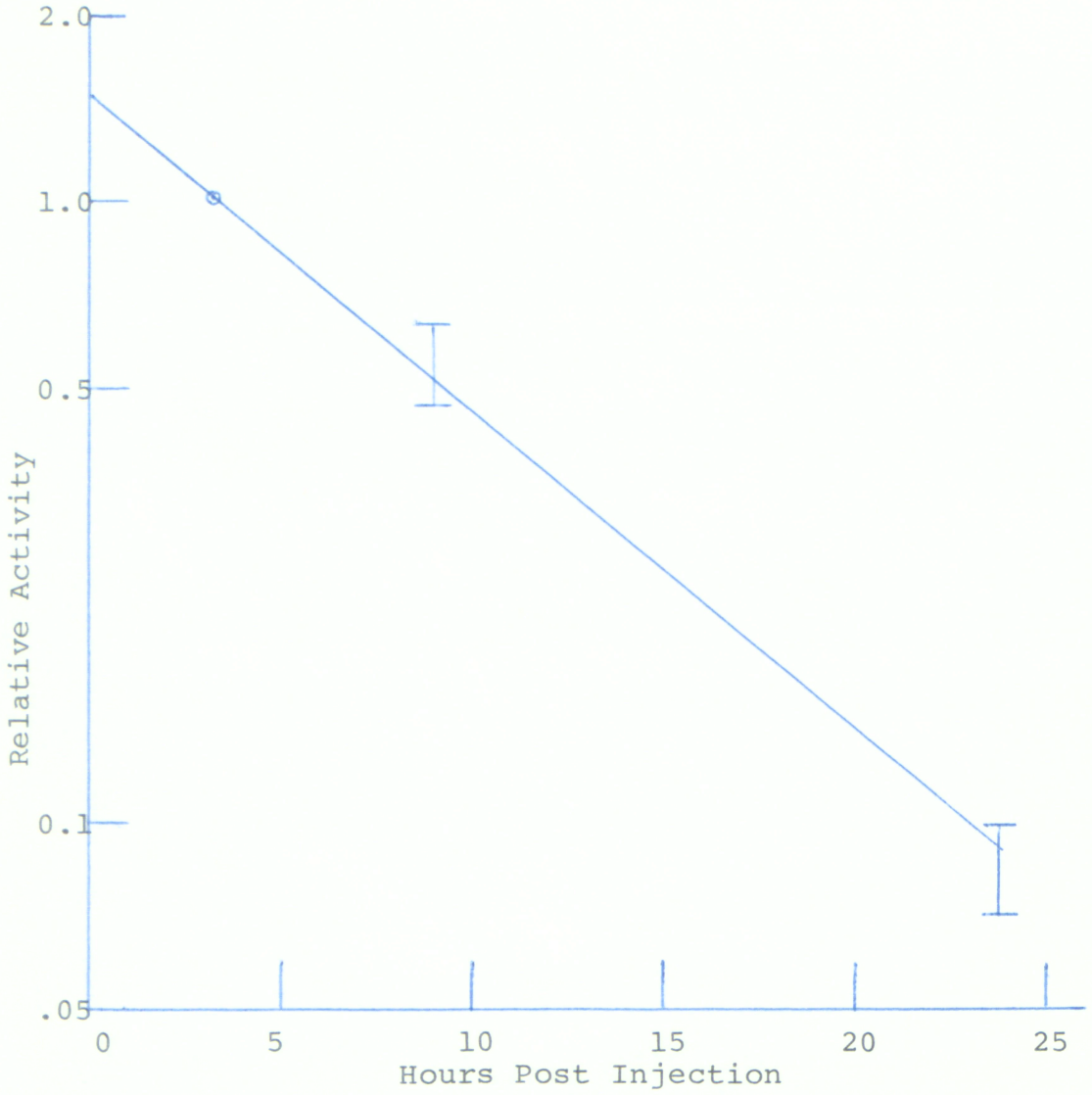

FIGURE 10: Relative activity for the growth plates of the knee, patient J.S. Activities of the right and left distal femurs and proximal tibias and fibulas have been normalized to 1.0 at 3.26 hours. Error bars denote 3 standard deviations.

Table 12

TS	JS
b = -.12	b = -.13
a = 1.66	a = 1.57
r = -.999	r = -.999

General equation of regression line:

$$A = ae^{bt}$$

Table 13

Summary of Parameters Obtained from Conjugate View Counting for Two Children

Child	Parameter	Area: Right Distal Femur	Right Proximal Tibia, Fibula	Left Distal Femur	Left Proximal Tibia, Fibula
T.S.	A'(o) μCi	41.2	22.2	46.1	27.6
	$T_{1/2(eff)}$ hr	5.8	from regression →		
	$\tilde{A}_\infty$ μCi-hr	344	185	385	231
J.S.	A'(o) μCi	129.5	87.8	131.9	81.5
	$T_{1/2(eff)}$ hr	5.3	from regression →		
	$\tilde{A}_\infty$ μCi-hr	988	670	1007	622

Table 14

Dosage to the Growth Plate Complex for Two Children

Child	Area	Disc Diameter (cm)	Dose (rads)
T.S.	right distal femur	4.6	3.1
	right proximal tibia, fibula	3.8	2.6
	left distal femur	4.8	3.1
	left proximal tibia, fibula	3.9	3.2
J.S.	right distal femur	5.8	4.9
	right proximal tibia, fibula	4.8	5.4
	left distal femur	5.9	5.0
	left proximal tibia, fibula	4.9	5.0

at the Children's Hospital and the number of channels counted. The experiment was also designed to measure the effects of different thicknesses of tissue equivalent absorber on the scale factor. The experimental setup is shown in figure 11, and the scale factor results are given in table 15.

Table 15 shows that the spatial response of the camera is not linear for small line source lengths. A two-way analysis of variance was performed on the data for line source lengths 2 cm and greater. Both source length and absorber thickness were significant at the $\alpha = .01$ level. A second two-way ANOVA was then performed for source length 3 cm and greater which showed no significance for both effects at the $\alpha = .01$ level (effect of line source length: $.01 < p < .025$; effect of absorber thickness: $.025 < p < .05$). Results of the second two-way ANOVA are given in table 16.

As a result of the above measurements and calculations, an average scale factor of .21 cm/channel may be applied for lengths greater than 3 cm, and absorber effects may be neglected. Growth plate diameters were measured for the two children in this study, and appear in table 14.

G. Dosage Calculation

From the diameters of the growth plates listed in table 14, an appropriate S factor is found in table 7,

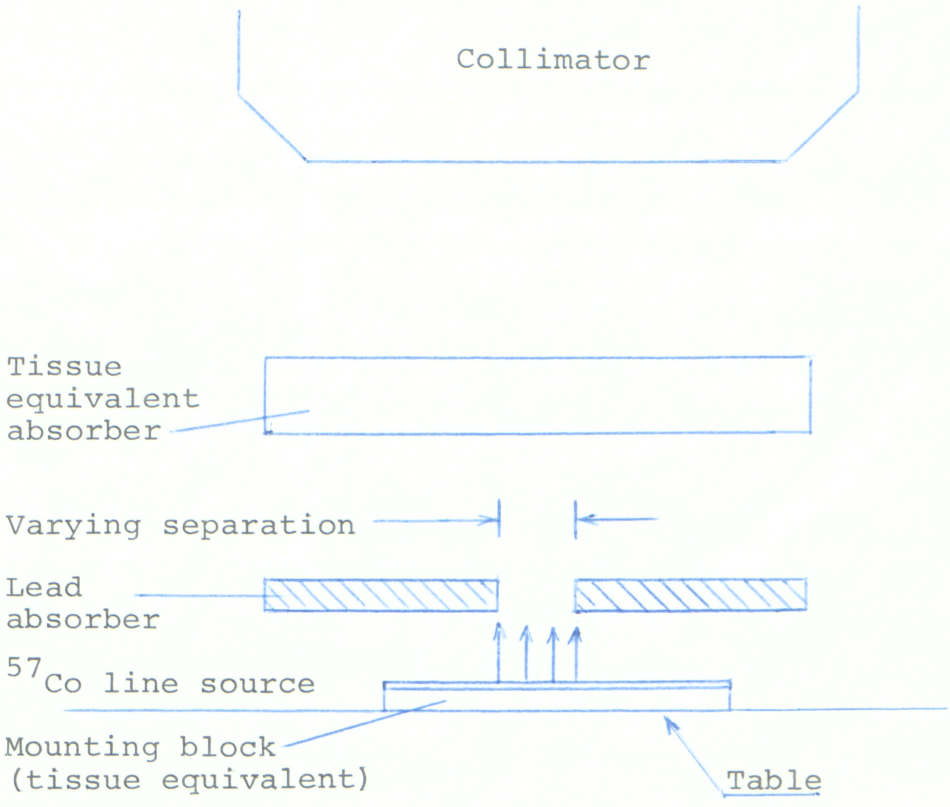

FIGURE 11: Experimental setup for scale factor determination.

Table 15

Cm Per Channel as a Function of Line Source Length and Absorber Thickness (Children's Hospital)

in. Rando Material	Average Cm/Channel* Length of line source (cm)										
	.5	1.0	1.5	2.0	2.5	3	3.5	4	5	6	8
0	.10	.12	.16	.17	.19	.20	.19	.19	.20	.20	.21
1	.08	.14	.17	.18	.22	.19	.20	.20	.21	.20	.22
2	.08	.15	.16	.20	.22	.21	.21	.21	.22	.21	.22

*Average of two readings per cell, originally recorded as channels per cm of line source.

Table 16

Results of Two-Way ANOVA on Effect of Absorber Thickness and Line Source Length (Experimental Data From Table 13)

Effect	df	SS	MS
Mean	1	15211.1111	
Absorber Thickness, 0-2"	2	10.7222	5.3611
Line source length, 3-8 cm	5	17.8889	3.5778
Interaction	10	4.2778	0.4278
Error	18	20.2778	1.1265

Conclusions: At $\alpha = .01$, effects not significant

Absorber thickness $.01 < p < .025$

Line source length $.025 < p < .05$

Interaction $p > .25$

and multiplied by the cumulated activity in table 13. The resulting dose in rads appears in table 14.

Conclusions

Dosages to the growth plates reported in this study are substantially higher than what other investigators have reported as total skeletal dosage from similar compounds. Yano et al. (34), for example, have determined that the total bone dose for a 70 kg man receiving 10 mCi of ^{99m}Tc-EHDP is .267 rads. Silberstein et al. have reported .45 rads total skeletal, for 10 mCi injected (43). Subramanian and McAfee, in a study of adult New Zealand albino rabbits receiving ^{99m}Tc-STPP (sodium tripolyphosphate) have estimated a total skeletal dose in man of .45 rads for 10 mCi injected (35). Scintigrams of the knee in children, however, continually show a "hot" area corresponding to the growth plates. The above dosages, while satisfactory estimates of total bone dose in man, cannot be applied to the epiphyses of children.

Subramanian and McAfee did obtain some data in their evaluation of ^{99m}Tc-STPP on rabbits which may be useful in understanding the dosage levels recorded for the growth plates in this study. The average percent of administered dose for total bone per percent of the body weight of the entire animal skeleton was 4.04, measured over 24 hours. For the callus of experimentally fractured tibia, the average distribution value over 24 hours reached 13.22, an increase of 3.27 over

total bone. Whether the findings for the healing fracture in rabbits can be applied to the metaphyses of children remains to be seen; the important point is that active bone will take up significantly more radionuclide than the average for total bone.

Subramanian et al., in a recent study of four technetium labeled bone seeking agents, have pointed out that total bone radiation levels given for the various agents must be viewed as "average skeletal doses" that assume uniform distribution (44). Biologic retention differs throughout all areas in the long bones, being greatest in the layer adjacent to the periosteum and relatively low in the interior of the cortex. In addition, the above authors suggest that adult dose estimates are not applicable to children. In an unpublished study submitted to the MIRD Committee, the biopsy specimens of the bones of children who had undergone bone scans showed the metaphyseal ends to contain about three times the average concentration of the cortex (45). In young rabbits subjected to radiostrontium assays, the metaphyses contained two and one-half to three times the concentration as the shaft of the bone (46).

The age of the child may also be an important factor in determining uptake and dosage to the growth plates of the knee. More data than presented here is needed to establish a relationship between cumulated

activity and administered activity. In terms of μCi-hrs per μCi administered, data from table 13 yields the following for the growth plates:

	$\frac{\mu Ci\text{-}hrs}{A_o}$	
	T.S. (4 yrs.)	J.S. (13 yrs.)
Right distal femur	.129	.090
Right proximal tibia and fibula	.070	.061
Left distal femur	.145	.092
Left proximal tibia and fibula	.087	.057

Future studies may delineate an age function for $\tilde{A}$ since the physiological processes of the growth plate complex are themselves dependent upon age.

The method of dosimetry outlined in this study allows dosage measurements on the growth plates of the knee, or any other tissue or organ of interest, to be obtained directly, using equipment commonly found in nuclear medicine labs. This method provides a means for quantitating dosage to a child from a nuclear medicine procedure while sparing the child the trauma of being placed in a whole body counter.

The overall accuracy of the growth plate dosages measured in this report is limited mainly by the S factor. Extrapolation was used to obtain values of absorbed fraction for the disc geometry; these values should be

verified by Monte Carlo techniques. S factors for the more common organs of interest, e.g. kidneys, gonads, bladder, etc. have been published for standard children ages one, five, and fifteen (23), (24). These have been computed by photon diffusion calculations specifically for ^{99m}Tc energies. S factors for several of the more commonly used radioisotopes for age groups: newborn, 1, 5, 10, and 15 years and for situations where target organ and source organ are different will be published in a future study by Kereiakes et al. (37). These values will hopefully allow more meaningful data to be gathered on children undergoing nuclear medicine procedures.

Since the S factor is closely tied to the physical dimensions of the organ or tissue under study, an accurate means of obtaining size must be used. Standard children may supply data for the common organs of interest; for other tissues or organs a method of measurement should be determined. While the scale factor presented is this paper sufficed for growth plate dimensions greater than 3 cm, the average thickness of the plate had to be taken from the literature and the dosages obtained apply only to this thickness. Futher pathological studies should be done to better substantiate the size of the growth plate complex as a function of age.

The method of quantitating activity in vivo by use of the gamma camera, outlined by Thomas et al. (29),

provides a means of obtaining cumulated activities in children when such data has been so terribly scarce in the past. The uniqueness of children, physiologically and structurally, and the rapid biological changes which take place between birth and 15 years of age, mandate more studies on cumulated activity and dosage to this segment of the population.

References

1. Loevinger, R., Holt, J.G. and Hine, G.J.: Internally administered radioisotopes, in: Hine, G.J. and Brownell, G.L.: Radiation Dosimetry. Academic Press, Inc., New York, 1956.

2. Johns, H.E. and Cunningham, J.R.: The Physics of Radiology. Third edition, Charles C. Thomas pub., Springfield, Illinois, 1969.

3. Bush, F.: The integral dose received from a uniformly distributed radioactive isotope. Brit. J. Radiol., 22: 96-105, Feb., 1949.

4. Widman, M.A. and Powsner, E.R.: Energy absorption in cylinders containing a uniformly distributed source. J.Nuc. Med., 8: 179-186, 1967.

5. Berger, R.T.: The x- or gamma ray energy absorption or transfer coefficient: tabulation and discussion. Rad. Res., 15:1, 1961.

6. Focht, E.F., Quimby, E.H. and Gershowitz, M.: Revised average geometric factors for cylinders in isotope dosage. Part I. Radiology, 85:151, 1965.

7. Loevinger, R. and Berman, M.: A schema for absorbed-dose calculations for biologically-distributed radionuclides. MIRD Pamphlet No. 1, J. Nuc. Med., 9: Suppl. 1, 7-14, 1968.

8. Loevinger, R. and Berman, M.: A revised schema for calculating the absorbed dose from biologically distributed radionuclides. To be published as a MIRD Pamphlet.

9. Dillman, L.T. and Von Der Lage, F.C.: Radionuclide decay schemas and nuclear parameters for use in radiation dose estimation. MIRD Pamphlet No. 10, New York, Society of Nuclear Medicine, 1975.

10. Brownell, G.L., Ellett, W.H. and Reddy, A.R.: absorbed fractions for photon dosimetry. MIRD Pamphlet No. 3, New York, Society of Nuclear Medicine, 1968.

11. Ellett, W.H., and Humes, R.M.: Absorbed fractions for small volumes containing photon-emitting radioactivity. MIRD Pamphlet No. 8, New York, Society of Nuclear Medicine, 1971.

12. Ellett, W.H., Callahan, A.B. and Brownell, G.L.: Gamma-ray dosimetry of internal emitters. I. Monte Carlo calculations of absorbed dose from point sources. Brit. J. Radiol., 37:45-52, 1964.

13. Ellett, W.H., Callahan, A.B. and Brownell, G.L.: Gamma-ray dosimetry of internal emitters. II. Monte Carlo calculations of absorbed dose from uniform sources. Brit. J. Radiol. 38:541-544, 1965.

14. Johnson, L.C.: The kinetics of skeletal remodeling. In: Structural Organization of the Skeleton, Birth Defects Article Series, Vol. II, No. 1; April, 1966.

15. Trueta, J.: Studies of the Development and Decay of the Human Frame. Saunders publishers, Philadelphia, 1968.

16. Evans, F.G.: Mechanical Properties of Bone. Charles C. Thomas publisher, Springfield, Illinois, 1973. pg. 239.

17. Anthony, C.P. and Kolthoff, N.J.: Textbook of Anatomy and Physiology. C.V. Mosby Co. publishers, St. Louis, 1971.

18. Ellett, W.H., Brownell, G.L. and Reddy, A.R.: Assessment of Monte Carlo calculations for determining the gamma ray dose from internal emitters. Phys. Med. Biol., 13:1968.

19. Snyder, W.S., Ford, M.R., Warner, G.G., and Fisher, H.L.: MIRD Pamphlet No. 5, J. Nucl. Med., 10, Suppl. No. 3, 1969.

20. Snyder, W.S., Ford, M.R., Warner, G.G. and Watson, S.B.: "A tabulation of dose equivalent per microcurie-day for source and target organs of an adult for various radionuclides," Oak Ridge National Laboratory Report ORNL-5000, 1974.

21. Kereiakes, J.G., Seltzer, R.A., Blackburn, B. and Saenger, E.L.: Radionuclide doses to infants and children: a plea for a standard child. Health Physics, 11:999, 1965.

22. Fisher, H.L. and Snyder, W.S.: Oak Ridge National Laboratory Report ORNL-4007, 211, 1966.

23. Hwang, J.M.L., Shoup, R.L., Warner, G.G. and Poston, J.W.: Oak Ridge National Laboratory Report ORNL/TM-5293, 1976.

24. Jones, R.M., Poston, J.W., Hwang, J.L., Jones, T.D. and Warner, G.G.: Oak Ridge National Laboratory Report ORNL/TM-5278, 1976.

25. Snyder, W.S., Ford, M.R., Warner, G.C. and Watson, S.D.: "S", absorbed dose per unit cumulated activity for selected radionuclides and organs. MIRD Pamphlet No. 11, New York, Society of Nuclear Medicine, 1975.

26. Kereiakes, J.G., Simmons, G.H. and Feller, P.A.: Whole body and critical organ dosimetry for ^{99m}Tc-labeled pharmaceuticals. Presented at the Symposium on Biophysical Aspects of the Medical Use of Technetium-^{99m}; Annual Meeting of the American Association of Physicists in Medicine, San Antonio, Texas, August 3-7, 1975.

27. Kereiakes, J.G., Wellman, H.N., Simmons, G.H. and Saenger, E.L.: Radiopharmaceutical dosimetry in pediatrics. Seminars in Nuclear Medicine, 2:316-327, 1972.

28. Webster, E.W., Alpert, N.M. and Brownell, G.L.: Radiation doses in pediatric nuclear medicine and diagnostic X-ray procedures. In:James, A.E., Wagner, H.N. and Cooke, R.E. (eds): Pediatric Nuclear Medicine, W.S. Saunders Co., Philadelphia Pa., 1974, pp. 34-58.

29. Thomas, S.R., Maxon, H.R. and Kereiakes, J.G.: In vivo quantitation of lesion radioactivity using external counting methods. To be published in Medical Physics, Vol. 3, No. 4, 1976.

30. Sorenson, J.A.: Methods for quantitating radioactivity in vivo by external counting measurements. Ph.D. Thesis, University of Wisconsin, Madison, Wisconsin, 1971.

31 Genna, S.: Analytical methods in whole-body counting; in:Clinical Uses of Whole-Body Counting; proceedings of a panel, Vienna, IAEA, 1965.

32. Ben-Haim, A. and Dudley, R.A.: Calibration problems in whole body counting with NaI(Te) detectors; in:Clinical Uses of Whole-Body Counting, proceedings of a panel, Vienna, IAEA, 1965.

33. Hicks, C.R.: Fundamental Concepts in the Design of Experiments, Holt, Rinehart and Winston Publishers, 1973.

34. Yano, Y., McRae, J., Van Dyke, D.C. and Anger, H.O.: ^{99m}Tc-Labeled Sm (II)- Diphosphate: A new bone scanning agent. J. Nucl. Med., 14:73-78, 1973.

35. Subramanian, G. and McAfee, J.G.: A new complex of ^{99m}Tc for skeletal imaging. Radiology, 99:192-196, 1971.

36. Kereiakes, J.G., Feller, P.A., Ascoli, F.A., Thomas, S.R., Gelfand, M.J. and Saenger, E.L.: Pediatric radiopharmaceutical dosimetry. Presented at: Radiopharmaceutical Dosimetry Symposium, April 26-29, 1976, Oak Ridge, Tennessee.

37. Kereiakes, J.G., Thomas, S.R., Ascoli, F.A., Gelfand, M.J., Saenger, E.L., Feller, P.A., Sodd, V.A., Paras, P., Poston, J.W., Warner, G.G. and Shoup, R.L.: Radiopharmaceutical dosimetry in pediatrics. Accepted for presentation at the 62nd RSNA annual meeting, November 14-19, 1976, Chicago.

38. Wellman, H.N., Kereiakes, J.G. and Branson, B.M.: Total and partial body counting of children for radiopharmaceutical dosimetry data. In:Cloutier, R.J., Edwards, C.L. and Snyder, W.S. (eds): Medical Radionuclides:Radiation Dose and Effects. (AEC Symposium Series 20). U.S. Atomic Energy Commission, Division of Technical Information, Washington, D.C., 1970, pp. 133-156.

39. Subramanian, G., McAfee, J.G., Bell, E.G., Blair, R.S., O'Mara, R.E. and Ralston, P.H.: Tc-99m labeled polyphosphate as a skeletal imaging agent. Radiology, 102:701-704, 1972.

40. NCRP, Scientific Committee Report 32: "Administered Radioactivity," to be published.

41. M. Gelfand, M.D.: Personal communication, 1976.

42. Kaul, A., Oeff, K., Roedler, H.A. and Vogelsang, T.: Radiopharmaceuticals-biokinetric data and results of radiation dose calculations. Klinikum Steglitz der Freien Universitat, 1000 Berlin 45, Hinberg-damm 30, 1973.

43. Silberstein, E.B., Saenger, E.L., Tofe, A.J., Alexander, G.W. and Perk, H.: Imaging of bone metastases with ^{99m}Tc-Sn-EHDP (diphosphonate), ^{18}F, and skeletal radiography. Radiology, 107:551-555, 1973.

44. Subramanian, G., McAfee, J.G., Blair, R.J., Kallfalz, F.A. and Thomas, F.D.: Technetium-99m-methylene diphosphonate-a superior agent for skeletal imaging: comparison with other technetium comlpexes. J. Nucl. Med., 16: 744-755, 1975.

45. Charkes, N.D.: Unpublished data submitted to MIRD Committee Society of Nuclear Medicine, November, 1965.

46. Tutt, M., Kidman, B., Rayner, B. et al.: The deposition of ^{89}Sr in rabbit bones following intravenous injection. Br. J. Exp. Pathol., 33:207-215, 1952.

47. Medi-physics, Inc.: Package insert.

48. Medi-physics, Inc.: Protocol for clinical evaluation of MPI bone scintigraphin.

49. Medi-physics, Inc.: Protocol for clinical evaluation of MPI ^{99m}Tc lungaggregate and instant lungaggragate reagent.

50. Clinical Evaluation Protocol of ^{99m}Tc-Stannous Glucoheptonate. New England Nuclear, North Billerica, Massachusetts.

51. Clinical Evaluation Protocol of Technetium-99m Electrolytically Labeled Human Serum Albumin (HSA). New England Nuclear, North Billerica, Massachusetts.

52. Medi-physics, Inc.: Protocol for clinical evaluation of ^{99m}Tc-liver colloid.

53. Clinical Evaluation Protocol of ^{99m}Tc-Stannous Phytate. New England Nuclear, North Billerica, Massachusetts.

54. Permissible Dosage for Internal Radiation. International Commission on Radiation Protection Report No. 2.

55. Lathrop, K.A., Johnston, R.E., Blau, M. and Rothschild, E.O.: Radiation dose to humans from ^{75}Se-L-selenomethionine. J.Nucl. Med., Suppl. 6, 1972.

56. Morin, R.L. and Brookeman, V.A.: ^{169}Yb-DTPA distribution and dosimetry in cisternography. J. Nucl. Med., 15:786, 1974.

57. Johnston, R.E. and Staab, E.V.: Radiation dose to the brain from ^{169}Yb-DTPA in cisternography. J. Nucl. Med., 16:101-102, 1975.

58. Smith, E.M.: Internal dose calculations for ^{99m}Tc. J. Nucl. Med., 6:231-251, 1965.

59. Harper, P.V., Lathrop, K.A. and Gottschalk, A.: Pharmacodynamics of some technetium-^{99m}preparations in radioactive pharmaceuticals; edited by Andrews, G.A., Kniseley, R.M. and Wagner, H.N.: AEC Symposium 6, U.S. Atomic Energy Commission, Division of Technical Information, Washington, D.C. (1966).

60. French, R.J., Johnson, P.E. and Trott, N.G.: Dosimetry of indium-113m, in Medical Radioisotope Scintigraphy. Vol. 1, IAEA, Vienna, pp. 843-862, 1969.

61. New England Nuclear, Massachusetts: Dosimetry. ^{99m}Tc-polyphosphate, products literature.

62. Kereiakes, J.G., Saenger, E.L. and Sodd, V.J.: Pediatric radiopharmaceutical dosimetry, Proceedings of the XIII International Congress of Radiology, Madrid, 15-20 October, 1973.

63. MIRD dose estimate report 8: Summary of current radiation dose estimates to normal humans from ^{99m}Tc as sodium pertechnetate. J. Nucl. Med., 17:74-77, 1976.

64. MIRD dose estimate report 5: Summary of current radiation dose estimates humans from ^{123}I, ^{124}I. ^{125}I, ^{126}I, ^{130}I, ^{131}I, ^{132}I, as sodium iodide. J. Nucl. Med., 16: 857, 860, 1975.

APPENDIX A

OUTPUT DATA

6 CARBON 11 HALF LIFE = 20.3 MINUTES

DECAY MODE- BETA PLUS

RADIATION		MEAN NUMBER/ DISINTE- GRATION n_i	MEAN ENERGY/ PAR- TICLE $\bar{E}_i$ (MeV)	EQUI- LIBRIUM DOSE CONSTANT Δ_i (g-rad/ μCi-h)
BETA PLUS	1	0.9980	0.3942	0.8380
ANNIH. RADIATION		1.9960	0.5110	2.1725

OUTPUT DATA

19 POTASSIUM 43 HALF LIFE = 22.4 HOURS

DECAY MODE- BETA MINUS

RADIATION		MEAN NUMBER/ DISINTE- GRATION n_i	MEAN ENERGY/ PAR- TICLE $\bar{E}_i$ (MeV)	EQUI- LIBRIUM DOSE CONSTANT Δ_i (g-rad/ μCi-h)
BETA MINUS	1	0.0450	0.1529	0.0146
BETA MINUS	2	0.8150	0.2972	0.5160
BETA MINUS	3	0.0620	0.4694	0.0620
BETA MINUS	4	0.0620	0.5680	0.0750
BETA MINUS	5	0.0160	0.7604	0.0259
GAMMA	1	0.0672	0.2192	0.0314
GAMMA	2	0.8992	0.3730	0.7144
K INT CON ELECT		0.0004	0.3689	0.0003
GAMMA	3	0.0896	0.3978	0.0759
GAMMA	4	0.0842	0.5925	0.1063
GAMMA	5	0.7252	0.6172	0.9534
K INT CON ELECT		0.0000	0.6131	0.0001
GAMMA	6	0.0449	1.0050	0.0963

OUTPUT DATA

20 CALCIUM 45 HALF LIFE = 163. DAYS

DECAY MODE- BETA MINUS

RADIATION		MEAN NUMBER/ DISINTE- GRATION n_i	MEAN ENERGY/ PAR- TICLE $\bar{E}_i$ (MeV)	EQUI- LIBRIUM DOSE CONSTANT Δ_i (g-rad/ μCi-h)
BETA MINUS	1	0.9999	0.0772	0.1645

OUTPUT DATA

24 CHROMIUM 51 HALF LIFE = 27.7 DAYS

DECAY MODE- ELECTRON CAPTURE

RADIATION		MEAN NUMBER/ DISINTE- GRATION n_i	MEAN ENERGY/ PAR- TICLE $\bar{E}_i$ (MeV)	EQUI- LIBRIUM DOSE CONSTANT Δ_i (g-rad/ μCi-h)
GAMMA	1	0.1018	0.3200	0.0694
K ALPHA-1 X-RAY		0.1289	0.0049	0.0013
K ALPHA-2 X-RAY		0.0659	0.0049	0.0006
K BETA-1 X-RAY		0.0224	0.0054	0.0002
KLL AUGER ELECT		0.5614	0.0044	0.0052
KLX AUGER ELECT		0.1240	0.0048	0.0012
LMM AUGER ELECT		1.5323	0.0004	0.0014
MXY AUGER ELECT		3.2177	0.0000	0.0002

OUTPUT DATA

27 COBALT 57 HALF LIFE = 270. DAYS

DECAY MODE- ELECTRON CAPTURE

RADIATION		MEAN NUMBER/ DISINTE- GRATION n_i	MEAN ENERGY/ PAR- TICLE $\bar{E}_i$ (MeV)	EQUI- LIBRIUM DOSE CONSTANT Δ_i (g-rad/ μCi-h)
GAMMA	1	0.0954	0.0144	0.0029
K INT CON ELECT		0.6979	0.0072	0.0108
L INT CON ELECT		0.0766	0.0136	0.0022
M INT CON ELECT		0.0098	0.0143	0.0003
GAMMA	2	0.8590	0.1220	0.2233
K INT CON ELECT		0.0173	0.1149	0.0042
L INT CON ELECT		0.0015	0.1213	0.0004
M INT CON ELECT		0.0005	0.1220	0.0001
GAMMA	3	0.1040	0.1364	0.0302
K INT CON ELECT		0.0137	0.1293	0.0037
L INT CON ELECT		0.0016	0.1356	0.0004
M INT CON ELECT		0.0005	0.1363	0.0001
GAMMA	4	0.0002	0.5701	0.0002
GAMMA	5	0.0015	0.6921	0.0022
K ALPHA-1 X-RAY		0.3083	0.0064	0.0042
K ALPHA-2 X-RAY		0.1554	0.0063	0.0021
K BETA-1 X-RAY		0.0499	0.0070	0.0007
KLL AUGER ELECT		0.8954	0.0056	0.0107
KLX AUGER ELECT		0.2185	0.0063	0.0029
LMM AUGER ELECT		2.6451	0.0006	0.0035
MXY AUGER ELECT		5.5781	0.0000	0.0006

OUTPUT DATA

31 GALLIUM 67 HALF LIFE = 78.1 HOURS

DECAY MODE- ELECTRON CAPTURE

RADIATION		MEAN NUMBER/ DISINTE-GRATION n_i	MEAN ENERGY/ PAR-TICLE $\bar{E}_i$ (MeV)	EQUI-LIBRIUM DOSE CONSTANT Δ_i (g-rad/ μCi-h)
GAMMA	1	0.0326	0.0913	0.0063
K INT CON ELECT		0.0021	0.0816	0.0003
GAMMA	2	0.3797	0.0933	0.0754
K INT CON ELECT		0.2830	0.0836	0.0504
L INT CON ELECT		0.0379	0.0922	0.0074
M INT CON ELECT		0.0126	0.0932	0.0025
GAMMA	3	0.2388	0.1846	0.0939
K INT CON ELECT		0.0026	0.1749	0.0009
L INT CON ELECT		0.0004	0.1835	0.0001
GAMMA	4	0.0247	0.2090	0.0110
GAMMA	5	0.1613	0.3002	0.1031
K INT CON ELECT		0.0005	0.2905	0.0003
GAMMA	6	0.0429	0.3936	0.0359
GAMMA	7	0.0009	0.4943	0.0010
GAMMA	8	0.0001	0.7036	0.0002
GAMMA	9	0.0006	0.7947	0.0010
GAMMA	10	0.0015	0.8880	0.0029
K ALPHA-1 X-RAY		0.3075	0.0086	0.0056
K ALPHA-2 X-RAY		0.1534	0.0086	0.0028
K BETA-1 X-RAY		0.0553	0.0095	0.0011
KLL AUGER ELECT		0.5185	0.0075	0.0083
KLX AUGER ELECT		0.1410	0.0085	0.0025
KXY AUGER ELECT		0.0067	0.0094	0.0001
LMM AUGER ELECT		1.7722	0.0008	0.0033
MXY AUGER ELECT		3.7779	0.0000	0.0006

OUTPUT DATA

34 SELENIUM 75 HALF LIFE = 120. DAYS

DECAY MODE- ELECTRON CAPTURE

RADIATION		MEAN NUMBER/ DISINTE-GRATION n_i	MEAN ENERGY/ PAR-TICLE $\bar{E}_i$ (MeV)	EQUI-LIBRIUM DOSE CONSTANT Δ_i (g-rad/ μCi-h)
GAMMA	1	0.0002	0.0244	0.0000
K INT CON ELECT		0.0418	0.0125	0.0011
L INT CON ELECT		0.0094	0.0230	0.0004
M INT CON ELECT		0.0031	0.0242	0.0001
GAMMA	2	0.0100	0.0660	0.0014
K INT CON ELECT		0.0026	0.0541	0.0003
GAMMA	3	0.0000	0.0810	0.0000
GAMMA	4	0.0291	0.0967	0.0060
K INT CON ELECT		0.0256	0.0848	0.0046
L INT CON ELECT		0.0031	0.0953	0.0006
M INT CON ELECT		0.0010	0.0965	0.0002
GAMMA	5	0.1563	0.1211	0.0403
K INT CON ELECT		0.0063	0.1092	0.0014
L INT CON ELECT		0.0005	0.1197	0.0001
GAMMA	6	0.5393	0.1360	0.1562
K INT CON ELECT		0.0154	0.1241	0.0040
L INT CON ELECT		0.0014	0.1346	0.0004
M INT CON ELECT		0.0004	0.1358	0.0001
GAMMA	7	0.0135	0.1986	0.0057
K INT CON ELECT		0.0002	0.1867	0.0001
GAMMA	8	0.5710	0.2646	0.3218
K INT CON ELECT		0.0035	0.2527	0.0019
L INT CON ELECT		0.0002	0.2632	0.0001
GAMMA	9	0.2388	0.2795	0.1421
K INT CON ELECT		0.0018	0.2676	0.0010
L INT CON ELECT		0.0001	0.2781	0.0001
GAMMA	10	0.0123	0.3038	0.0080
K INT CON ELECT		0.0005	0.2919	0.0003
GAMMA	11	0.1164	0.4005	0.0993
K INT CON ELECT		0.0001	0.3886	0.0001
GAMMA	12	0.0001	0.4193	0.0001
GAMMA	13	0.0003	0.5726	0.0004
GAMMA	14	0.0000	0.6177	0.0000
K ALPHA-1 X-RAY		0.3175	0.0105	0.0071
K ALPHA-2 X-RAY		0.1581	0.0105	0.0035
K BETA-1 X-RAY		0.0625	0.0117	0.0015
KLL AUGER ELECT		0.3394	0.0091	0.0065
KLX AUGER ELECT		0.0994	0.0103	0.0021
KXY AUGER ELECT		0.0076	0.0115	0.0001
LMM AUGER ELECT		1.3522	0.0010	0.0031
MXY AUGER ELECT		2.9144	0.0001	0.0008

OUTPUT DATA

26 IRON 59 HALF LIFE = 45.0 DAYS

DECAY MODE- BETA MINUS

RADIATION		MEAN NUMBER/ DISINTE-GRATION n_i	MEAN ENERGY/ PAR-TICLE $\bar{E}_i$ (MeV)	EQUI-LIBRIUM DOSE CONSTANT Δ_i (g-rad/ μCi-h)
BETA MINUS	2	0.0122	0.0381	0.0009
BETA MINUS	3	0.4609	0.0808	0.0793
BETA MINUS	4	0.5228	0.1496	0.1666
BETA MINUS	5	0.0030	0.6396	0.0040
GAMMA	1	0.0096	0.1420	0.0029
GAMMA	2	0.0292	0.1922	0.0119
GAMMA	3	0.0023	0.3347	0.0017
GAMMA	4	0.0002	0.3810	0.0001
GAMMA	5	0.5548	1.0990	1.2987
K INT CON ELECT		0.0000	1.0912	0.0002
GAMMA	6	0.4411	1.2920	1.2140
K INT CON ELECT		0.0000	1.2842	0.0001
GAMMA	7	0.0009	1.4810	0.0028

OUTPUT DATA

43 TECHNETIUM 99M HALF LIFE = 6.03 HOURS

DECAY MODE- ISOMERIC LEVEL

RADIATION		MEAN NUMBER/ DISINTE-GRATION n_i	MEAN ENERGY/ PAR-TICLE $\bar{E}_i$ (MeV)	EQUI-LIBRIUM DOSE CONSTANT Δ_i (g-rad/ μCi-h)
GAMMA	1	0.0000	0.0021	0.0000
M INT CON ELECT		0.9860	0.0016	0.0035
GAMMA	2	0.8787	0.1405	0.2630
K INT CON ELECT		0.0913	0.1194	0.0232
L INT CON ELECT		0.0118	0.1377	0.0034
M INT CON ELECT		0.0039	0.1400	0.0011
GAMMA	3	0.0003	0.1426	0.0001
K INT CON ELECT		0.0088	0.1215	0.0022
L INT CON ELECT		0.0035	0.1398	0.0010
M INT CON ELECT		0.0011	0.1422	0.0003
K ALPHA-1 X-RAY		0.0441	0.0183	0.0017
K ALPHA-2 X-RAY		0.0221	0.0182	0.0008
K BETA-1 X-RAY		0.0105	0.0206	0.0004
KLL AUGER ELECT		0.0152	0.0154	0.0005
KLX AUGER ELECT		0.0055	0.0178	0.0002
LMM AUGER ELECT		0.1093	0.0019	0.0004
MXY AUGER ELECT		1.2359	0.0004	0.0011

OUTPUT DATA

49 INDIUM 111 HALF LIFE = 2.81 DAYS

DECAY MODE- ELECTRON CAPTURE

RADIATION		MEAN NUMBER/ DISINTE-GRATION n_i	MEAN ENERGY/ PAR-TICLE $\bar{E}_i$ (MeV)	EQUI-LIBRIUM DOSE CONSTANT Δ_i (g-rad/ μCi-h)
GAMMA	1	0.8959	0.1720	0.3282
K INT CON ELECT		0.0896	0.1452	0.0277
L INT CON ELECT		0.0108	0.1682	0.0038
M INT CON ELECT		0.0036	0.1713	0.0013
GAMMA	2	0.9395	0.2470	0.4942
K INT CON ELECT		0.0507	0.2202	0.0238
L INT CON ELECT		0.0073	0.2432	0.0037
M INT CON ELECT		0.0024	0.2463	0.0012
K ALPHA-1 X-RAY		0.4663	0.0231	0.0230
K ALPHA-2 X-RAY		0.2364	0.0229	0.0115
K BETA-1 X-RAY		0.1198	0.0260	0.0066
K BETA-2 X-RAY		0.0237	0.0267	0.0013
L X-RAYS		0.1108	0.0030	0.0007
KLL AUGER ELECT		0.1103	0.0192	0.0045
KLX AUGER ELECT		0.0441	0.0223	0.0021
KXY AUGER ELECT		0.0067	0.0254	0.0003
LMM AUGER ELECT		0.9867	0.0024	0.0052
MXY AUGER ELECT		2.2886	0.0006	0.0030

OUTPUT DATA

54 XENON 127 HALF LIFE = 36.4 DAYS

DECAY MODE- ELECTRON CAPTURE

RADIATION		MEAN NUMBER/ DISINTE-GRATION n_i	MEAN ENERGY/ PAR-TICLE $\bar{E}_i$ (MeV)	EQUI-LIBRIUM DOSE CONSTANT Δ_i (g-rad/ μCi-h)
GAMMA	1	0.0137	0.0576	0.0016
K INT CON ELECT		0.0403	0.0244	0.0021
L INT CON ELECT		0.0059	0.0527	0.0006
M INT CON ELECT		0.0019	0.0567	0.0002
GAMMA	2	0.0413	0.1452	0.0128
K INT CON ELECT		0.0142	0.1120	0.0033
L INT CON ELECT		0.0039	0.1404	0.0011
M INT CON ELECT		0.0013	0.1443	0.0004
GAMMA	3	0.2504	0.1721	0.0918
K INT CON ELECT		0.0395	0.1389	0.0117
L INT CON ELECT		0.0052	0.1672	0.0018
M INT CON ELECT		0.0017	0.1712	0.0006
GAMMA	4	0.6756	0.2028	0.2918
K INT CON ELECT		0.0658	0.1696	0.0238
L INT CON ELECT		0.0101	0.1980	0.0042
M INT CON ELECT		0.0033	0.2019	0.0014
GAMMA	5	0.1797	0.3749	0.1435
K INT CON ELECT		0.0026	0.3417	0.0019
L INT CON ELECT		0.0004	0.3701	0.0003
GAMMA	6	0.0001	0.6184	0.0001
K ALPHA-1 X-RAY		0.4795	0.0286	0.0292
K ALPHA-2 X-RAY		0.2467	0.0283	0.0148
K BETA-1 X-RAY		0.1309	0.0322	0.0090
K BETA-2 X-RAY		0.0273	0.0331	0.0019
L X-RAYS		0.1419	0.0039	0.0011
KLL AUGER ELECT		0.0842	0.0235	0.0042
KLX AUGER ELECT		0.0361	0.0274	0.0021
KXY AUGER ELECT		0.0059	0.0314	0.0003
LMM AUGER ELECT		0.9413	0.0030	0.0061
MXY AUGER ELECT		2.2374	0.0008	0.0041

OUTPUT DATA

49 INDIUM 113M HALF LIFE = 99.4 MINUTES

DECAY MODE- ISOMERIC LEVEL

RADIATION		MEAN NUMBER/ DISINTE-GRATION n_i	MEAN ENERGY/ PAR-TICLE $\bar{E}_i$ (MeV)	EQUI-LIBRIUM DOSE CONSTANT Δ_i (g-rad/ μCi-h)
GAMMA	1	0.6206	0.3916	0.5178
K INT CON ELECT		0.2668	0.3637	0.2067
L INT CON ELECT		0.0503	0.3877	0.0415
M INT CON ELECT		0.0620	0.3910	0.0516
K ALPHA-1 X-RAY		0.1243	0.0242	0.0064
K ALPHA-2 X-RAY		0.0632	0.0240	0.0032
K BETA-1 X-RAY		0.0324	0.0272	0.0018
K BETA-2 X-RAY		0.0065	0.0279	0.0003
L X-RAYS		0.0325	0.0032	0.0002
KLL AUGER ELECT		0.0274	0.0201	0.0011
KLX AUGER ELECT		0.0110	0.0233	0.0005
LMM AUGER ELECT		0.2715	0.0025	0.0014
MXY AUGER ELECT		0.6846	0.0006	0.0009

OUTPUT DATA

54 XENON 133 HALF LIFE = 5.31 DAYS

DECAY MODE- BETA MINUS

RADIATION		MEAN NUMBER/ DISINTE-GRATION n_i	MEAN ENERGY/ PAR-TICLE $\bar{E}_i$ (MeV)	EQUI-LIBRIUM DOSE CONSTANT Δ_i (g-rad/ μCi-h)
BETA MINUS	2	0.0163	0.0750	0.0026
BETA MINUS	3	0.9830	0.1006	0.2106
GAMMA	1	0.0061	0.0796	0.0010
K INT CON ELECT		0.0084	0.0436	0.0007
L INT CON ELECT		0.0012	0.0742	0.0001
GAMMA	2	0.3603	0.0809	0.0621
K INT CON ELECT		0.5261	0.0450	0.0504
L INT CON ELECT		0.0848	0.0756	0.0136
M INT CON ELECT		0.0282	0.0799	0.0048
GAMMA	3	0.0000	0.1606	0.0000
GAMMA	4	0.0000	0.2230	0.0000
GAMMA	5	0.0000	0.3028	0.0000
GAMMA	6	0.0002	0.3839	0.0001
K ALPHA-1 X-RAY		0.2552	0.0309	0.0168
K ALPHA-2 X-RAY		0.1321	0.0306	0.0086
K BETA-1 X-RAY		0.0712	0.0349	0.0053
K BETA-2 X-RAY		0.0150	0.0359	0.0011
L X-RAYS		0.0823	0.0043	0.0007
KLL AUGER ELECT		0.0402	0.0253	0.0021
KLX AUGER ELECT		0.0177	0.0296	0.0011
KXY AUGER ELECT		0.0029	0.0339	0.0002
LMM AUGER ELECT		0.4894	0.0033	0.0034
MXY AUGER ELECT		1.1847	0.0009	0.0025

••OUTPUT DATA••

53 IODINE 123 HALF LIFE = 13.0 HOURS

DECAY MODE- ELECTRON CAPTURE

RADIATION		MEAN NUMBER/ DISINTE-GRATION n_i	MEAN ENERGY/ PAR-TICLE E_i (MeV)	EQUI-LIBRIUM DOSE CONSTANT Δ_i (g-rad/ μCi-h)
GAMMA	1	0.8356	0.1591	0.2831
K INT CON ELECT		0.1343	0.1272	0.0364
L INT CON ELECT		0.0174	0.1545	0.0057
M INT CON ELECT		0.0058	0.1582	0.0019
GAMMA	2	0.0002	0.1837	0.0000
GAMMA	3	0.0002	0.1927	0.0001
GAMMA	4	0.0006	0.2483	0.0003
GAMMA	5	0.0006	0.2810	0.0003
GAMMA	6	0.0010	0.3466	0.0007
GAMMA	7	0.0034	0.4404	0.0032
GAMMA	8	0.0026	0.5056	0.0028
GAMMA	9	0.0105	0.5290	0.0118
GAMMA	10	0.0026	0.5385	0.0030
GAMMA	11	0.0006	0.6249	0.0009
GAMMA	12	0.0002	0.6877	0.0003
GAMMA	13	0.0002	0.7361	0.0004
GAMMA	14	0.0004	0.7844	0.0007
K ALPHA-1 X-RAY		0.4715	0.0274	0.0275
K ALPHA-2 X-RAY		0.2419	0.0272	0.0140
K BETA-1 X-RAY		0.1273	0.0309	0.0084
K BETA-2 X-RAY		0.0264	0.0318	0.0017
L X-RAYS		0.1332	0.0037	0.0010
KLL AUGER ELECT		0.0877	0.0226	0.0042
KLX AUGER ELECT		0.0370	0.0264	0.0020
KXY AUGER ELECT		0.0059	0.0301	0.0003
LMM AUGER ELECT		0.9242	0.0029	0.0057
MXY AUGER ELECT		2.1864	0.0008	0.0038

••OUTPUT DATA••

53 IODINE 125 HALF LIFE = 60.2 DAYS

DECAY MODE- ELECTRON CAPTURE

RADIATION		MEAN NUMBER/ DISINTE-GRATION n_i	MEAN ENERGY/ PAR-TICLE $\bar{E}_i$ (MeV)	EQUI-LIBRIUM DOSE CONSTANT Δ_i (g-rad/ μCi-h)
GAMMA	1	0.0666	0.0354	0.0050
K INT CON ELECT		0.8000	0.0036	0.0062
L INT CON ELECT		0.1142	0.0309	0.0075
M INT CON ELECT		0.0190	0.0346	0.0014
K ALPHA-1 X-RAY		0.7615	0.0274	0.0445
K ALPHA-2 X-RAY		0.3906	0.0272	0.0226
K BETA-1 X-RAY		0.2056	0.0309	0.0135
K BETA-2 X-RAY		0.0426	0.0318	0.0028
L X-RAYS		0.2226	0.0037	0.0017
KLL AUGER ELECT		0.1416	0.0226	0.0068
KLX AUGER ELECT		0.0597	0.0264	0.0033
KXY AUGER ELECT		0.0096	0.0301	0.0006
LMM AUGER ELECT		1.5442	0.0029	0.0096
MXY AUGER ELECT		3.6461	0.0008	0.0063

••OUTPUT DATA••

53 IODINE 131 HALF LIFE = 8.06 DAYS

DECAY MODE- BETA MINUS

RADIATION		MEAN NUMBER/ DISINTE-GRATION n_i	MEAN ENERGY/ PAR-TICLE $\bar{E}_i$ (MeV)	EQUI-LIBRIUM DOSE CONSTANT Δ_i (g-rad/ μCi-h)
BETA MINUS	1	0.0200	0.0691	0.0029
BETA MINUS	2	0.0067	0.0867	0.0012
BETA MINUS	3	0.0664	0.0964	0.0136
BETA MINUS	5	0.8980	0.1916	0.3666
BETA MINUS	6	0.0080	0.2839	0.0048
GAMMA	1	0.0258	0.0801	0.0044
K INT CON ELECT		0.0343	0.0456	0.0033
L INT CON ELECT		0.0043	0.0751	0.0007
M INT CON ELECT		0.0014	0.0792	0.0002
GAMMA	2	0.0029	0.1772	0.0011
K INT CON ELECT		0.0004	0.1426	0.0001
GAMMA	3	0.0006	0.2723	0.0003
GAMMA	4	0.0578	0.2843	0.0350
K INT CON ELECT		0.0023	0.2497	0.0012
L INT CON ELECT		0.0004	0.2792	0.0002
GAMMA	5	0.0010	0.3180	0.0007
GAMMA	6	0.0003	0.3250	0.0002
GAMMA	7	0.0036	0.3257	0.0025
GAMMA	8	0.0001	0.3585	0.0001
GAMMA	9	0.8201	0.3644	0.6366
K INT CON ELECT		0.0147	0.3299	0.0103
L INT CON ELECT		0.0023	0.3594	0.0017
M INT CON ELECT		0.0007	0.3635	0.0006
GAMMA	10	0.0006	0.4048	0.0005
GAMMA	11	0.0029	0.5029	0.0031
GAMMA	12	0.0653	0.6367	0.0886
K INT CON ELECT		0.0002	0.6021	0.0003
GAMMA	13	0.0014	0.6430	0.0020
GAMMA	14	0.0173	0.7228	0.0267
K ALPHA-1 X-RAY		0.0249	0.0297	0.0015
K ALPHA-2 X-RAY		0.0128	0.0294	0.0008
K BETA-1 X-RAY		0.0068	0.0336	0.0004
K BETA-2 X-RAY		0.0014	0.0345	0.0001
KLL AUGER ELECT		0.0041	0.0244	0.0002
KLX AUGER ELECT		0.0018	0.0285	0.0001
LMM AUGER ELECT		0.0477	0.0031	0.0003
MXY AUGER ELECT		0.1147	0.0009	0.0002

DAUGHTER NUCLIDE, XENON 131M IS RADIOACTIVE AND MAY CONTRIBUTE TO THE DOSE.

BRANCHING TO 0.1639 MEV, 11.8 DAY HALF LIFE, ISOMERIC LEVEL IN XENON-131 IS 0.0144 PER DISINTEGRATION OF IODINE-131.

••OUTPUT DATA••

70 YTTERBIUM 169 HALF LIFE = 32.0 DAYS

DECAY MODE- ELECTRON CAPTURE

RADIATION		MEAN NUMBER/ DISINTE- GRATION n_i	MEAN ENERGY/ PAR- TICLE $\bar{E}_i$ (MeV)	EQUI- LIBRIUM DOSE CONSTANT Δ_i (g-rad/ μCi-h)
	GAMMA 1	0.0000	0.0084	0.0000
M INT CON	ELECT	0.9540	0.0065	0.0132
	GAMMA 2	0.0021	0.0207	0.0000
L INT CON	ELECT	0.0921	0.0113	0.0022
M INT CON	ELECT	0.0307	0.0188	0.0012
	GAMMA 3	0.4516	0.0631	0.0607
K INT CON	ELECT	0.4080	0.0037	0.0032
L INT CON	ELECT	0.0722	0.0537	0.0082
M INT CON	ELECT	0.0240	0.0612	0.0031
	GAMMA 4	0.0078	0.0936	0.0015
K INT CON	ELECT	0.0240	0.0342	0.0017
L INT CON	ELECT	0.0038	0.0842	0.0006
M INT CON	ELECT	0.0953	0.0917	0.0186
	GAMMA 5	0.0382	0.1097	0.0089
K INT CON	ELECT	0.0788	0.0503	0.0084
L INT CON	ELECT	0.0117	0.1003	0.0025
M INT CON	ELECT	0.4711	0.1078	0.1082
	GAMMA 6	0.0004	0.1172	0.0001
	GAMMA 7	0.0190	0.1181	0.0048
K INT CON	ELECT	0.0132	0.0587	0.0016
L INT CON	ELECT	0.0140	0.1087	0.0032
M INT CON	ELECT	0.0046	0.1162	0.0011
	GAMMA 8	0.1142	0.1305	0.0317
K INT CON	ELECT	0.0628	0.0711	0.0095
L INT CON	ELECT	0.0539	0.1211	0.0139
M INT CON	ELECT	0.0179	0.1286	0.0049
	GAMMA 9	0.1731	0.1771	0.0653
K INT CON	ELECT	0.0831	0.1177	0.0208
L INT CON	ELECT	0.0136	0.1677	0.0048
M INT CON	ELECT	0.0801	0.1752	0.0299
	GAMMA 10	0.2616	0.1979	0.1103
K INT CON	ELECT	0.0915	0.1385	0.0270
L INT CON	ELECT	0.0150	0.1885	0.0060
M INT CON	ELECT	0.1506	0.1960	0.0629
	GAMMA 11	0.0012	0.2404	0.0006
	GAMMA 12	0.0174	0.2610	0.0097
K INT CON	ELECT	0.0004	0.2016	0.0002
	GAMMA 13	0.1104	0.3076	0.0724
K INT CON	ELECT	0.0054	0.2482	0.0028
L INT CON	ELECT	0.0015	0.2982	0.0010
M INT CON	ELECT	0.0005	0.3057	0.0003
K ALPHA-1	X-RAY	0.7750	0.0507	0.0837
K ALPHA-2	X-RAY	0.4154	0.0497	0.0440
K BETA-1	X-RAY	0.2472	0.0575	0.0302
K BETA-2	X-RAY	0.0569	0.0593	0.0072
L	X-RAYS	0.4027	0.0075	0.0064
KLL AUGER	ELECT	0.0626	0.0405	0.0054
KLX AUGER	ELECT	0.0322	0.0481	0.0033
KXY AUGER	ELECT	0.0055	0.0556	0.0006
LMM AUGER	ELECT	1.3635	0.0056	0.0163
MXY AUGER	ELECT	5.2840	0.0018	0.0212

DOSIMETRY PARAMETERS OF ^{129}Cs

Radiation (i)	Mean number per disintegration (n_i)	Mean Energy MeV (E_i)	Equilibrium dose constant $\frac{\text{g-rad}}{\mu\text{Ci-hr}}$ (Δ_i)
Gamma-1	.0292	.0394	.0025
K conv elect.	.3121	.0048	.0032
Gamma-2	.0076	.0935	.0015
K conv elect.	.0054	.0589	.0007
L conv elect.	.0008	.0886	.0001
M conv elect.	.0003	.0925	.0001
Gamma-3	.0030	.1772	.0011
K conv elect.	.0004	.1426	.0001
L conv elect.	.0001	.1723	.0000
M conv elect.	.00003	.1762	.0000
Gamma-4	.0046	.2681*	.0026
K conv elect.	.0002	.2335	.0001
Gamma-5	.0165	.2787*	.0098
K conv elect.	.0007	.2441	.0004
Gamma-6	.0247	.3179	.0167
K conv elect.	.0007	.2833	.0004
Gamma-7	.0005	.3220	.0003
Gamma-8	.317	.3719	.2511
K conv elect.	.0060	.3373	.0043
L conv elect.	.0010	.3670	.0008
M conv elect.	.0003	.3709	.0003
Gamma-9	.219	.4113	.1916
K conv elect.	.0033	.3767	.0027
L conv elect.	.0005	.4064	.0004
M conv elect.	.0002	.4103	.0001
Gamma-10	.0001	.4928	.0001
Gamma-11	.0003	.5348	.0004
Gamma-12	.0327	.5493	.0382
K conv elect.	.0002	.5147	.0002
L conv elect.	.00002	.5444	.0000
M conv elect.	.00001	.5483	.0000
Gamma-13	.0055	.5888	.0070
Gamma-14	.0003	.6245	.0004
Gamma-15	.0003	.8655	.0006
Gamma-16	.0023	.9070	.0044
Gamma-17	.0007	.9463	.0013
X-rays			
Kα-1	.558	.0298	.0355
Kα-2	.290	.0295	.0182
Kβ-1	.156	.0336	.0112
Kβ-2	.0335	.0344	.0025
K Auger Electrons	.1415	.0346	.0104
N. P. Radiation from L vacancies	.9701	.0050	.0103
N. P. Radiation from H.O. vacancies	.2208	.0011	.0005
		TOTAL Δ_p =	.5970
		TOTAL Δ_{np} =	.0351

* Weighted Averages

DOSIMETRY PARAMETERS OF ^{201}Tl.

Radiation (i)	Mean number per disintegration (n_i)	Mean Energy MeV (E_i)	Equilibrium dose constant g-rad μCi-hr (Δ_i)
Gamma 1	.0000	.0016	.0000
N int. conv. elect.	.6559	.0016	.0022
Gamma 2	.0029	.0306	.0002
L int. conv. elect.	.0742	.0168	.0027
M int. conv. elect.	.0268	.0277	.0016
Gamma 3	.0025	.0322	.0002
L int. conv. elect.	.0730	.0184	.0029
M int. conv. elect.	.0234	.0293	.0015
Gamma 4	.0289	.1353	.0083
K int. conv. elect.	.0736	.0522	.0082
L int. conv. elect.	.0115	.1215	.0030
M int. conv. elect.	.0037	.1324	.0010
Gamma 5	.0013	.1659	.0005
K int. conv. elect.	.0022	.0828	.0004
L int. conv. elect.	.0004	.1521	.0001
Gamma 6	.0881	.1674	.0314
K int. conv. elect.	.1315	.0843	.0236
L int. conv. elect.	.0215	.1536	.0070
M int. conv. elect.	.0071	.1645	.0025
X rays:			
Kα-1	.4616	.0708	.0696
Kα-2	.2539	.0689	.0373
Kβ-1	.1616	.0802	.0276
Kβ-2	.0462	.0825	.0081
L	.4292	.0108	.0099
Auger electrons:			
KLL	.0238	.0557	.0028
KLX	.0135	.0665	.0019
KXY	.0022	.0773	.0004
LXY	.7153	.0079	.0120
MXY	2.204	.0029	.0136

Total $\Delta_p{}^a$ = .1931

Total $\Delta_{np}{}^b$ = .0874

APPENDIX B

ABSORBED FRACTIONS FOR UNIFORMLY DISTRIBUTED SOURCES IN SMALL UNIT-DENSITY SPHERES SURROUNDED BY SCATTERING MEDIUM

Mass (g)	Photon energy (MeV)									
	0.030	0.040	0.060	0.080	0.100	0.140	0.364	0.662	1.460	2.750
1	0.050	0.023	0.011	0.009	0.009	0.010	0.011	0.011	0.010	0.008
2	0.064	0.030	0.014	0.012	0.012	0.012	0.014	0.014	0.012	0.010
4	0.081	0.038	0.019	0.016	0.015	0.016	0.018	0.018	0.016	0.013
6	0.092	0.043	0.022	0.018	0.017	0.018	0.020	0.020	0.018	0.014
8	0.103	0.049	0.024	0.020	0.020	0.020	0.023	0.023	0.020	0.016
10	0.111	0.054	0.027	0.022	0.021	0.022	0.025	0.024	0.021	0.017
20	0.139	0.070	0.035	0.029	0.027	0.028	0.031	0.031	0.027	0.022
40	0.174	0.090	0.046	0.037	0.036	0.036	0.039	0.038	0.033	0.027
60	0.230	0.121	0.064	0.050	0.048	0.048	0.053	0.052	0.045	0.035
80	0.286	0.152	0.079	0.064	0.061	0.061	0.066	0.065	0.056	0.046
100	0.306	0.165	0.087	0.070	0.067	0.066	0.072	0.070	0.061	0.050

ABSORBED FRACTIONS FOR UNIFORMLY DISTRIBUTED SOURCES IN SMALL UNIT-DENSITY ELLIPSOIDS SURROUNDED BY SCATTERING MEDIUM (AXES 1:2:4)

Mass (g)	Photon energy (MeV)									
	0.030	0.040	0.060	0.080	0.100	0.140	0.364	0.662	1.460	2.750
1	0.045	0.021	0.010	0.008	0.008	0.009	0.010	0.010	0.009	0.007
2	0.058	0.027	0.013	0.011	0.011	0.011	0.013	0.013	0.011	0.009
4	0.073	0.035	0.017	0.014	0.014	0.014	0.016	0.016	0.014	0.012
6	0.082	0.040	0.020	0.016	0.016	0.016	0.018	0.018	0.016	0.014
8	0.092	0.045	0.022	0.018	0.018	0.018	0.021	0.020	0.018	0.015
10	0.100	0.049	0.024	0.020	0.019	0.020	0.022	0.022	0.019	0.016
20	0.125	0.063	0.032	0.026	0.025	0.025	0.028	0.028	0.024	0.020
40	0.155	0.081	0.042	0.034	0.032	0.032	0.035	0.035	0.030	0.025
60	0.192	0.101	0.052	0.043	0.040	0.041	0.044	0.044	0.037	0.031
80	0.229	0.121	0.063	0.051	0.049	0.049	0.053	0.052	0.045	0.037
100	0.244	0.131	0.069	0.056	0.053	0.053	0.057	0.056	0.049	0.040

ABSORBED FRACTIONS FOR UNIFORMLY DISTRIBUTED SOURCES IN SMALL ELLIPSOIDS SURROUNDED BY SCATTERING MEDIUM (AXES 1:3:8)

Mass (g)	Photon energy (MeV)									
	0.030	0.040	0.060	0.080	0.100	0.140	0.364	0.662	1.460	2.750
1	0.041	0.019	0.009	0.008	0.007	0.008	0.009	0.009	0.008	0.007
2	0.049	0.023	0.011	0.009	0.009	0.010	0.011	0.011	0.010	0.008
4	0.063	0.030	0.015	0.012	0.012	0.012	0.014	0.014	0.012	0.010
6	0.071	0.034	0.017	0.014	0.013	0.014	0.016	0.016	0.013	0.012
8	0.079	0.038	0.019	0.016	0.015	0.016	0.018	0.018	0.015	0.013
10	0.085	0.042	0.021	0.017	0.017	0.017	0.019	0.019	0.016	0.014
20	0.117	0.059	0.031	0.024	0.024	0.024	0.027	0.027	0.022	0.019
40	0.158	0.080	0.041	0.034	0.032	0.033	0.036	0.036	0.031	0.025
60	0.179	0.093	0.048	0.039	0.037	0.038	0.041	0.041	0.035	0.029
80	0.197	0.104	0.054	0.045	0.042	0.043	0.046	0.045	0.039	0.032
100	0.212	0.113	0.060	0.049	0.046	0.046	0.050	0.049	0.043	0.035

ABSORBED FRACTIONS FOR A UNIFORM DISTRIBUTION OF ACTIVITY IN ELLIPSOIDS*

Mass (kg)	ϕ 0.020 MeV	0.030 MeV	0.040 MeV	0.060 MeV	0.080 MeV	0.100 MeV	0.160 MeV	0.364 MeV	0.662 MeV	1.460 MeV	2.750 MeV
2	0.702	0.407	0.317	0.131	0.072	0.099	0.113	0.112	0.134	0.099	0.096
4	0.762	0.485	0.325	0.176	0.127	0.133	0.144	0.148	0.155	0.133	0.120
6	0.795	0.529	0.345	0.206	0.157	0.155	0.163	0.170	0.173	0.155	0.134
8	0.815	0.560	0.366	0.228	0.179	0.172	0.178	0.187	0.189	0.171	0.147
10	0.830	0.583	0.385	0.247	0.196	0.185	0.190	0.200	0.202	0.183	0.156
20	0.868	0.649	0.460	0.308	0.250	0.233	0.234	0.245	0.250	0.223	0.187
30	0.884	0.685	0.508	0.346	0.284	0.265	0.264	0.273	0.280	0.248	0.207
40	0.893	0.709	0.541	0.374	0.310	0.290	0.287	0.294	0.301	0.267	0.222
50	0.900	0.727	0.567	0.397	0.332	0.312	0.305	0.312	0.317	0.282	0.235
60	0.905	0.741	0.585	0.416	0.351	0.330	0.321	0.327	0.330	0.294	0.247
70	0.909	0.753	0.600	0.432	0.368	0.346	0.335	0.340	0.341	0.306	0.257
80	0.912	0.763	0.613	0.446	0.383	0.361	0.348	0.351	0.351	0.316	0.265
90	0.916	0.772	0.624	0.459	0.397	0.374	0.359	0.362	0.360	0.325	0.274
100	0.918	0.780	0.634	0.471	0.409	0.386	0.369	0.371	0.368	0.334	0.283
120	0.924	0.793	0.652	0.492	0.431	0.407	0.388	0.389	0.384	0.350	0.298
140	0.929	0.804	0.670	0.511	0.450	0.425	0.405	0.405	0.399	0.364	0.310
160	0.933	0.814	0.688	0.528	0.466	0.440	0.421	0.420	0.415	0.378	0.321
180	0.937	0.821	0.708	0.544	0.480	0.454	0.436	0.433	0.432	0.391	0.331
200	0.940	0.828	0.729	0.559	0.491	0.466	0.451	0.446	0.449	0.403	0.340

* The principal axes of the ellipsoids are in the ratio of 1/1.8/9.27.

Not surrounded by scattering medium

ABSORBED FRACTIONS FOR UNIFORM DISTRIBUTION OF ACTIVITY IN SMALL SPHERES* AND THICK ELLIPSOIDS*

Mass (kg)	ϕ 0.020 MeV	0.030 MeV	0.040 MeV	0.060 MeV	0.080 MeV	0.100 MeV	0.160 MeV	0.364 MeV	0.662 MeV	1.460 MeV	2.750 MeV
0.3	0.684	0.357	0.191	0.109	0.086	0.085	0.087	0.099	0.096	0.092	0.077
0.4	0.712	0.388	0.212	0.121	0.096	0.093	0.097	0.108	0.108	0.099	0.083
0.5	0.731	0.412	0.229	0.131	0.104	0.099	0.104	0.116	0.117	0.104	0.089
0.6	0.745	0.431	0.244	0.140	0.111	0.105	0.111	0.122	0.124	0.109	0.093
1.0	0.780	0.486	0.289	0.167	0.135	0.125	0.130	0.142	0.144	0.125	0.106
2.0	0.818	0.559	0.360	0.212	0.173	0.160	0.162	0.174	0.173	0.153	0.127
3.0	0.840	0.600	0.405	0.245	0.201	0.188	0.186	0.197	0.195	0.174	0.143
4.0	0.856	0.629	0.438	0.271	0.222	0.209	0.205	0.216	0.213	0.190	0.156
5.0	0.868	0.652	0.464	0.294	0.241	0.227	0.222	0.231	0.228	0.204	0.167
6.0	0.876	0.671	0.485	0.312	0.258	0.241	0.236	0.245	0.240	0.216	0.177

* The principal axes of the small spheres and thick ellipsoids are in the ratios of 1/1/1 and 1/0.667/1.333.

Not surrounded by scattering medium

ABSORBED FRACTIONS FOR UNIFORM DISTRIBUTION OF ACTIVITY IN FLAT ELLIPSOIDS*

	ϕ								
Mass (kg)	0.020 MeV	0.030 MeV	0.040 MeV	0.060 MeV	0.080 MeV	0.100 MeV	0.160 MeV	0.662 MeV	2.75 MeV
0.3	0.627	0.306	0.164	0.090	0.075	0.072	0.078	0.084	0.062
0.4	0.654	0.334	0.179	0.098	0.081	0.079	0.085	0.095	0.069
0.5	0.674	0.356	0.192	0.106	0.087	0.085	0.090	0.103	0.074
0.6	0.690	0.374	0.204	0.112	0.092	0.090	0.095	0.109	0.079
1.0	0.731	0.423	0.243	0.134	0.109	0.106	0.112	0.128	0.093
2.0	0.779	0.492	0.305	0.173	0.140	0.133	0.140	0.154	0.112
3.0	0.803	0.533	0.344	0.200	0.162	0.154	0.159	0.171	0.125
4.0	0.820	0.564	0.372	0.221	0.181	0.171	0.174	0.185	0.136
5.0	0.833	0.588	0.394	0.238	0.197	0.185	0.187	0.197	0.146
6.0	0.844	0.608	0.414	0.254	0.211	0.198	0.198	0.209	0.156

* The principal axes of the flat ellipsoids are in the ratio of 1/0.5/2.0.

Not surrounded by scattering medium

FRACTIONAL INCREASE OF ABSORBED FRACTION IN CENTRAL ORGAN DUE TO BACKSCATTERED RADIATION FROM 70-kg PHANTOM SURROUNDING ORGAN

Energy (MeV)	0.020	0.030	0.040	0.060	0.080	0.100	0.160	0.364	0.662	1.46	2.75
Fractional increase of ϕ	1.01	1.08	1.19	1.24	1.28	1.26	1.17	1.05	1.04	1.02	1.01

```
IV G LEVEL  21                    MAIN                    DATE = 76099          08/56/48

      C THE FOLLOWING PROGRAM ATTEMPTS TO CALCULATE S-FACTORS. S IS DEFINED AS
      C DOSE EQUIVALENT PER UNIT CUMMULATED ACTIVITY. ITS UNITS ARE RADS PER
      C MICRO-CURIE HOUR. IT IS THE SUM TOTAL OF ALL THE EQUILIBRIUM DOSE
      C CONSTANTS OF A PARTICULAR ISOTOPE TIMES THEIR RESPECTIVE ABSORBED
      C DOSE FRACTIONS DIVIDED BY THE MASS OF A DEFINED ORGAN SHAPE.
      C THE S-FACTORS CALCULATED IN THIS PROGRAM ARE VALID ONLY FOR
      C TARGET ORGAN- SOURCE ORGAN THE SAME.
      C
      C THE FOLLOWING READS PERTAIN TO THE ISOTOPE OF INTEREST
      C
      C READS THE MAXIMUM NUMBER OF PENETRATING DELTAS, ALSO THE
      C NON-PENETRATING COMPONENT
            DIMENSION DELTPN (50)
            DIMENSION ENISO (50)
            DIMENSION M(6), ME(6)
            DIMENSION MASS (6,50)
            DIMENSION ENERGY (6,50)
            DIMENSION PHI (6,50,50)
            READ(5,1) MAXNOD
          1 FORMAT (I10)
            DO 2 I=1, MAXNOD
            READ(5,3) DELTPN(I)
          3 FORMAT (F10.0)
          2 CONTINUE
            READ (5,4) DELTNP
          4 FORMAT (F10.0)
      C READS THE PENETRATING ENERGIES
            DO 5 I=1, MAXNOD
            READ (5,6) ENISO(I)
          6 FORMAT (F10.0)
          5 CONTINUE
```

```
C THE FOLLOWING READS RECONSTRUCTS THE ABSORBED DOSE FRACTIONS IN
C ARRAY FORM
C
C READS MASS VALUE (INTEGER) AS A FUNCTION OF ORGAN SHAPE 1,2,3,4,5,6
      READ (5,7) M(1), M(2), M(3), M(4), M(5), M(6), ME(1), ME(2),
     1ME(3), ME(4), ME(5), ME(6)
    7 FORMAT (12I2)
      DO 8 I=1, 6
      KNOX=M(I)
      DO 8 J=1, KNOX
      READ (5,9) MASS(I,J)
    9 FORMAT (I10)
    8 CONTINUE
C READS ENERGY (REAL) AS A FUNCTION OF ORGAN SHAPE 1,2,3,4,5,6
      DO 10 I=1, 6
      KNOY=ME(I)
      DO 10 J=1, KNOY
      READ (5,11) ENERGY(I,J)
   11 FORMAT (F10.0)
   10 CONTINUE
C READS PHI (REAL) AS A FUNCTION OF ORGAN SHAPE, MASS, AND ENERGY
      DO 12 I=1, 6
      KNOZ=M(I)
      KNOXX=ME(I)
      DO 12 J=1, KNOZ
      DO 12 K=1, KNOXX
      READ (5,13) PHI(I,J,K)
   13 FORMAT (F10.0)
   12 CONTINUE
C THE FOLLOWING CHECKS TO SEE IF THE ENISO VALUE IS WITHIN
C THE RANGE OF THE ENERGY VALUES FOR THE VARIOUS ORGAN SHAPES
      DO 14 MO=1, 6
```

```
      DO 14 L=1, MAXNOD
      IF (ENISO(L) .LT. ENERGY(MO,1) .OR. ENISO(L) .GT. ENERGY(MO,ME(MO)
     1)) GO TO 555
   14 CONTINUE
C THE FOLLOWING IS THE LINEAR INTERPOLATION OF PHI BASED ON THE INDIVIDU
C AL ENISO AS A FUNCTION OF ORGAN SHAPE AND MASS
      WRITE (6,30)
   30 FORMAT (1H1,11HORGAN SHAPE,20X,10HMASS-GRAMS,20X, 8HS-FACTOR///)
      DO 15 I=1,6
      KNOYY=M(I)
      DO 15 J=1, KNOYY
C SET THE SUM TOTAL OF PHI TIMES DELPN EQUAL
C TO ZERO
      SIGMA = 0.0
      DO 16 L=1,MAXNOD
C BEGIN SEARCH FOR NEXT HIGHEST ENERGY ABOVE ENISO
      K=2
   20 IF (ENISO(L)-ENERGY(I,K)) 200,18,19
C NOT FOUND YET
   19 K=K+1
C CHECK TO SEE IF K IS LARGER THAN MAXIMUM NO. OF ENERGIES AVAILABLE
      IF (K .GT. ME (I)) GO TO 666
      GO TO 20
C EQUAL
   18 PHIO=PHI (I,J,K)
      GO TO 21
C TWO ENERGY VALUES BRACKET GIVEN
C ENISO VALUE
  200 IF (PHI(I,J,K) - PHI(I,J,K-1)) 202,201,201
C PHI INCREASING
  201 PHIO = PHI(I,J,K-1) + (ENISO(L) - ENERGY(I,K-1)) * (PHI(I,J,K) - P
     1HI(I,J,K-1)) / (ENERGY(I,K) - ENERGY(I,K-1))
      GO TO 21
C PHI DECREASING
  202 PHIO = PHI(I,J,K) + (ENERGY(I,K) - ENISO(L)) * (PHI(I,J,K-1) - PHI
     1(I,J,K)) / (ENERGY(I,K) - ENERGY(I,K-1))
      GO TO 21
```

```
C CALCULATE PHI TIMES DELTA PENETRATING
   21 PHIDEL=PHIO * DELTPN(L)
C SUM UP ALL PHI TIMES DELTAS OVER ALL PENETRATING ENERGIES OF THE
C ISOTOPE
      SIGMA = SIGMA + PHIDEL
   16 CONTINUE

C ADD NON PENETRATING COMPONENT
      SIGMA=SIGMA+DELTNP
      AMASS=MASS (I,J)
      SIGMA=SIGMA/AMASS
      WRITE (6,25) I, MASS (I,J), SIGMA
   25 FORMAT (1H0,5X,I1,21X,I10,1PE34.4)
   15 CONTINUE
      GO TO 100
  555 WRITE (6,556)
  556 FORMAT (41HENERGY OF ISOTOPE EXCEEDS RANGE OF TABLES)
      GO TO 999
  666 WRITE (6,667)
  667 FORMAT (43HINTERPOLATION INDEX EXCEEDS NO. OF ENERGIES)
      GO TO 999
  100 WRITE (6,101) DELTNP
  101 FORMAT (///,' TOTAL EQUILIBRIUM DOSE CONSTANT FOR NON PENETRATING
     1RADIATION IS ', F10.4,///,' ORGAN CODE ',//,' 1.     SMALL UNIT DE
     2NSITY SPHERES AXES RATIO 1/1/1 ',//,' 2.     SMALL UNIT DENSITY EL
     3LIPSOIDS AXES RATIO 1/2/4 ',//,' 3.     SMALL UNIT DENSITY ELLIPSO
     4IDS AXES RATIO 1/3/8 ',//,' 4.     SMALL UNIT DENSITY SPHERES AND
     5THICK ELLIPSOIDS AXES RATIO 1/1/1 AND 1/0.667/1.333 ',//,' 5.
     6UNIT DENSITY FLAT ELLIPSOIDS AXES RATIO 1/0.5/2.0 ',//,' 6.     UN
     7IT DENSITY ELLIPSOIDS AXES RATIO 1/1.8/9.27 ')
      WRITE (6,102)
  102 FORMAT (///,' THE ISOTOPE IS INDIUM-113M ')
  999 STOP
      END
```

1 gram	S =	8.6190E-01
2		4.3421E-01
4		2.1928E-01
6		1.4691E-01
8		1.1100E-01
10		8.9124E-02
20		4.5267E-02
40		2.3041E-02
60		1.5868E-02
80		1.2254E-02
100		9.9228E-03

Small Unit Density Spheres (With Backscatter)

1gram	S=	8.5972E-01
2		4.3312E-01
4		2.1819E-01
6		1.4618E-01
8		1.1032E-01
10		8.8579E-02
20		4.4941E-02
40		2.2851E-02
60		1.5560E-02
80		1.1901E-02
100		9.6076E-03

Small Unit Density Ellipsoids, Axes Ratio 1/2/4 (With Backscatter)

1gram	S =	8.5755E-01
2		4.3095E-01
4		2.1710E-01
6		1.4546E-01
8		1.0964E-01
10		8.7928E-02
20		4.4833E-02
40		2.2905E-02
60		1.5451E-02
80		1.1711E-02
100		9.4555E-03

Small Unit Density Ellipsoids, Axes Ratio 1/3/8 (With Backscatter)

300 gram	S =	3.5322E-03
400		2.7061E-03
500		2.2061E-03
600		1.8619E-03
1000		1.1628E-03
2000		6.1618E-04
3000		4.2781E-04
4000		3.3145E-04
5000		2.7190E-04
6000		2.3147E-04

Small Unit Density Spheres and Thick Ellipsoids, Axes Ratio 1/.667/1.333 (With Backscatter)

^{11}C

300 gram	Unit Density Flat Ellipsoids, Axes Ratio 1/.5/2.0 (With Backscatter)	S =	3.4321E-03
400			2.6327E-03
500			2.1383E-03
600			1.8036E-03
1000			1.1256E-03
2000			5.9411E-04
3000			4.0998E-04
4000			3.1574E-04
5000			2.5850E-04
6000			2.1987E-04
2000 gram	Unit Density Ellipsoids, Axes Ratio 1/1.8/9.27 (No Backscatter)	S =	5.5245E-04
4000			2.9176E-04
6000			2.0176E-04
8000			1.5580E-04
10000			1.2746E-04
20000			6.8781E-05
30000			4.7953E-05
40000			3.7105E-05
50000			3.0424E-05
60000			2.5860E-05
70000			2.2539E-05
80000			2.0007E-05
90000			1.8026E-05
100000			1.6408E-05
120000			1.3981E-05
140000			1.2225E-05

Small Unit Density Spheres (With Backscatter)

1	gram	S = 7.1559E-01
2		3.6073E-01
4		1.8234E-01
6		1.2222E-01
8		9.2400E-02
10		7.4214E-02
20		3.7749E-02
40		1.9244E-02
60		1.3288E-02
80		1.0287E-02
100		8.3376E-03

Small Unit Density Ellipsoids, Axes Ratio 1/2/4 (With Backscatter)

1	gram	S = 7.1362E-01
2		3.5974E-01
4		1.8135E-01
6		1.2156E-01
8		9.1784E-02
10		7.3724E-02
20		3.7452E-02
40		1.9071E-02
60		1.3009E-02
80		9.9666E-03
100		8.0524E-03

Small Unit Density Ellipsoids, Axes Ratio 1/3/8 (With Backscatter)

1	gram	S = 7.1164E-01
2		3.5780E-01
4		1.8037E-01
6		1.2090E-01
8		9.1167E-02
10		7.3131E-02
20		3.7352E-02
40		1.9121E-02
60		1.2911E-02
80		9.7943E-03
100		7.9144E-03

Small Unit Density Spheres and Thick Ellipsoids, Axes Ratio 1/.667/1.333 (With Backscatter)

300	gram	S = 2.9841E-03
400		2.2898E-03
500		1.8690E-03
600		1.5789E-03
1000		9.8875E-04
2000		5.2596E-04
3000		3.6613E-04
4000		2.8422E-04
5000		2.3351E-04
6000		1.9904E-04

^{43}K

300 gram	S =	2.8930E-03
400		2.2231E-03
500		1.8077E-03
600		1.5261E-03
1000		9.5516E-04
2000		5.0595E-04
3000		3.4991E-04
4000		2.6992E-04
5000		2.2130E-04
6000		1.8847E-04

Unit Density Flat Ellipsoids, Axes Ratio 1/.5/2.0 (With Backscatter)

2000gram	S =	4.6819E-04
4000		2.4818E-04
6000		1.7204E-04
8000		1.3310E-04
10000		1.0905E-04
20000		5.9108E-05
30000		4.1314E-05
40000		3.2023E-05
50000		2.6289E-05
60000		2.2367E-05
70000		1.9511E-05
80000		1.7332E-05
90000		1.5625E-05
100000		1.4231E-05
120000		1.2139E-05
140000		1.0624E-05

Unit Density Ellipsoids, Axes Ratio 1/1.8/9.27 (No Backscatter)

1	gram	S = 1.6450E-01
2		8.2250E-02
4		4.1125E-02
6		2.7417E-02
8		2.0562E-02
10		1.6450E-02
20		8.2250E-03
40		4.1125E-03
60		2.7417E-03
80		2.0562E-03
100		1.6450E-03

Small Unit Density Spheres (With Backscatter)

1	gram	S = 1.6450E-01
2		8.2250E-02
4		4.1125E-02
6		2.7417E-02
8		2.0562E-02
10		1.6450E-02
20		8.2250E-03
40		4.1125E-03
60		2.7417E-03
80		2.0562E-03
100		1.6450E-03

Small Unit Density Ellipsoids, Axes Ratio 1/2/4 (With Backscatter)

1	gram	S = 1.6450E-01
2		8.2250E-02
4		4.1125E-02
6		2.7417E-02
8		2.0562E-02
10		1.6450E-02
20		8.2250E-03
40		4.1125E-03
60		2.7417E-03
80		2.0562E-03
100		1.6450E-03

Small Unit Density Ellipsoids, Axes Ratio 1/3/8 (With Backscatter)

300	gram	S = 5.4833E-04
400		4.1125E-04
500		3.2900E-04
600		2.7417E-04
1000		1.6450E-04
2000		8.2250E-05
3000		5.4833E-05
4000		4.1125E-05
5000		3.2900E-05
6000		2.7417E-05

Small Unit Density Spheres and Thick Ellipsoids, Axes Ratio 1/.667/1.333 (With Backscatter)

^{45}Ca

Unit Density Flat Ellipsoids, Axes Ratio 1/.5/2.0 (With Backscatter)

300	gram	S = 5.4833E-04
400		4.1125E-04
500		3.2900E-04
600		2.7417E-04
1000		1.6450E-04
2000		8.2250E-05
3000		5.4833E-05
4000		4.1125E-05
5000		3.2900E-05
6000		2.7417E-05

Unit Density Ellipsoids, Axes Ratio 1/1.8/9.27 (No Backscatter)

2000	gram	S = 8.2250E-05
4000		4.1125E-05
6000		2.7417E-05
8000		2.0562E-05
10000		1.6450E-05
20000		8.2250E-06
30000		5.4833E-06
40000		4.1125E-06
50000		3.2900E-06
60000		2.7417E-06
70000		2.3500E-06
80000		2.0562E-06
90000		1.8278E-06
100000		1.6450E-06
120000		1.3708E-06
140000		1.1750E-06

^{51}Cr

1 gram	S =	1.0850E-02
2		5.5222E-03
4		2.8305E-03
6		1.9101E-03
8		1.4569E-03
10		1.1794E-03
20		6.1052E-04
40		3.1914E-04
60		2.2850E-04
80		1.8265E-04
100		1.5015E-04

Small Unit Density Spheres (With Backscatter)

1 gram	S =	1.0780E-02
2		5.4875E-03
4		2.7958E-03
6		1.8870E-03
8		1.4396E-03
10		1.1600E-03
20		6.0011E-04
40		3.1220E-04
60		2.1854E-04
80		1.7155E-04
100		1.4001E-04

Small Unit Density Ellipsoids, Axes Ratio 1/2/4 (With Backscatter)

1 gram	S =	1.0711E-02
2		5.4249E-03
4		2.7611E-03
6		1.8639E-03
8		1.4152E-03
10		1.1391E-03
20		5.9664E-04
40		3.1394E-04
60		2.1507E-04
80		1.6564E-04
100		1.3515E-04

Small Unit Density Ellipsoids, Axes Ratio 1/3/8 (With Backscatter)

300 gram	S =	5.7625E-05
400		4.4855E-05
500		3.7134E-05
600		3.1689E-05
1000		2.0485E-05
2000		1.1452E-05
3000		8.2101E-06
4000		6.5121E-06
5000		5.4437E-06
6000		4.7034E-06

Small Unit Density Spheres and Thick Ellipsoids, Axes Ratio 1/.667/1.333 (With Backscatter)

^{51}Cr

300	gram	S =	5.4423E-05
400			4.2426E-05
500			3.4862E-05
600			2.9746E-05
1000	Unit Density Flat Ellipsoids, Axes Ratio 1/.5/2.0 (With Backscatter)		1.9236E-05
2000			1.0697E-05
3000			7.6105E-06
4000			5.9980E-06
5000			4.9978E-06
6000			4.3115E-06
2000	gram	S =	8.9439E-06
4000			5.0778E-06
6000			3.6322E-06
8000			2.8679E-06
10000			2.3830E-06
20000			1.3469E-06
30000			9.6372E-07
40000	Unit Density Ellipsoids, Axes Ratio 1/1.8/9.27 (No Backscatter)		7.5997E-07
50000			6.3296E-07
60000			5.4507E-07
70000			4.8030E-07
80000			4.3018E-07
90000			3.9087E-07
100000			3.5817E-07
120000			3.0901E-07
140000			2.7291E-07

^{57}Co

Small Unit Density Spheres (With Backscatter)

1	gram	S = 5.1765E-02
2		2.6195E-02
4		1.3330E-02
6		8.9727E-03
8		6.8074E-03
10		5.4870E-03
20		2.8211E-03
40		1.4647E-03
60		1.0264E-03
80		8.1310E-04
100		6.6441E-04

Small Unit Density Ellipsoids, Axes Ratio 1/2/4 (With Backscatter)

1	gram	S = 5.1507E-02
2		2.6065E-02
4		1.3227E-02
6		8.9038E-03
8		6.7425E-03
10		5.4352E-03
20		2.7875E-03
40		1.4389E-03
60		9.9627E-04
80		7.7432E-04
100		6.2977E-04

Small Unit Density Ellipsoids, Axes Ratio 1/3/8 (With Backscatter)

1	gram	S = 5.1249E-02
2		2.5882E-02
4		1.3097E-02
6		8.8003E-03
8		6.6647E-03
10		5.3680E-03
20		2.7745E-03
40		1.4428E-03
60		9.8336E-04
80		7.5360E-04
100		6.1169E-04

Small Unit Density Spheres and Thick Ellipsoids, Axes Ratio 1/.667/1.333 (With Backscatter)

300	gram	S = 2.5442E-04
400		1.9755E-04
500		1.6238E-04
600		1.3850E-04
1000		8.9378E-05
2000		5.0022E-05
3000		3.6098E-05
4000		2.8637E-05
5000		2.4026E-05
6000		2.0755E-05

^{57}Co

Unit Density Flat Ellipsoids, Axes Ratio 1/.5/2.0 (With Backscatter)

300	gram	S = 2.4225E-04
400		1.8729E-04
500		1.5326E-04
600		1.3031E-04
1000		8.3499E-05
2000		4.6068E-05
3000		3.2799E-05
4000		2.5868E-05
5000		2.1556E-05
6000		1.8596E-05

Unit Density Ellipsoids, Axes Ratio 1/1.8/9.27 (No Backscatter)

2000	gram	S = 3.8145E-05
4000		2.1182E-05
6000		1.5014E-05
8000		1.1782E-05
10000		9.7495E-06
20000		5.4709E-06
30000		3.9140E-06
40000		3.0904E-06
50000		2.5768E-06
60000		2.2206E-06
70000		1.9589E-06
80000		1.7594E-06
90000		1.5986E-06
100000		1.4674E-06
120000		1.2659E-06
140000		1.1172E-06

1 gram	S =	2.7727E-01
2		1.4159E-01
4		7.3327E-02
6		4.9729E-02
8		3.8036E-02
10		3.0683E-02
20		1.6143E-02
40		8.4734E-03
60		6.1836E-03
80		5.0074E-03
100		4.1325E-03

Small Unit Density Spheres (With Backscatter)

1 gram	S =	2.7474E-01
2		1.4032E-01
4		7.2061E-02
6		4.8885E-02
8		3.7297E-02
10		3.0176E-02
20		1.5764E-02
40		8.2831E-03
60		5.8461E-03
80		4.6379E-03
100		3.8116E-03

Small Unit Density Ellipsoids, Axes Ratio 1/2/4 (With Backscatter)

1 gram	S =	2.7220E-01
2		1.3863E-01
4		7.0795E-02
6		4.7762E-02
8		3.6454E-02
10		2.9417E-02
20		1.5553E-02
40		8.3464E-03
60		5.7474E-03
80		4.4374E-03
100		3.6511E-03

Small Unit Density Ellipsoids, Axes Ratio 1/3/8 (With Backscatter)

300 gram	S =	1.6477E-03
400		1.2908E-03
500		1.0665E-03
600		9.1275E-04
1000		5.9415E-04
2000		3.3345E-04
3000		2.4062E-04
4000		1.9167E-04
5000		1.6061E-04
6000		1.3906E-04

Small Unit Density Spheres and Thick Ellipsoids, Axes Ratio 1/.667/1.333 (With Backscatter)

^{59}Fe

300	gram	S =	1.5204E-03
400			1.2081E-03
500			1.0031E-03
600			8.5591E-04
1000	Unit Density Flat Ellipsoids, Axes Ratio 1/.5/2.0 (With Backscatter)		5.6291E-04
2000			3.1313E-04
3000			2.2290E-04
4000			1.7557E-04
5000			1.4667E-04
6000			1.2718E-04
2000	gram	S =	2.6575E-04
4000			1.5165E-04
6000			1.0982E-04
8000			8.7426E-05
10000			7.3064E-05
20000			4.1937E-05
30000	Unit Density Ellipsoids, Axes Ratio 1/1.8/9.27 (No Backscatter)		3.0211E-05
40000			2.3905E-05
50000			1.9901E-05
60000			1.7106E-05
70000			1.5085E-05
80000			1.3516E-05
90000			1.2268E-05
100000			1.1261E-05
120000			9.7221E-06
140000			8.5928E-06

^{67}Ga

1 gram	S =	8.9561E-02
2		4.5220E-02
4		2.2927E-02
6		1.5395E-02
8		1.1653E-02
10		9.3821E-03
20		4.7920E-03
40		2.4633E-03
60		1.7133E-03
80		1.3390E-03
100		1.0899E-03

Small Unit Density Spheres (With Backscatter)

1 gram	S =	8.9230E-02
2		4.5055E-02
4		2.2775E-02
6		1.5294E-02
8		1.1569E-02
10		9.3031E-03
20		4.7451E-03
40		2.4311E-03
60		1.6694E-03
80		1.2874E-03
100		1.0434E-03

Small Unit Density Ellipsoids, Axes Ratio 1/2/4 (With Backscatter)

1 gram	S =	8.8928E-02
2		4.4781E-02
4		2.2610E-02
6		1.5174E-02
8		1.1464E-02
10		9.2092E-03
20		4.7271E-03
40		2.4373E-03
60		1.6524E-03
80		1.2602E-03
100		1.0203E-03

Small Unit Density Ellipsoids, Axes Ratio 1/3/8 (With Backscatter)

300 gram	S =	4.0212E-04
400		3.0941E-04
500		2.5400E-04
600		2.1562E-04
1000		1.3699E-04
2000		7.4808E-05
3000		5.2987E-05
4000		4.1583E-05
5000		3.4541E-05
6000		2.9669E-05

Small Unit Density Spheres and Thick Ellipsoids, Axes Ratio 1/.667/1.333 (With Backscatter)

^{67}Ga

Unit Density Flat Ellipsoids, Axes Ratio 1/.5/2.0 (With Backscatter)

300	gram	S = 3.8734E-04
400		2.9780E-04
500		2.4260E-04
600		2.0551E-04
1000		1.3003E-04
2000		7.0428E-05
3000		4.9420E-05
4000		3.8586E-05
5000		3.1899E-05
6000		2.7340E-05

Unit Density Ellipsoids, Axes Ratio 1/1.8/9.27 (No Backscatter)

2000	gram	S = 6.0843E-05
4000		3.3323E-05
6000		2.3399E-05
8000		1.8238E-05
10000		1.5019E-05
20000		8.2688E-06
30000		5.8425E-06
40000		4.5705E-06
50000		3.7816E-06
60000		3.2404E-06
70000		2.8443E-06
80000		2.5413E-06
90000		2.3013E-06
100000		2.1045E-06
120000		1.8066E-06
140000		1.5885E-06

1 gram	S=	4.9695E-02
2		2.5838E-02
4		1.3691E-02
6		9.3878E-03
8		7.2880E-03
10		5.9816E-03
20		3.2261E-03
40		1.7701E-03
60		1.3488E-03
80		1.1388E-03
100		9.5416E-04

Small Unit Density Spheres (With Backscatter)

1 gram	S =	4.8913E-02
2		2.5447E-02
4		1.3310E-02
6		9.1339E-03
8		7.0911E-03
10		5.7890E-03
20		3.1108E-03
40		1.6923E-03
60		1.2448E-03
80		1.0168E-03
100		8.4473E-04

Small Unit Density Ellipsoids, Axes Ratio 1/2/4 (With Backscatter)

1 gram	S =	4.8133E-02
2		2.4847E-02
4		1.2919E-02
6		8.8666E-03
8		6.8453E-03
10		5.5585E-03
20		3.0717E-03
40		1.7107E-03
60		1.2057E-03
80		9.5296E-04
100		7.9000E-04

Small Unit Density Ellipsoids, Axes Ratio 1/3/8 (With Backscatter)

300 gram	S =	4.0809E-04
400		3.2563E-04
500		2.7445E-04
600		2.3782E-04
1000		1.5993E-04
2000		9.4372E-05
3000		6.9957E-05
4000		5.6683E-05
5000		4.8244E-05
6000		4.2201E-05

Small Unit Density Spheres and Thick Ellipsoids, Axes Ratio 1/.667/1.333 (With Backscatter)

^{75}Se

300 gram		S = 3.7359E-04
400		2.9758E-04
500		2.4825E-04
600		2.1469E-04
1000	Unit Density Flat Ellipsoids, Axes Ratio 1/.5/2.0 (With Backscatter)	1.4455E-04
2000		8.4774E-05
3000		6.2175E-05
4000		5.0071E-05
5000		4.2399E-05
6000		3.7049E-05
2000 gram		S = 6.4210E-05
4000		3.8641E-05
6000		2.8456E-05
8000		2.2919E-05
10000		1.9320E-05
20000		1.1419E-05
30000		8.3777E-06
40000	Unit Density Ellipsoids, Axes Ratio 1/1.8/9.27 (No Backscatter)	6.7197E-06
50000		5.6643E-06
60000		4.9255E-06
70000		4.3755E-06
80000		3.9489E-06
90000		3.6075E-06
100000		3.3231E-06
120000		2.8914E-06
140000		2.5713E-06

1	gram	S = 4.1331E-02
2		2.0937E-02
4		1.0737E-02
6		7.2475E-03
8		5.5031E-03
10		4.4560E-03
20		2.3086E-03
40		1.2079E-03
60		8.5500E-04
80		6.8781E-04
100		5.6364E-04

Small Unit Density Spheres (With Backscatter)

1	gram	S = 4.1062E-02
2		2.0802E-02
4		1.0603E-02
6		7.1579E-03
8		5.4357E-03
10		4.4021E-03
20		2.2683E-03
40		1.1811E-03
60		8.2755E-04
80		6.4751E-04
100		5.2871E-04

Small Unit Density Ellipsoids, Axes Ratio 1/2/4 (With Backscatter)

1	gram	S = 4.0794E-02
2		2.0665E-02
4		1.0468E-02
6		7.0681E-03
8		5.3680E-03
10		4.3214E-03
20		2.2547E-03
40		1.1877E-03
60		8.1414E-04
80		6.2731E-04
100		5.0992E-04

Small Unit Density Ellipsoids, Axes Ratio 1/3/8 (With Backscatter)

300	gram	S = 2.2103E-04
400		1.7296E-04
500		1.4303E-04
600		1.2261E-04
1000		7.9785E-05
2000		4.5194E-05
3000		3.2803E-05
4000		2.6145E-05
5000		2.2025E-05
6000		1.9088E-05

Small Unit Density Spheres and Thick Ellipsoids, Axes Ratio 1/.667/1.333 (With Backscatter)

^{99m}Tc

300	gram	S =	2.0949E-04
400			1.6276E-04
500			1.3364E-04
600			1.1406E-04
1000	Unit Density Flat Ellipsoids, Axes Ratio 1/.5/2.0 (With Backscatter)		7.3882E-05
2000			4.1384E-05
3000			2.9653E-05
4000			2.3498E-05
5000			1.9645E-05
6000			1.6988E-05
2000	gram	S =	3.3803E-05
4000			1.9041E-05
6000			1.3583E-05
8000			1.0708E-05
10000			8.8944E-06
20000			5.0478E-06
30000			3.6353E-06
40000	Unit Density Ellipsoids, Axes Ratio 1/1.8/9.27 (No Backscatter)		2.8826E-06
50000			2.4080E-06
60000			2.0798E-06
70000			1.8379E-06
80000			1.6532E-06
90000			1.5037E-06
100000			1.3814E-06
120000			1.1943E-06

Small Unit Density Spheres (With Backscatter)

1 gram	S = 1.0148E-01
2	5.1900E-02
4	2.6892E-02
6	1.8254E-02
8	1.3970E-02
10	1.1363E-02
20	5.9676E-03
40	3.1729E-03
60	2.2184E-03
80	1.8899E-03
100	1.5615E-03

Small Unit Density Ellipsoids, Axes Ratio 1/2/4 (With Backscatter)

1 gram	S = 1.0052E-01
2	5.1405E-02
4	2.6425E-02
6	1.7933E-02
8	1.3726E-02
10	1.1139E-02
20	5.8245E-03
40	3.0773E-03
60	2.1922E-03
80	1.7430E-03
100	1.4315E-03

Small Unit Density Ellipsoids, Axes Ratio 1/3/8 (With Backscatter)

1 gram	S = 9.9581E-02
2	5.0725E-02
4	2.5943E-02
6	1.7607E-02
8	1.3439E-02
10	1.0850E-02
20	5.7722E-03
40	3.1000E-03
60	2.1450E-03
80	1.6665E-03
100	1.3649E-03

Small Unit Density Spheres and Thick Ellipsoids, Axes Ratio 1/.667/1.333 (With Backscatter)

300 gram	S = 6.2093E-04
400	4.9032E-04
500	4.0888E-04
600	3.5208E-04
1000	2.3100E-04
2000	1.3179E-04
3000	9.5649E-05
4000	7.6379E-05
5000	6.4350E-05
6000	5.5831E-05

^{111}In

300	gram	S = 5.7990E-04
400		4.5539E-04
500		3.7634E-04
600		3.2307E-04
1000		2.1221E-04
2000		1.2063E-04
3000		8.6770E-05
4000		6.8926E-05
5000		5.7721E-05
6000		4.9973E-05

Unit Density Flat Ellipsoids, Axes Ratio 1/.5/2.0 (With Backscatter)

2000	gram	S = 9.7627E-05
4000		5.6179E-05
6000		4.0433E-05
8000		3.2052E-05
10000		2.6727E-05
20000		1.5286E-05
30000		1.1031E-05
40000		8.7497E-06
50000		7.3051E-06
60000		6.3089E-06
70000		5.5730E-06
80000		5.0072E-06
90000		4.5541E-06
100000		4.1804E-06
120000		3.6150E-06
140000		3.1989E-06

Unit Density Ellipsoids, Axes Ratio 1/1.8/9.27 (No Backscatter)

Small Unit Density Spheres (With Backscatter)

1 gram	S = 3.1328E-01
2	1.5748E-01
4	7.9292E-02
6	5.3049E-02
8	3.9993E-02
10	3.2100E-02
20	1.6219E-02
40	8.2194E-03
60	5.5792E-03
80	4.2963E-03
100	3.4693E-03

Small Unit Density Ellipsoids, Axes Ratio 1/2/4 (With Backscatter)

1 gram	S = 3.1272E-01
2	1.5719E-01
4	7.9016E-02
6	5.2862E-02
8	3.9846E-02
10	3.1940E-02
20	1.6136E-02
40	8.1648E-03
60	5.5261E-03
80	4.2061E-03
100	3.3869E-03

Small Unit Density Ellipsoids, Axes Ratio 1/3/8 (With Backscatter)

1 gram	S = 3.1217E-01
2	1.5664E-01
4	7.8736E-02
6	5.2674E-02
8	3.9644E-02
10	3.1772E-02
20	1.6107E-02
40	8.1784E-03
60	5.4984E-03
80	4.1574E-03
100	3.3479E-03

Small Unit Density Spheres and Thick Ellipsoids, Axes Ratio 1/.667/1.333 (With Backscatter)

300 gram	S = 1.2132E-03
400	9.2281E-04
500	7.4819E-04
600	6.2908E-04
1000	3.8887E-04
2000	2.0348E-04
3000	1.3990E-04
4000	1.0757E-04
5000	8.7749E-05
6000	7.4352E-05

^{113m}In

300	gram	S = 1.1860E-03
400		9.0311E-04
500		7.3016E-04
600		6.1399E-04
1000	Unit Density Flat Ellipsoids, Axes Ratio 1/.5/2.0 (With Backscatter)	3.7930E-04
2000		1.9783E-04
3000		1.3550E-04
4000		1.0379E-04
5000		8.4532E-05
6000		7.1557E-05
2000	gram	S = 1.8477E-04
4000		9.7065E-05
6000		6.6651E-05
8000		5.1120E-05
10000		4.1591E-05
20000		2.1998E-05
30000	Unit Density Ellipsoids, Axes Ratio 1/1.8/9.27 (No Backscatter)	1.5161E-05
40000		1.1648E-05
50000		9.5054E-06
60000		8.0508E-06
70000		6.9968E-06
80000		6.1937E-06
90000		5.5686E-06
100000		5.0584E-06
120000		4.2931E-06

Small Unit Density Spheres (With Backscatter)

1 gram	S = 7.2210E-02
2	3.6754E-02
4	1.8877E-02
6	1.2770E-02
8	9.7225E-03
10	7.8745E-03
20	4.0936E-03
40	2.1477E-03
60	1.3829E-03
80	1.2346E-03
100	1.0125E-03

Small Unit Density Ellipsoids, Axes Ratio 1/2/4 (With Backscatter)

1 gram	S = 7.1677E-02
2	3.6464E-02
4	1.8632E-02
6	1.2592E-02
8	9.5820E-03
10	7.7597E-03
20	4.0158E-03
40	2.0957E-03
60	1.4712E-03
80	1.1556E-03
100	9.4357E-04

Small Unit Density Ellipsoids, Axes Ratio 1/3/8 (With Backscatter)

1 gram	S = 7.1189E-02
2	3.6083E-02
4	1.8366E-02
6	1.2407E-02
8	9.4271E-03
10	7.5997E-03
20	3.9823E-03
40	2.1068E-03
60	1.4460E-03
80	1.1138E-03
100	9.0754E-04

Small Unit Density Spheres and Thick Ellipsoids, Axes Ratio 1/.667/1.333 (With Backscatter)

300 gram	S = 3.8506E-04
400	3.0131E-04
500	2.4912E-04
600	2.1324E-04
1000	1.3753E-04
2000	7.6361E-05
3000	5.4431E-05
4000	4.2867E-05
5000	3.5735E-05
6000	3.0748E-05

$^{123}_{I}$

300	gram	S =	3.6387E-04
400			2.8312E-04
500			2.3255E-04
600			1.9851E-04
1000	Unit Density Flat Ellipsoids, Axes Ratio 1/.5/2.0 (With Backscatter)		1.2785E-04
2000			7.0723E-05
3000			5.0084E-05
4000			3.9315E-05
5000			3.2610E-05
6000			2.8010E-05
2000	gram	S =	6.0059E-05
4000			3.3338E-05
6000			2.3559E-05
8000			1.8435E-05
10000			1.5229E-05
20000			8.4505E-06
30000	Unit Density Ellipsoids, Axes Ratio 1/1.8/9.27 (No Backscatter)		5.9957E-06
40000			4.6997E-06
50000			3.8866E-06
60000			3.3307E-06
70000			2.9234E-06
80000			2.6128E-06
90000			2.3645E-06
100000			2.1620E-06
120000			1.8550E-06
140000			1.6308E-06

1	gram	S= 5.6650E-02
2		2.8862E-02
4		1.4757E-02
6		9.9783E-03
8		7.5895E-03
10		6.1335E-03
20		3.1747E-03
40		1.6548E-03
60		9.1783E-04
80		9.3520E-04
100		7.6365E-04

Small Unit Density Spheres (With Backscatter)

1	gram	S= 5.6268E-02
2		2.8632E-02
4		1.4604E-02
6		9.8518E-03
8		7.4848E-03
10		6.0493E-03
20		3.1209E-03
40		1.6184E-03
60		1.1264E-03
80		8.8036E-04
100		7.1592E-04

Small Unit Density Ellipsoids, Axes Ratio 1/2/4 (With Backscatter)

1	gram	S = 5.5961E-02
2		2.8288E-02
4		1.4412E-02
6		9.7107E-03
8		7.3598E-03
10		5.9343E-03
20		3.0902E-03
40		1.6239E-03
60		1.1096E-03
80		8.4960E-04
100		6.9126E-04

Small Unit Density Ellipsoids, Axes Ratio 1/3/8 (With Backscatter)

300	gram	S = 2.7426E-04
400		2.1268E-04
500		1.7444E-04
600		1.4812E-04
1000		9.3717E-05
2000		4.9995E-05
3000		3.4510E-05
4000		2.6514E-05
5000		2.1612E-05
6000		1.8283E-05

Small Unit Density Spheres and Thick Ellipsoids, Axes Ratio 1/.667/1.333 (With Backscatter)

I

300	gram	S= 2.5799E-04
400		2.0007E-04
500		1.6394E-04
600		1.3941E-04
1000	Unit Density Flat Ellipsoids, Axes Ratio 1/.5/2.0 (With Backscatter)	8.8086E-05
2000		4.7090E-05
3000		3.2595E-05
4000		2.5105E-05
5000		2.0497E-05
6000		1.7374E-05
2000	gram	S = 4.2130E-05
4000		2.2631E-05
6000		1.5685E-05
8000		1.2076E-05
10000		9.8483E-06
20000		5.1928E-06
30000		3.5578E-06
40000		2.7157E-06
50000	Unit Density Ellipsoids, Axes Ratio 1/1.8/9.27 (No Backscatter)	2.2011E-06
60000		1.8525E-06
70000		1.6012E-06
80000		1.4107E-06
90000		1.2619E-06
100000		1.1418E-06
120000		9.6019E-07
140000		8.2942E-07

1	gram	S= 4.1748E-01
2		2.0995E-01
4		1.0579E-01
6		7.0798E-02
8		5.3400E-02
10		4.2871E-02
20		2.1686E-02
40		1.1003E-02
60		7.5153E-03
80		5.7752E-03
100		4.6676E-03

Small Unit Density Spheres (With Backscatter)

1	gram	S= 4.1666E-01
2		2.0954E-01
4		1.0538E-01
6		7.0526E-02
8		5.3182E-02
10		4.2641E-02
20		2.1564E-02
40		1.0924E-02
60		7.4046E-03
80		5.6433E-03
100		4.5471E-03

Small Unit Density Ellipsoids, Axes Ratio 1/2/4 (With Backscatter)

1	gram	S = 4.1585E-01
2		2.0874E-01
4		1.0497E-01
6		7.0254E-02
8		5.2893E-02
10		4.2397E-02
20		2.1522E-02
40		1.0944E-02
60		7.3639E-03
80		5.5723E-03
100		4.4902E-03

Small Unit Density Ellipsoids, Axes Ratio 1/3/8 (With Backscatter)

300	gram	S = 1.6417E-03
400		1.2503E-03
500		1.0152E-03
600		8.5432E-04
1000		5.2965E-04
2000		2.7840E-04
3000		1.9205E-04
4000		1.4806E-04
5000		1.2102E-04
6000		1.0272E-04

Small Unit Density Spheres and Thick Ellipsoids, Axes Ratio 1/.667/1.333 (With Backscatter)

131

131
I

300	gram	S = 1.6029E-03
400		1.2222E-03
500		9.8906E-04
600		8.3233E-04
1000	Unit Density Flat Ellipsoids, Axes Ratio 1/.5/2.0 (With Backscatter)	5.1559E-04
2000		2.6999E-04
3000		1.8541E-04
4000		1.4231E-04
5000		1.1612E-04
6000		9.8450E-05
2000	gram	S = 2.5084E-04
4000		1.3228E-04
6000		9.1068E-05
8000		7.0000E-05
10000		5.7049E-05
20000		3.0355E-05
30000	Unit Density Ellipsoids, Axes Ratio 1/1.8/9.27 (No Backscatter)	2.0997E-05
40000		1.6172E-05
50000		1.3223E-05
60000		1.1217E-05
70000		9.7613E-06
80000		8.6509E-06
90000		7.7857E-06
100000		7.0787E-06
120000		6.0179E-06
140000		5.2494E-06

1	gram	S = 8.2936E-02
2		4.2481E-02
4		2.1996E-02
6		1.4936E-02
8		1.1437E-02
10		9.2977E-03
20		4.8823E-03
40		2.5935E-03
60		1.7239E-03
80		1.5426E-03
100		1.2737E-03

Small Unit Density Spheres (With Backscatter)

1	gram	S = 8.2145E-02
2		4.2060E-02
4		2.1625E-02
6		1.4673E-02
8		1.1232E-02
10		9.1108E-03
20		4.7659E-03
40		2.5157E-03
60		1.7894E-03
80		1.4225E-03
100		1.1673E-03

Small Unit Density Ellipsoids, Axes Ratio 1/2/4 (With Backscatter)

1	gram	S = 8.1403E-02
2		4.1444E-02
4		2.1229E-02
6		1.4400E-02
8		1.0986E-02
10		8.8732E-03
20		4.7187E-03
40		2.5328E-03
60		1.7514E-03
80		1.3587E-03
100		1.1132E-03

Small Unit Density Ellipsoids, Axes Ratio 1/3/8 (With Backscatter)

300	gram	S = 4.9942E-04
400		3.9285E-04
500		3.2679E-04
600		2.8061E-04
1000		1.8323E-04
2000		1.0354E-04
3000		7.4578E-05
4000		5.9221E-05
5000		4.9639E-05
6000		4.2922E-05

Small Unit Density Spheres and Thick Ellipsoids, Axes Ratio 1/.667/1.333 (With Backscatter)

^{127}Xe

300	gram	S = 4.6684E-04
400		3.6599E-04
500		3.0211E-04
600		2.5894E-04
1000	Unit Density Flat Ellipsoids, Axes Ratio 1/.5/2.0 (With Backscatter)	1.6903E-04
2000		9.5151E-05
3000		6.8076E-05
4000		5.3839E-05
5000		4.4933E-05
6000		3.8796E-05
2000	gram	S = 7.8245E-05
4000		4.4565E-05
6000		3.1911E-05
8000		2.5203E-05
10000		2.0955E-05
20000		1.1855E-05
30000		8.4948E-06
40000	Unit Density Ellipsoids, Axes Ratio 1/1.8/9.27 (No Backscatter)	6.7034E-06
50000		5.5766E-06
60000		4.8001E-06
70000		4.2284E-06
80000		3.7891E-06
90000		3.4394E-06
100000		3.1516E-06
120000		2.7160E-06
140000		2.3964E-06

1	gram	S =	2.9482E-01
2			1.4771E-01
4			7.4039E-02
6			4.9434E-02
8			3.7132E-02
10			2.9742E-02
20			1.4934E-02
40			7.5057E-03
60			4.9534E-03
80			3.8153E-03
100			3.0620E-03

Small Unit Density Spheres (With Backscatter)

1	gram	S =	2.9461E-01
2			1.4759E-01
4			7.3951E-02
6			4.9366E-02
8			3.7077E-02
10			2.9697E-02
20			1.4904E-02
40			7.4871E-03
60			5.0189E-03
80			3.7841E-03
100			3.0349E-03

Small Unit Density Ellipsoids, Axes Ratio 1/2/4 (With Backscatter)

1	gram	S =	2.9449E-01
2			1.4740E-01
4			7.3847E-02
6			4.9291E-02
8			3.7013E-02
10			2.9635E-02
20			1.4887E-02
40			7.4889E-03
60			5.0083E-03
80			3.7676E-03
100			3.0211E-03

Small Unit Density Ellipsoids, Axes Ratio 1/3/8 (With Backscatter)

300	gram	S =	1.0373E-03
400			7.8099E-04
500			6.2885E-04
600			5.2602E-04
1000			3.1943E-04
2000			1.6249E-04
3000			1.0957E-04
4000			8.2861E-05
5000			6.6757E-05
6000			5.5975E-05

Small Unit Density Spheres and Thick Ellipsoids, Axes Ratio 1/.667/1.333 (With Backscatter)

133 Xe

131

133
Xe

300	gram	S = 1.0288E-03
400		7.7515E-04
500		6.2238E-04
600		5.2040E-04
1000	Unit Density Flat Ellipsoids, Axes Ratio 1/.5/2.0 (With Backscatter)	3.1528E-04
2000		1.6007E-04
3000		1.0776E-04
4000		8.1476E-05
5000		6.5598E-05
6000		5.4972E-05
2000	gram	S = 1.5495E-04
4000		7.8856E-05
6000		5.3095E-05
8000		4.0110E-05
10000		3.2265E-05
20000		1.6410E-05
30000	Unit Density Ellipsoids, Axes Ratio 1/1.8/9.27 (No Backscatter)	1.1052E-05
40000		8.3499E-06
50000		6.7200E-06
60000		5.6277E-06
70000		4.8448E-06
80000		4.2552E-06
90000		3.7955E-06
100000		3.4262E-06
120000		2.8704E-06
140000		2.4716E-06

Small Unit Density Spheres (With Backscatter)

1	gram	S = 4.4987E-02
2		2.3736E-02
4		1.2671E-02
6		8.7423E-03
8		6.8432E-03
10		5.6256E-03
20		3.0667E-03
40		1.6945E-03
60		1.1012E-03
80		1.1168E-03
100		9.3752E-04

Small Unit Density Ellipsoids, Axes Ratio 1/2/4 (With Backscatter)

1	gram	S = 4.4137E-02
2		2.3276E-02
4		1.2279E-02
6		8.4604E-03
8		6.6141E-03
10		5.4043E-03
20		2.9419E-03
40		1.6127E-03
60		1.1946E-03
80		9.8455E-04
100		8.1871E-04

Small Unit Density Ellipsoids, Axes Ratio 1/3/8 (With Backscatter)

1	gram	S = 4.3349E-02
2		2.2463E-02
4		1.1852E-02
6		8.1639E-03
8		6.3200E-03
10		5.1487E-03
20		2.8893E-03
40		1.6303E-03
60		1.1539E-03
80		9.1236E-04
100		7.6078E-04

Small Unit Density Spheres and Thick Ellipsoids, Axes Ratio 1/.667/1.333 (With Backscatter)

300	gram	S = 3.8629E-04
400		3.0774E-04
500		2.5935E-04
600		2.2383E-04
1000		1.4949E-04
2000		8.6332E-05
3000		6.2803E-05
4000		5.0277E-05
5000		4.2258E-05
6000		3.6683E-05

$^{129}_{Cs}$

300	gram	S =	3.4862E-04
400			2.7969E-04
500			2.3417E-04
600			2.0267E-04
1000	Unit Density Flat Ellipsoids, Axes Ratio 1/.5/2.0 (With Backscatter)		1.3578E-04
2000			7.8392E-05
3000			5.6830E-05
4000			4.5315E-05
5000			3.8092E-05
6000			3.3100E-05
2000	gram	S =	6.1952E-05
4000			3.6666E-05
6000			2.6805E-05
8000			2.1472E-05
10000			1.8018E-05
20000			1.0437E-05
30000	Unit Density Ellipsoids, Axes Ratio 1/1.8/9.27 (No Backscatter)		7.5410E-06
40000			5.9761E-06
50000			4.9938E-06
60000			4.3076E-06
70000			3.8004E-06
80000			3.4061E-06
90000			3.0976E-06
100000			2.8403E-06
120000			2.4527E-06
140000			2.1679E-06

^{169}Yb

1	gram	S = 4.2059E-01
2		2.1113E-01
4		1.0619E-01
6		7.1030E-02
8		5.3453E-02
10		4.2902E-02
20		2.1659E-02
40		1.0967E-02
60		7.4568E-03
80		5.6976E-03
100		4.5957E-03

Small Unit Density Spheres (With Backscatter)

1	gram	S = 4.1999E-01
2		2.1080E-01
4		1.0592E-01
6		7.0845E-02
8		5.3304E-02
10		4.2751E-02
20		2.1567E-02
40		1.0906E-02
60		7.3645E-03
80		5.5934E-03
100		4.5030E-03

Small Unit Density Ellipsoids, Axes Ratio 1/2/4 (With Backscatter)

1	gram	S = 4.1940E-01
2		2.1029E-01
4		1.0560E-01
6		7.0597E-02
8		5.3097E-02
10		4.2567E-02
20		2.1530E-02
40		1.0908E-02
60		7.3298E-03
80		5.5375E-03
100		4.4556E-03

Small Unit Density Ellipsoids, Axes Ratio 1/3/8 (With Backscatter)

300	gram	S = 1.6064E-03
400		1.2226E-03
500		9.9025E-04
600		8.3397E-04
1000		5.1594E-04
2000		2.7089E-04
3000		1.8675E-04
4000		1.4364E-04
5000		1.1741E-04
6000		9.9498E-05

Small Unit Density Spheres and Thick Ellipsoids, Axes Ratio 1/.667/1.333 (With Backscatter)

^{169}Yb

300	gram	S =	1.5748E-03
400			1.1949E-03
500			9.6427E-04
600			8.1038E-04
1000	Unit Density Flat Ellipsoids, Axes Ratio 1/.5/2.0 (With Backscatter)		4.9966E-04
2000			2.6109E-04
3000			1.7904E-04
4000			1.3724E-04
5000			1.1172E-04
6000			9.4565E-05
2000	gram	S =	2.4472E-04
4000			1.2681E-04
6000			8.6583E-05
8000			6.6151E-05
10000			5.3725E-05
20000			2.8276E-05
30000			1.9459E-05
40000			1.4933E-05
50000	Unit Density Ellipsoids, Axes Ratio 1/1.8/9.27 (No Backscatter)		1.2166E-05
60000			1.0290E-05
70000			8.9311E-06
80000			7.9017E-06
90000			7.0930E-06
100000			6.4397E-06
120000			5.4525E-06
140000			4.7404E-06

1	gram	S = 9.9112E-02
2		4.9815E-02
4		2.5105E-02
6		1.6807E-02
8		1.2652E-02
10		1.0164E-02
20		5.1469E-03
40		2.6143E-03
60		1.7855E-03
80		1.3724E-03
100		1.1097E-03

Small Unit Density Spheres (With Backscatter)

1	gram	S = 9.8928E-02
2		4.9723E-02
4		2.5013E-02
6		1.6746E-02
8		1.2606E-02
10		1.0121E-02
20		5.1193E-03
40		2.5981E-03
60		1.7605E-03
80		1.3409E-03
100		1.0820E-03

Small Unit Density Ellipsoids, Axes Ratio 1/2/4 (With Backscatter)

1	gram	S = 9.8832E-02
2		4.9556E-02
4		2.4921E-02
6		1.6675E-02
8		1.2552E-02
10		1.0066E-02
20		5.1056E-03
40		2.5978E-03
60		1.7490E-03
80		1.3250E-03
100		1.0681E-03

Small Unit Density Ellipsoids, Axes Ratio 1/3/8 (With Backscatter)

300	gram	S = 3.9522E-04
400		3.0021E-04
500		2.4573E-04
600		2.0772E-04
1000		1.3007E-04
2000		6.9453E-05
3000		4.8489E-05
4000		3.7622E-05
5000		3.0998E-05
6000		2.6463E-05

Small Unit Density Spheres and Thick Ellipsoids, Axes Ratio 1/.667/1.333 (With Backscatter)

^{201}Tl

300	gram	S = 3.8536E-04
400		2.9312E-04
500		2.3710E-04
600		1.9975E-04
1000	Unit Density Flat Ellipsoids, Axes Ratio 1/.5/2.0 (With Backscatter)	1.2408E-04
2000		6.5803E-05
3000		4.5562E-05
4000		3.5261E-05
5000		2.8913E-05
6000		2.4630E-05
2000	gram	S = 5.7682E-05
4000		3.0985E-05
6000		2.1501E-05
8000		1.6595E-05
10000		1.3578E-05
20000		7.2825E-06
30000		5.0644E-06
40000	Unit Density Ellipsoids, Axes Ratio 1/1.8/9.27 (No Backscatter)	3.9171E-06
50000		3.2124E-06
60000		2.7330E-06
70000		2.3846E-06
80000		2.1193E-06
90000		1.9104E-06
100000		1.7406E-06
120000		1.4827E-06
140000		1.2951E-06

Appendix E

S Factor Calculations for Discs, ^{99m}Tc Energies, Standard Height = 0.3 cm

Radius = 1 cm

$$\sum_i \Delta_i \phi_i = (.2630)(.009) + (.0001)(.009)+(.0017)(.205) +(.0008)(.205) + (.0004)(.148) + NP$$

$$= .03984$$

$$S_1 = \frac{.03984}{.94} = .042$$

Radius = 2 cm

$$\sum_i \Delta_i \phi_i = (.2630)(.012)+(.0001)(.012)+(.0017)(.235) +(.0008)(.235)+(.0004)(.180)+NP$$

$$= .04072$$

$$S_2 = \frac{.04072}{3.77} = .011$$

Radius = 3 cm

$$\sum_i \Delta_i \phi_i = (.2630)(.014)+(.0001)(.014)+(.0017)(.270) +(.0008)(.270)+(.0004)(.210)+NP$$

$$= .04134$$

$$S_3 = \frac{.04134}{8.48} = .005$$

Radius = 4 cm

$$\sum_i \Delta_i \phi_i = (.2630)(.016)+(.0001)(.016)+(.0017)(.290) +(.0008)(.290)+(.0004)(.230)+NP$$

$$= .04192$$

$$S_4 = \frac{.04192}{15.08} = .003$$

Radius = 5 cm

$$\sum_i \Delta_i \phi_i = (.2630)(.017)+(.0001)(.017)+(.0017)(.310) +(.0008)(.310)+(.0004)(.240)+NP$$

$$= .04224$$

$$S_5 = \frac{.04224}{23.56} = .002$$

Appendix F

Cumulated Activities for Various Radionuclides, $\tilde{A}$ μCi-hr Per 1 μCi Administered

Radionuclide	Radiopharmaceutical	Reference	$\tilde{A}$ Rest of body	$\tilde{A}$ Critical organ
^{51}Cr	DTPA or EDTA	(42)	.852	7.66 (kidney)
	Human serum albumen	(42)	319.2	
	RBC	(42)	450	150 (spleen)
^{55}Fe	Ferric chloride	(42)	10,418	448 (kidney) 3406 (liver) 315 (lungs) 565 (spleen) 144 (testes)
^{57}Fe	Vitamin B12	(42)	18.3	2215 (liver) 96.2 (stomach) 16.8 (spleen) 69.3 (kidney) 0.87 (overies) 48.1 (bone) 36.5 (testes)
^{59}Fe	Ferric chloride	(42)	1005	43 (kidney) 329 (liver) 30 (lungs) 56 (spleen) 1387 (tested)
^{67}Ga	Citrate	(28)	88(total)	4.0 (spleen)
^{68}Ga	Albumen macro-aggregates	(42)	.082	.135 (liver) 1.15 (lung)
	DTPA or EDTA	(42)	.138	1.24 (kidney)

^{75}Se	L-Selenomethionine	(55)		190 (blood) 81 (fat) 35 (kidneys) 190 (liver) 41 (lungs) 660 (muscle) 0.3 (ovaries) 1.4 (pancreas) 81 (skin) 12 (spleen) 1.3 (testes) 1.1 (thyroid)
^{99m}Tc	Albumen macro-aggregates	(42)	.42	.42 (liver) 3.94 (lung)
	DTPA or EDTA	(42)	.432	3.89 (kidney)
	DTPA	(28)	3.2(total)	.16 (kidney) 5.0 (bladder)
	EHDP	(34)	8.6(total)	2.6 (bone)
	FeOH Colloid	(42)	.578	.290 (liver) 4.92 (lung)
	HSA	(51)		6.480 (blood)
	HSA	(28)	4.3(total)	4.3 (blood)
	HSA	(42)	8.5(total)	
	HSA	(58)	4.3(total)	4.3 (blood)
	Heat treated RBC	(42)	8.7	7.8 (spleen)
	Iron complex	(59)	3.7(total)	1.7 (renal cortex)
	Iron complex	(28)	3.7(total)	1.7 (renal cortex)
	Isotopes	(62)		
	Newborn			.26 (thyroid)
	1-15 years			.26 (thyroid)

Liver colloid	(52)	8.64(total)	7.78 (liver) 0.432 (spleen) 0.432 (marrow)
MAA	(60)	8.0(total)	5.6 (lungs)
MAA or microspheres	(28)	7.6(total)	3.9 (lung)
MPI bone scintigraphin	(48)	.346(total)	3.030 (bone) .0866 (kidney)
MPI lung-aggregate	(49)	8.66(total)	2.23 (lung) 1.46 (liver and spleen) 1.33 (liver) .13 (spleen) .91 (GIT) .52 (kidney) .10 (bladder)
Pertechnetate	(58)	7.0(total)	0.1 (thyroid)
Pertechnetate	(28)	7.0(total)	.092 (thyroid)*
Pertechnetate	(a)	Resting Population 7.13(total)	3.48 (extra-vascular) .61 (LI) .73 (plasma) .21 (RBC) .08 (salivary glands) 1.81 (Stomach) .04 (thyroid)
		Nonresting Population 5.69(total)	2.57 (extra-vascular) 1.26 (LI) .71 (plasma) .20 (RBC) .07 (salivary glands) .30 (stomach) .04 (thyroid)

*no blocking dose
a) calculated from reference 63.

	Polyphosphate	(61)	7.1(total)	4.3 (bone)
	Polyphosphate	(42)	1.14	4.34 (bone)
	Polyphosphate	(28)	6.7(total)	4.2 (bone)
	RBC	(42)	8.7(total)	
	Stannous gluco-heptonate	(50)	1.368(total)	1.584(kidney) 1.800(bladder) 8.640(gonads) 6.480(blood)
	Stannous phytate	(53)	0.432(total)	7.776(liver) 0.432(spleen)
	Sulfur colloid	(28)	8.7(total)	7.4 (liver)
^{111}In	Chloride	(47)	32	32 (liver) 32 (red marrow)
^{113m}In	Albumen macro-aggregates	(42)	.120	.176 (liver) 1.58 (lung)
	Colloid	(42)		2.2 (liver) .07 (spleen) .17 (red-marrow)
	Colloid	(28)	2.5(total)	2.1 (liver)
	DTPA	(28)	1.2(total)	1.4 (bladder)
	DTPA	(42)	.187	1.68 (kidney)
	Fe-hydroxide	(28)	2.4(total)	1.7 (lung)
	Fe OH Colloid	(42)	.21	.105 (liver) 1.786 (lung)
	Microspheres	(42)	.143	1.94 (lung)*

*thyroid blocked

^{123}I	Hippuran	(42)	.370(total)	.187(kidneys)
	Isotopes	(62)		
	newborn			13.3(thyroid)
	1-15 yrs			5.1(thyroid)
	Sodium iodide	(b)	9.4(total)	3.2(thyroid)
^{125}I	Human serum albumen	(42)	391.2(total)*	
	Hippuran	(42)	.432(total)	.271(kidney)
	Isotopes	(62)		
	newborn			772(thyroid)
	1-15 yrs			297(thyroid)
	Rose bengal	(42)		2.16(liver) 3.98(SI) 13.3(ULI) 23.5(LLI)
	Sodium iodide	(b)	28.5(total)	21.3(thyroid)
^{131}I	HSA	(28)	163(total)	163(blood)
	Isotopes	(62)		
	newborn			174(thyroid)
	1-15 yrs			67.2(thyroid)
	MAA	(28)	35(total)	8.9(lung)
	Rose bengal	(28)	30(total)	2.2(liver)
	Sodium iodide	(b)	6.8(total)	1.67(thyroid)
^{129}Cs	Chloride	(54)	46(total)	
^{131}Cs	Chloride	(54)	314(total)	

*thyroid blocked

b) Calculated from reference 64. Assumes maximum thyroid uptake of 25%

^{132}Cs	Chloride	(54)	2.15(total)	
^{134}Cs	Chloride	(54)	4085(total)	
^{169}Yb	DTPA	(56)		1005(blood) 2922(C1-C7) 2630(C8-T6) 3151(T7-L1) 5376(L2-Col) 6160(nerve roots) 4688(nerve roots)

DTPA	(57)		54,880	(brain)
DTPA or EDTA	(42)	.852	7.68	(kidney)

The following data is from reference 27:

Table 3. Measured Effective Half-Lives and Calculated Cumulative Activities and Doses for Various Radiopharmaceuticals in Children

Age	Weight (kg)	Effective Half-Lives T_e (days) T_{e1} (C_1)*	T_{e2} (C_2)*	Cumulative Activity A (μCi•h) (1 μCi administered) Whole Body	Organ	Dose (mrad/μCi Administered) Whole Body	Organ
^{131}I-triolein							
3 mo	3.18	0.4(98)	6.4(0.02)	18.0		7.2	
2 yr	9.55	0.4(98)	6.0(0.02)	17.7		2.5	
^{131}I-serum albumin							
2 yr	7.50	4.7		163.0		12.3	
^{131}I-rose bengal							
5 yr	19.30	0.4(0.90)	3.0(0.10)	10.4	12.5	0.4	1.9 (liver)
13 yr	59.00	0.6(0.80)	4.3(0.20)	29.8	16.6	0.3	0.8 (liver)
^{51}Cr-sodium chromate							
4 mo	8.18	15.0		519		1.8	
14 mo	12.60	20.0		692		1.7	
5 yr	20.00	20.0		692		1.2	
6 yr	13.62	19.4		672		1.6	
6 yr	18.60	16.5		571		0.8	
^{59}Fe-ferrous citrate							
4 yr	19.00	26.0		900		49.3	
5 yr	20.00	38.0		1315		70.3	
6 yr	13.62	31.0		1072		78.0	
15 yr	55.00	39.0		1350		32.0	
^{197}Hg-chlormerodrin							
3 yr	14.55	0.8(0.82)	2.6(0.18)	38.9	38.9	0.16	68.1 (kidney)
12 yr	47.28	0.9(0.84)	2.6(0.16)	40.6	40.6	0.07	39.0 (kidney)
^{75}Se-selenomethionine							
7 yr	24.50	0.8(0.15)	23.3(0.85)	689	689 (liver) 689 (muscle)	10.3	34.0 (liver) 8.7 (muscle) 4.9 (pancreas)
^{47}Ca-calcium chloride							
7 yr	25.00	0.7(0.94)	4.6(0.06)	22.8	9.6 (bone)	2.8	4.5 (bone)
^{85}Sr-strontium nitrate							
4 yr	15.47	3.5(0.38)	58.0(0.62)	46.0	1224 (bone)	16.3	68.3 (bone)
10 yr	32.70	1.3(0.48)	44.0(0.53)	21.6	792 (bone)	6.0	40.8 (bone)
11 yr	54.50	3.2(0.20)	55.0(0.80)	22.1	1524 (bone)	9.2	62.5 (bone)
12 yr	40.00	1.4(0.30)	53.0(0.70)	14.5	1283 (bone)	8.6	32.8 (bone)
12 yr	60.00	1.5(0.65)	30.0(0.35)	33.8	364 (bone)	2.5	14.0 (bone)

* C_1 and C_2 are fractional components of administered activity.